Improved Fast Inverse Nonlinear Fourier Transform for Multi-solitons

A Discrete Darboux Based Approach

Shrinivas Chimmalgi

Master of Science Thesis

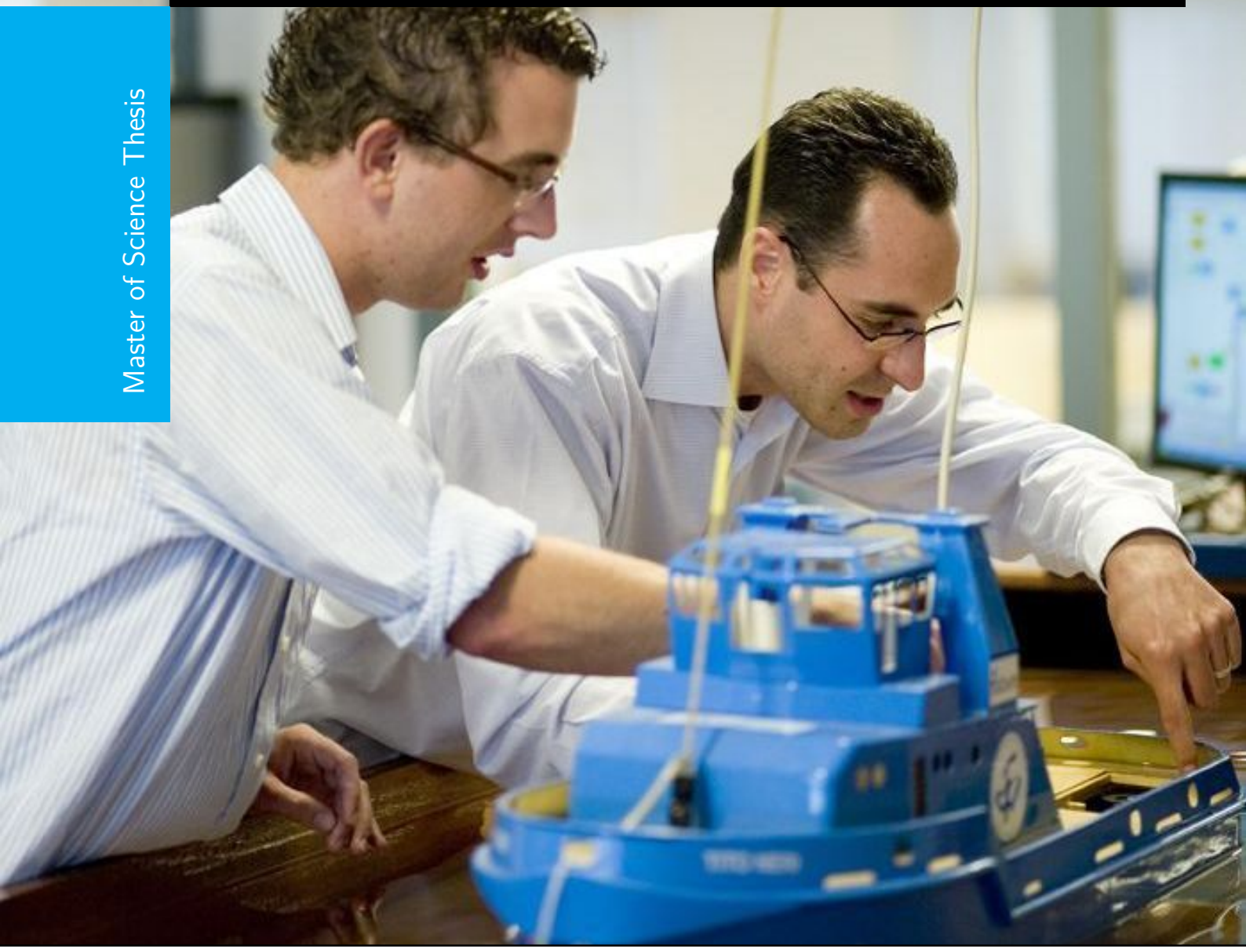

TU Delft Delft University of Technology

Delft Center for Systems and Control

Improved Fast Inverse Nonlinear Fourier Transform for Multi-solitons

A Discrete Darboux Based Approach

Master of Science Thesis

For the degree of Master of Science in Systems and Control at Delft University of Technology

Shrinivas Chimmalgi

August 31, 2017

Faculty of Mechanical, Maritime and Materials Engineering (3mE) · Delft University of Technology

Delft University of Technology
Department of
Delft Center for Systems and Control (dcsc)

The undersigned hereby certify that they have read and recommend to the Faculty of Mechanical, Maritime and Materials Engineering (3mE) for acceptance a thesis entitled

Improved Fast Inverse Nonlinear Fourier Transform for Multi-solitons

by

Shrinivas Chimmalgi

in partial fulfillment of the requirements for the degree of

Master of Science Systems and Control

Dated: August 31, 2017

Supervisor(s):

Dr.-Ing. S. Wahls

Reader(s):

Prof.dr.ir. M. Verhaegen

Dr.ir. R. F. Remis

Table of Contents

List of Figures

Abstract

The relation between the input of an ideal optical single-mode fiber and the corresponding fiber output constitutes a nonlinear system that can be described using the nonlinear Schrödinger equation. This nonlinear system has the interesting property that it can be solved analytically using nonlinear Fourier transforms. To utilize this property, new methods of optical communication are being developed by embedding information in the nonlinear Fourier domain and employing fast nonlinear Fourier transforms. Many of the recent works use a specialized form of inverse nonlinear Fourier transform to generate information-bearing fiber inputs in the form of so-called multi-soliton pulses. Recently, multiple fast inverse nonlinear Fourier transform algorithms that can generate multi-solitons have been proposed. The goal of this thesis is to study and improve these algorithms, in particular, with respect to their computational complexity.

Based on the literature survey, discrete Darboux transform combined with other discrete techniques is studied and a new algorithm is proposed. The algorithm employs a single-start approach in which discrete Darboux matrix is computed at only one sample point and rest of the samples are computed by evolution of the Darboux matrix. The algorithm is hence named as discrete Darboux evolution algorithm (DDE). The errors in the generated signal and run-time are studied by comparison with the classical Darboux transform (CDT). The DDE algorithm is shown to have floating point operations complexity of $\mathcal{O}(KN)$ for K eigenvalues and N samples. However, in a limited precision environment the number of samples that can be generated is found to be limited. To better understand the effects of machine precision, both the CDT and DDE algorithms are studied in a multi-precision environment. Certain insights from the study are used to develop two modifications to overcome the limitations. The first modification computes the signal using multiple single-start runs while the second one uses a multi-start approach. The second modification is shown to have errors comparable with other fast algorithms in literature. Additionally, in a qualitative comparison it is shown to be potentially faster than existing algorithms in a certain regime.

Acknowledgements

I would like to thank my thesis advisor Dr.-Ing. Sander Wahls for giving me this opportunity to work under his guidance. He was always very welcoming and helped me when I had any questions about my research or writing. He encouraged me to work independently, but steered me in the right direction whenever he thought I needed it.
I would also like to thank my daily supervisor Dr. Vishal Vaibhav for his guidance and helpful discussions.
Finally, I must express my very profound gratitude to my parents for providing me with unfailing support and continuous encouragement. I am grateful to my friends for all the help. It would not have been possible without them. Thank you.

Delft, University of Technology — Shrinivas Chimmalgi
August 31, 2017

Chapter 1

Introduction

Fiber-optic cables are nonlinear channels for transmission of light and they form the basis of modern communication systems. The propagation of light in the single-mode optical fibers can be modeled using the nonlinear Schrödinger equation. However, it is important to understand the link between the physical systems and the mathematical models. With this view in mind, the physical phenomena occurring during light propagation are mentioned first. The discussion on these phenomena naturally leads to the nonlinear Schrödinger equation which governs the propagation of light. The solitons which arise from the interaction of various physical phenomena are explained next. Once the significance of the solitons is discussed, nonlinear Fourier transform is introduced.

1-1 The Nonlinear Schrödinger Equation

James Clerk Maxwell showed in the 1860's that light is an electromagnetic phenomenon and derived the celebrated Maxwell equations which model light as electromagnetic waves. He showed that light propagates as an electromagnetic planewave. Later, in 1926, Erwin Schrödinger formulated the Schrödinger equation to describe how the quantum state of a quantum system changes with time. Owing to its particle-wave duality, light also obeys the Schrödinger equation. To understand the propagation of light according to the Schrödinger equation, it is necessary to understand the underlying linear and nonlinear phenomena.

Many of the phenomena arise due to the refractive index n of an optical medium, which is defined as the ratio of the speed of light in vacuum c and the phase velocity v of light in the medium ($n = c/v$). The phase velocity is the rate at which phase of any one frequency component changes while it propagates. In an isotropic (same properties in all directions) medium such as glass optical fiber, the refractive index is independent of the direction of the electric field. The refractive index is given by (p.63 in [2])

$$n = n(\omega, |A|^2) \approx n_0(\omega_0) + n_2|A|^2, \tag{1-1}$$

where $|A|^2$ is the intensity of the pulse, n_2 is the intensity-dependent refractive index coefficient (generally positive), ω_0 is the carrier frequency and n_0 is the frequency dependent refractive index. Such a variation in refractive index of the material proportional to the intensity of the electric field is known as the Optical-Kerr effect and n_2 is known as the Optical-Kerr coefficient. In purely one dimensional propagation (like propagation of light along an optical fiber), the intensity dependent refractive index (n) imposes a self-phase shift on the pulse envelope during propagation which is given by (p.64 in [2])

$$\frac{\partial A(x,t)}{\partial x} = -i\gamma |A(x,t)|^2 A(x,t), \tag{1-2}$$

where γ is the self-phase modulation coefficient, $A(x,t)$ is the complex electromagnetic field envelope, x is the position along the wave's direction of travel, t is the coordinate time with respect to a frame of reference moving at the group velocity. Such a phase-shift is known as self-phase modulation (SPM). The intensity profile does not change, only the spectrum of the pulse changes. Energy redistribution occurs during SPM and for positive SPM, the low frequency contributions move to the front and the high frequencies to the back of the pulse. The other important effect to be understood is optical-dispersion. Dispersion is the phenomenon in which the phase velocity of a wave depends on its frequency,

$$\omega(k) = v(k)k, \tag{1-3}$$

where k is the wavenumber. Such a variation of the phase velocity leads to a phase difference between the different frequency components as light travels through the medium. Dispersion is a linear effect while SPM is a nonlinear effect. The effects of positive SPM and negative dispersion can be seen in Figure 1-1.

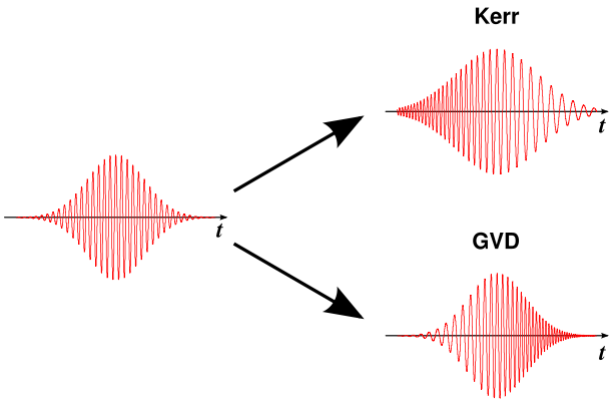

Figure 1-1: Linear and nonlinear effects on Gaussian pulses (modified from [1])

There are other nonlinear phenomena which affect the light propagating through a medium. The high order nonlinear Schrödinger equation (NSE) provides a model for light traveling through an optical fiber [5],

$$\frac{\partial A}{\partial x} + \frac{\alpha}{2}A + \frac{i}{2}\beta_2 \frac{\partial^2 A}{\partial t^2} - \frac{1}{6}\beta_3 \frac{\partial^3 A}{\partial t^3} = i\gamma\left[|A|^2 A + \frac{2i}{\omega_0}\frac{\partial}{\partial t}(|A|^2 A) - T_R \frac{\partial |A|^2}{\partial t}\right], \tag{1-4}$$

where α is the fiber loss coefficient, β_2 is the dispersion (with respect to frequency), β_3 is the third order dispersion (dispersion slope), γ is the nonlinear coefficient, ω_0 is the angular

carrier frequency and T_R is the Raman term. The coefficients $\alpha, \beta_2, \beta_3, \gamma, \omega_0$ and T_R represent the physical properties of the optical fiber.
The reduced NSE ,

$$\frac{\partial A(x,t)}{\partial x} = -\frac{i}{2}\frac{\partial^2 A}{\partial t^2} + i\gamma|A|^2 A, \tag{1-5}$$

represents a scalar approximation to the light propagation i.e. it ignores polarization effects and considers only SPM and dispersion [5].
The terms in the reduced NSE Eq. (1-5) can be normalized to obtain the normalized NSE [2],

$$i\frac{\partial A'(x',t)}{\partial x'} = \frac{\partial^2 A'}{\partial t^2} + 2|A'|^2 A', \tag{1-6}$$

where A' is the normalized field amplitude, x' is the normalized propagation distance and t' is the normalized time.
Under certain circumstances, the SPM due to the positive Kerr effect is canceled by the negative dispersion, leading to non dispersive wave-packets or pulses known as solitary waves. They are also known as bound solutions or bright solitons (Figure 1-2). These solitary waves have special shapes and properties.

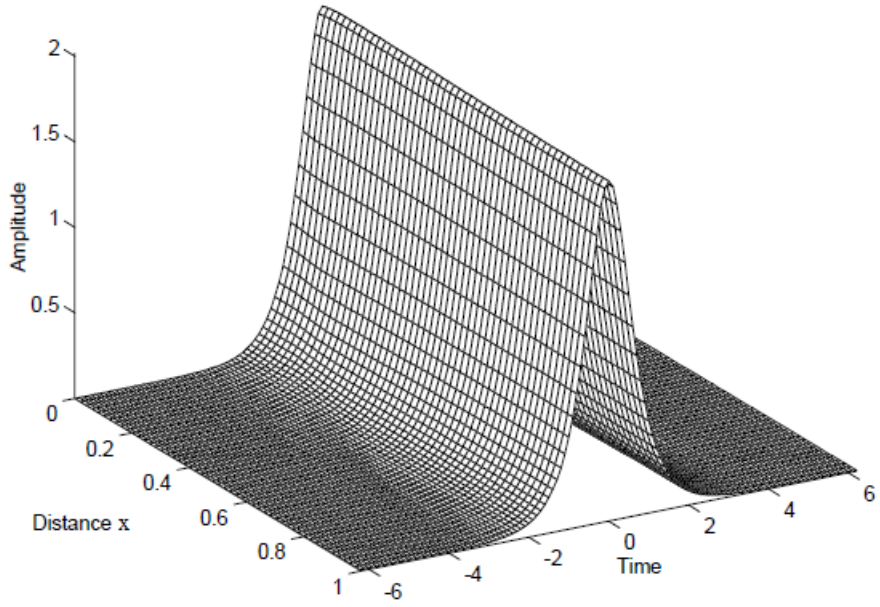

Figure 1-2: Propagation of a soliton taken from p.69 of [2]

1-2 The Fundamental Soliton

Now we look at few properties of self-consistent (non-dispersive) pulses which are formed when the effect of SPM cancels effect of dispersion. The shape of such a solitary pulse or fundamental soliton is given by [2],

$$A_s(x,t) = A_0 \operatorname{sech}\left(\frac{t}{\tau}\right) e^{-i\theta(x,t)} \tag{1-7}$$

where $\theta(x,t)$ is the nonlinear phase shift of the soliton, A_s is the complex envelope of the soliton pulse and sech(x) is the hyberbolic secant function. In order to achieve balance between the nonlinear and linear effects, the nonlinear phase shift

$$\theta = \frac{1}{2}\gamma A_0^2 x, \tag{1-8}$$

should equal the dispersive spreading of the pulse,

$$\theta(x,t) = \frac{|D_2|}{\tau^2}x. \tag{1-9}$$

The soliton energy fluence (energy per cross-sectional area) of such a soliton is given by,

$$w = \int_{-\infty}^{\infty} |A_s(x,t)|^2 dt = 2A_0^2\tau. \tag{1-10}$$

For a lossless fiber the energy fluence is constant and the width of the soliton (p.68 in [2]),

$$\tau = \frac{4|D_2|}{\delta w}, \tag{1-11}$$

is proportional to the amount of negative dispersion (D_2). The pulse area of the fundamental soliton is determined by only the dispersion and the self-phase modulation coefficient,

$$\textbf{Pulse Area} = \int_{-\infty}^{\infty} |A_s(x,t)|dt = \pi A_0\tau = \pi\sqrt{\frac{|D_2|}{2\delta}}. \tag{1-12}$$

The balance between the nonlinear and linear effects occurs only at specific amplitudes of the complex envelope. Thus the initial amplitude required for soliton propagation is fixed uniquely in terms of the fiber dispersion, nonlinear Kerr coefficient and effective area for a given pulse width and carrier wavelength. The distance after which the soliton acquires a phase shift of $\pi/4$ is called the soliton period. Only the pulse area is fixed and for a certain dispersion and SPM-coefficient, the energy fluence and the width are determined if either one of them is specified.
The loss during transmission through real fibers is generally not modeled. Instead periodic amplification is used and the power is averaged over the given length of the fiber. This leads to the guiding-center soliton or average soliton. The periodic amplification acts like a periodic perturbation. Perturbation analysis shows that the soliton energy has to be kept small enough, so that the soliton period is much longer than the distance between amplifiers to prevent significant loss of information (p.87 in [2]).

The NSE possesses higher order soliton solutions. Such solutions are known as multi-solitons or N-solitons formed from N individual solitons. When all the solitons travel with the same speed, i.e. they posses the same carrier frequency, they are known as breather solutions (Figure 1-3). Due to the interaction of two or more solitons, the temporal shape and the spectrum exhibit complicated but periodic behaviour with a period $x = \pi/4$. The multi-soliton solutions which result from the interaction of solitons traveling at different speeds break down into N individual solitons as the signals propagate through the fiber.

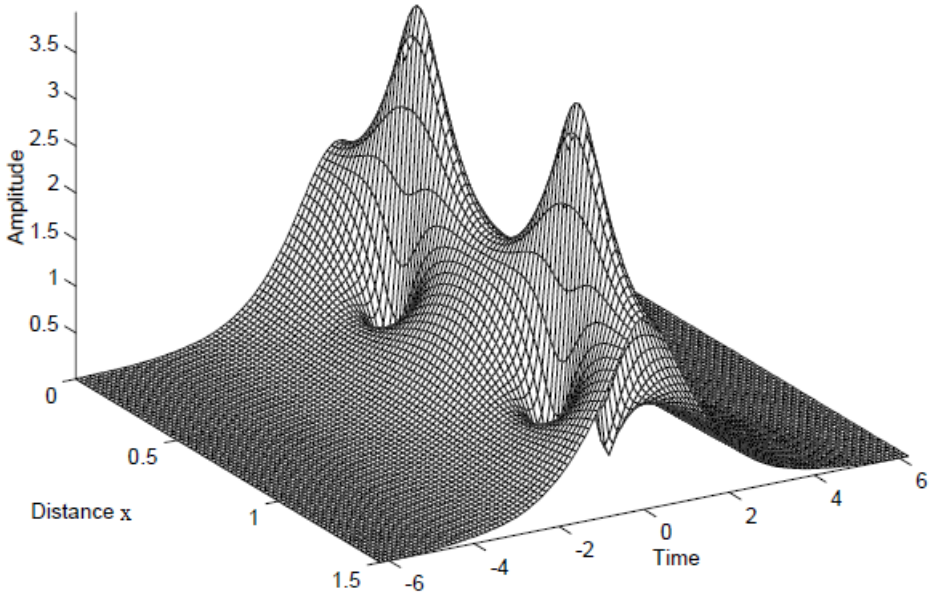

Figure 1-3: Breather solution composed of two fundamental solitons, taken from p.72 of [2]

1-3 Scattering Theory

To understand solitons and their behaviour, a mechanism is required to solve the nonlinear Schrödinger equation. More specifically, a method of solution is needed to solve initial value problems for the nonlinear Schrödinger equation. The application of scattering theory provides an elegant method to solve such problems. Scattering theory is a framework for studying and understanding the scattering of waves and particles. The solutions of the nonlinear PDE can be viewed as waves and hence scattering theory can be used to understand and solve for them. To better understand the method of solution for the Nonlinear Schrödinger Equation (NSE) Eq. (1-5), it is first applied to a linear PDE [6].
A general first order linear PDE is given as,

$$\frac{\partial q(x,t)}{\partial t} = -i\omega \left(-i\frac{\partial}{\partial x}\right) q(x,t). \tag{1-13}$$

Given the initial ($t = 0$) waveform $q(x,0)$, the goal is to find the waveform $q(x,t)$ for some specified time t. The first step is to map $q(x,0)$ to its Fourier transform $K(k,0)$ where k is the wavenumber. Then the time evolution of $K(k)$ for each k can be traced separately as,

$$K_t(k,t) = -i\omega(k)K(k,t), \tag{1-14}$$

where the subscript t represents the partial differential of $K(k,t)$ with respect to t. It is worth noting that the time evolution of $K(k,t)$ is only determined by functionals evaluated at k. This property is known as separability. Thus, knowing $K(k,0)$, $K(k,t)$ can be found. The inverse Fourier transform of $K(k,t)$ gives the solution $q(x,t)$.

Such a mechanism is now extended to nonlinear PDE. For ease of comparing different literature sources, the notations used in [6] will be followed from here on in the report. The

normalized nonlinear Schrödinger Eq. (1-6) is written as

$$q_t - iq_{xx} - 2iq^2q^* = 0, \tag{1-15}$$

where q^* denotes the complex conjugate of the complex valued solution $q(x,t)$ and the subscripts represent the parital derivative of $q(x,t)$ with respect to the subscript.
It can be shown that Eq. (1-15) is associated with the linear system,

$$\begin{aligned} v_{1x} + i\zeta v_1 &= q(x,t)v_2, \\ v_{2x} - i\zeta v_2 &= -q^*(x,t)v_1, \end{aligned} \tag{1-16}$$

where $\zeta \in \mathbb{C}$ is a parameter which is independent of x and $v(\zeta, x, t) \in \mathbb{C}^2$. The subscript 1 in v_1 corresponds to first of the two terms. The solution $q(x,t)$ is assumed to satisfy $q(x,t) \to 0$ sufficiently rapidly as $|x| \to \infty$. For $q(x,t)$ real, the parameter ζ is a set of all real ζ (continuous spectrum) and a finite number of distinct complex numbers $\zeta = K_n, n = 1, ..., N$ (the discrete spectrum). The function v corresponding to parameter ζ can be computed and in particular the asymptotic behavior may be fixed as,

$$\begin{aligned} v(k,x,t) &\to e^{-ikx} + R(k,t)e^{ikx}, \qquad x \to +\infty, \\ v(k,x,t) &\to T(k,t)e^{-ikx}, \qquad x \to -\infty, \end{aligned} \tag{1-17}$$

for $\zeta = k, k$ real, and

$$\begin{aligned} v_n(x,t) &\to C_n(t)e^{-K_n x}, \qquad x \to +\infty, \\ v_n(x,t) &\to D_n(t)e^{K_n x}, \qquad x \to -\infty, \end{aligned} \tag{1-18}$$

for $\zeta = K_n$. The linear problem Eq. (1-16) is also referred to as the scattering problem hence the name scattering theory. In this framework the function $v(\zeta, x, t)$ is scattered by the solution $q(x,t)$ which is analogous to the scattering potential. The scattering can be characterized by the reflection coefficient $R(k,t)$ and transmission coefficient $T(k,t)$.
Essentially, the association of the solution of Eq. (1-15) with the scattering problem Eq. (1-16) gives a mapping between $q(x,t)$ and what shall be called as the scattering data [6],

$$q(x,t) \mapsto S(\{K_n, C_n(t)\}_{n=1}^N, T(k,t), R(k,t)), \tag{1-19}$$

which is composed of the spectrum $(\{K_n\}_{n=1}^N, -\infty < k < \infty)$ and the coefficients representing the asymptotic behavior of the corresponding functions (v). The process of computing the function $v(\zeta, x, t)$ from $q(x,0)$ is known as forward or direct scattering. The reflection coefficient $R(k,0)$ and transmission coefficient $T(k,0)$ at $t = 0$ can be computed from the functions $v(\zeta, x, 0)$ and the complete process of computing the scattering data from $q(x,t)$ is known as the nonlinear Fourier transform. The scattering data corresponding to the initial condition $q(x,0)$ shall be denoted by $S(0)$. By analogy to the linear problem, the time evolution of scattering data can be found. The details will be given in a later section, but for now it suffices to know that under such a time evolution the discrete parameters $\zeta = K_n$ remain invariant. The evolution of the related functions $v(\zeta, x, t)$ can also be described by simple relations. While the determination of $v(\zeta, x, t)$ at later times depends on the knowledge of $q(x,t)$, the asymptotic behavior of $v(\zeta, x \to \pm\infty, t)$ does not, this is crucial for existence of an inverse mapping. The time evolution of the scattering data S is directly related to the

dispersion relation of the linearized Schrödinger equation. This will be clearer in subsequent sections.
Given the scattering data at initial time $S(0)$, time evolved scattering data at some future time t denoted by $S(t)$ can be computed. So the next question is whether this mapping can be inverted. This question was answered by Gelfand and Levitan [2]. For sake of brevity the mathematics is not explained here but it can be found in the paper by Ablowitz et al. [6]. Thus the solution (potential) $q(x,t)$ can be computed from $S(t)$. This step is known as the inverse scattering transform.
The scheme for solving initial value problem can be summarized as follows [6].
For linear problems,

$$q(x,0) \mapsto K(k,0) \xrightarrow{\omega(k)} K(k,t) \mapsto q(x,t), \tag{1-20}$$

and for nonlinear problems,

$$\begin{aligned} q(x,0) &\mapsto S(\{K_n, C_n(0)\}_{n=1}^{N}, T(k,0), R(k,0)) \\ &\xrightarrow{\omega(2k)} S(\{K_n, C_n(t)\}_{n=1}^{N}, T(k,t), R(k,t)) \\ &\mapsto q(x,t), \end{aligned} \tag{1-21}$$

where $\xrightarrow{\omega(k)}$ denotes the time evolution of the scattering data based on the dispersion relation. The method for solving nonlinear PDE is therefore analogous to the Fourier transform method of linear problem and hence known as the nonlinear Fourier transform.

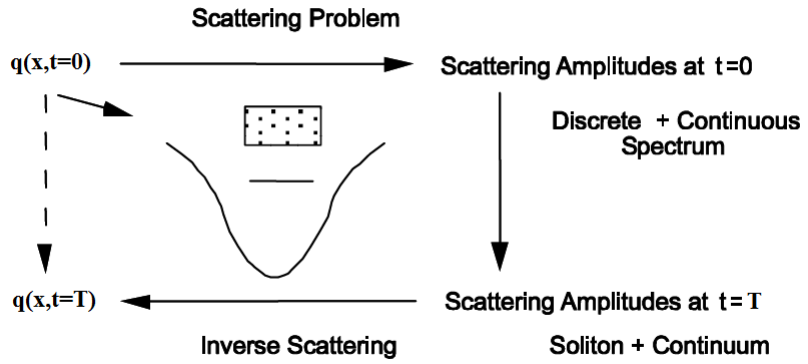

Figure 1-4: Schematic representation of the inverse scattering theory for the solution of integrable nonlinear partial differential equations, taken from p.74 of [2].

From a physical perspective, the discrete parameters correspond to the solitons (bound states) and the real parameters correspond to a continuum of scattering states. The continuum states disperse during propagation while the solitons do not, and hence only the solitons can be recognized after a while i.e. as $t \gg 0$. It is found that the speed of the soliton is function of ζ. In general there is a locus of ζ in the complex plane such that the solitons corresponding to the values of ζ on such a locus have the same speed. If the initial solution contains two or more solitons moving at the same speed, then a multi-soliton bound structure is formed termed as the breather solution (so called because it pulsates as it travels)(Figure 1-3). If the speed of the solitons is not the same, then as $t \to \infty$ the multi-soliton solution breaks

up into solitons arranged in such a way that the fastest soliton is in front and the slowest at the rear. In Figure 1-5 a multi-soliton is shown to break up into four individual solitons as it travels through the fiber. The solitons always recover completely after an interaction but acquire a phase shift. The total soliton phase shift is equal to the algebraic sum of its shifts during paired collisions, so that there is no effect of multi-particle collisions.

Outline

Starting from the basic physical phenomena and building up to the concept of nonlinear Fourier transform makes it easier to comprehend the significance of multi-solitons. The non-dispersive nature of these types of signals make them appealing to be used for information transmission. The association of solitons with the discrete nonlinear Fourier spectrum is fascinating. In Chapter 2, essential details about nonlinear Fourier transform will be covered. The classical Darboux transform which is a special form of inverse NFT for generating multi-solitons is then introduced. Chapter 3 covers NFT in a discrete setting. An analogy between continuous and discrete time NFT is drawn. In Chapter 4 a new algorithm based on discrete Darboux transform is proposed. In Chapter 5 the newly proposed algorithm is tested and modifications are introduced to overcome limitations found during testing.

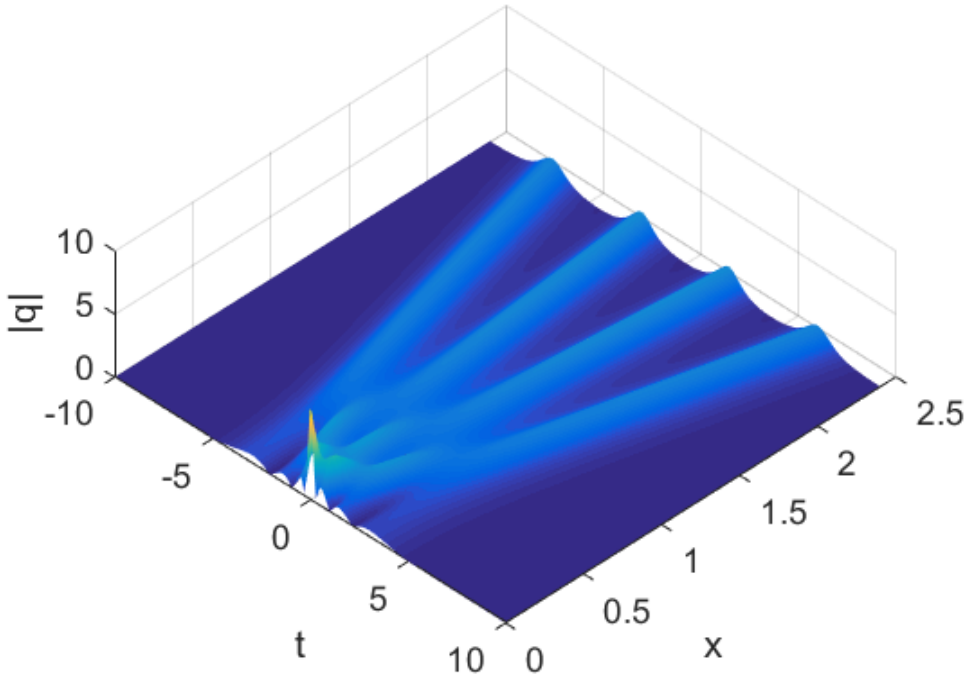

Figure 1-5: Multi-soliton breaking into four separate solitons

Chapter 2

Nonlinear Fourier Transform

Having introduced the notion of nonlinear Fourier transform (NFT) in Chapter 1, the underlying assumptions and other relevant details will be covered in this chapter. The classical Darboux transform which is an inverse NFT method for generating multi-solitons is also explained.

2-1 Forward Nonlinear Fourier Transform

Obtaining the spectral data from the potential is known as the forward NFT. In this section, the most important question of the relationship between a particular nonlinear partial differential equation PDE and the associated eigenvalue problem will be addressed. More details about the method of computing the scattering data and its properties will be covered.

2-1-1 Relation of Eigenvalue Problem to Evolution Equations

The technique of inverse scattering transform was first discovered by Gardner et al. [7] and applied by them to the Korteweg de Vries (KdV) equation. It was initially speculated to be a fluke [8] and specific to only the KdV equation. But in 1972, Zakharov and Shabat [9] applied the scattering problem Eq. (1-16) to find the initial value solution for the nonlinear Schrödinger equation. In 1974, Ablowitz et al. [6] developed a systematic method which allows one to identify certain important classes of evolution equations which can be solved by the method of inverse scattering. The central point of their paper is that given a dispersion relation $\omega(k)$ meromorphic[1], and real for real k, there is a nonlinear evolution equation whose linearized version has this dispersion relation and for which appropriate initial value problems can be solved exactly (p.253 [6]). All the equations under this subclass are integrable[2] and can be shown to have infinite sequence of conservation laws [9]. Ablowitz et al. also showed

[1] A meromorphic function on an open subset D of the complex plane is a function that is holomorphic on all D except for a set of isolated points, which are the poles of the function

[2] Liouville Integrability

the relationship between the scattering theory and Bäcklund transformations. Details of a special type of Bäcklund transformation known as the Darboux transform will be discussed in Section 2-2-2.

The systematic method referred to as the 'AKNS formalism' which was developed by Ablowitz et al. [6] will now be detailed further.
They started by considering the eigenvalue problem,

$$\begin{aligned} v_{1x} + i\zeta v_1 &= q(x,t)v_2, \\ v_{2x} - i\zeta v_2 &= r(x,t)v_1, \end{aligned} \tag{2-1}$$

on the interval $-\infty < x < \infty$, where the parameter ζ plays the role of the eigenvalue, the potentials $q(x,t)$ and $r(x,t)$ are the solutions of a coupled pair of special nonlinear evolution equations and $v(\zeta,x,t) \in \mathbb{C}$ are the eigenfunctions. The subscript 1 in v_1 corresponds to first of the two terms in the eigenfunction while subscript x in v_x means the partial derivative of v with respect to x. The eigenvalues and eigenfunctions evolve with time as the potentials evolve according to some evolution equation.
Eq. (2-1) is known as an eigenvalue problem because the eigenvalues of the system of equations are constants over all space x and for all time t if $q(x,t)$ and $r(x,t)$, are the complex valued solutions of a coupled pair of nonlinear evolution equations. This scattering problem was first mentioned by Zakharov and Shabat [9]. The terms scattering problem and eigenvalue problem will be used interchangeably throughout this report. The eigenvalue problem Eq. (2-1) when combined with equations describing the time dependence of $v(\zeta,x,t)$, results in the nonlinear evolution equations. The time dependence of $v_1(x,t)$ and $v_2(x,t)$ is chosen to be,

$$\begin{aligned} v_{1t} &= A(x,t,\zeta)v_1 + B(x,t,\zeta)v_2, \\ v_{2t} &= C(x,t,\zeta)v_1 + D(x,t,\zeta)v_2, \end{aligned} \tag{2-2}$$

where different functions $A(x,t,\zeta), B(x,t,\zeta), C(x,t,\zeta)$ and $D(x,t,\zeta)$ result in different coupled nonlinear differential equations.
Eq. (2-2) and Eq. (2-1) can be written for a more general case as,

$$\begin{aligned} v_x &= Xv, \\ v_t &= Tv, \end{aligned} \tag{2-3}$$

where $v \in \mathbb{C}^n$ and $X, T \in \{\mathbb{C}^n \text{ x } \mathbb{C}^n\}$. By cross-differentiating X and T, and equating the results we get

$$X_t - T_x + [X,T] = 0, \tag{2-4}$$

where $[X,T]$ is the commutator bracket $[X,T] = XT - TX$. Eq. (2-4) is also known as the zero-curvature condition or compatibility condition.
For the scattering problem Eq. (2-1) to be meaningful, the eigenvalues of X, ζ should be constant i.e. $\zeta_t = 0$ (spectrum should be time invariant). Applying compatibility condition Eq. (2-4) to Eq. (2-1) and Eq. (2-2), and taking $\zeta_t = 0$ gives

$$D = -A + d(t).$$

Without loss of generality $d(t) \equiv 0$, then for $A(x,t,\zeta), B(x,t,\zeta)$ and $C(x,t,\zeta)$ (p.257 of [6]),

$$\begin{aligned} A_x &= qC - rB, \\ B_x + 2i\zeta B &= q_t - 2Aq, \\ C_x - 2i\zeta C &= r_t + 2Ar. \end{aligned} \tag{2-5}$$

The set of Eq. (2-5) can be solved for A, B and C which will ensure that Eq. (2-2) and Eq. (2-1) are compatible. Solving for A, B and C results in the evolution equation. Eq. (2-1) is used to find the discrete eigenvalues (which are time invariant). The asymptotic behaviour of all eigenfunctions $v(x, 0, \zeta)$ at the initial time can be found as it is known that the solutions $q(x,t), r(x,t) \to 0$ sufficiently rapidly as $|x| \to \infty$. The sufficient rate of decay of the potentials can be found on p.268 of [6].
To find simple solutions which are still representative of a very broad variety of evolution equations, the functions are chosen as

$$A = \sum_{0}^{N} A^{(n)} \zeta^n, \quad B = \sum_{0}^{N} B^{(n)} \zeta^n, \quad C = \sum_{0}^{N} C^{(n)} \zeta^n. \tag{2-6}$$

It is found (p.257 of [6]) that $A^{(N)} = a_N$ and $B^{(N)} = C^{(N)} = 0$, where a_N is a constant which is independent of x but can depend on t. Now Eq. (2-5) can be used to compute rest of the coefficients. As a special case,

$$a_0 = a_1 = a_3 = 0, a_2 = -2i,$$

leads to the nonlinear Schrödinger equation,

$$r = -q^*, q_t - iq_{xx} - 2iq^2 q^* = 0. \tag{2-7}$$

In Section 3 of their paper [6], they show how a broader class of equations can be derived and how each is related to its linearized dispersion relation. The AKNS formalism provides a systematic method for arriving at evolutions equations which can be solved using inverse scattering transform.

2-1-2 Computing Scattering Data

The rest of the report will focus on the nonlinear Schrödinger equation but similar steps can be applied to other nonlinear evolution equations as well. In the previous section it was shown how the scattering problem Eq. (1-16) is related to the nonlinear Schrödinger equation Eq. (2-7). So the next step is to compute the scattering data given the initial ($t = 0$) potentials $q(\zeta, x, 0)$ and $r(\zeta, x, 0)$.
If $v(\zeta_1, x, t)$ and $w(\zeta_2, x, t)$ are eigenfunctions of the system Eq. (2-1) then by substitution and some simplification gives,

$$\frac{d}{dx}(v_1 w_2 - w_1 v_2) + i(\zeta_1 - \zeta_2)(v_1 w_2 + v_2 w_1) = 0. \tag{2-8}$$

Also if v is an eigenfunction of the system at $\zeta_1 = \xi_1 + i\eta_1$, let the adjoint of v be defined as

$$\bar{v} = \begin{bmatrix} v_2^* \\ -v_1^* \end{bmatrix}. \tag{2-9}$$

The adjoint $\bar{v}$ satisfies the system Eq. (1-16) at $\zeta_2 = \zeta_1^* = \xi_1 - i\eta_1$.
Assuming $q(x,t)$ and $r(x,t) \to 0$ sufficiently fast [6] as $|x| \to \infty$ in Eq. (2-7), the eigenfunctions

$(v(\zeta, x, t))$ of Eq. (2-1) are chosen to have the asymptotic forms (p.260 in [6]),

$$\begin{aligned} \phi &\to \begin{pmatrix} 1 \\ 0 \end{pmatrix} e^{-i\zeta x} \quad x \to -\infty, \\ \bar{\phi} &\to \begin{pmatrix} 0 \\ -1 \end{pmatrix} e^{i\zeta x} \quad x \to -\infty, \\ \psi &\to \begin{pmatrix} 0 \\ 1 \end{pmatrix} e^{i\zeta x} \quad x \to +\infty, \\ \bar{\psi} &\to \begin{pmatrix} 1 \\ 0 \end{pmatrix} e^{-i\zeta x} \quad x \to +\infty, \end{aligned} \tag{2-10}$$

where $v(\zeta, x, t) = \psi(\zeta, t)$ and $v(\zeta, x, t) = \phi(\zeta, t)$ are known as Jost functions.
Two vectors or functions are linearly independent if their Wronskian is non-zero. The Wronskian for two dimensional vectors f and g is defined as,

$$W(f, g) = f_1 g_2 - g_1 f_2.$$

Applying the Wronskian to Jost functions in Eq. (2-10),

$$W(\psi, \bar{\psi}) = -1, \qquad W(\phi, \bar{\phi}) = -1. \tag{2-11}$$

Hence the Jost function $\psi(t)$ and its adjoint $\bar{\psi}(t)$, and the pair $\psi(t)$, $\bar{\psi}(t)$ are linearly independent vectors. However, Eq. (2-1) is a two-dimensional system and hence can have a maximum of two independent eigenfunctions. Therefore $(\psi(t),\bar{\psi}(t))$ are arbitrarily chosen to form the basis. Hence ϕ and $\bar{\phi}$ can be expressed as a linear combination of ψ and $\bar{\psi}$. These can be expressed as,

$$\begin{aligned} \phi = a\bar{\psi} + b\psi &\to \begin{pmatrix} ae^{-i\zeta x} \\ be^{i\zeta x} \end{pmatrix} \quad x \to +\infty, \\ \bar{\phi} = \bar{b}\bar{\psi} - \bar{a}\psi &\to \begin{pmatrix} \bar{b}e^{-i\zeta x} \\ -\bar{a}e^{i\zeta x} \end{pmatrix} \quad x \to +\infty. \end{aligned} \tag{2-12}$$

The coefficients $a(\zeta, t), b(\zeta, t), \bar{a}(\zeta, t)$ and $\bar{b}(\zeta, t)$ are complex valued functions. They are given by the Wronskian relations,

$$\begin{aligned} a &= W(\phi, \psi), \\ b &= -W(\phi, \bar{\psi}), \\ \bar{a} &= W(\bar{\phi}, \bar{\psi}), \\ \bar{b} &= W(\bar{\phi}, \psi). \end{aligned} \tag{2-13}$$

Applying Eq. (2-8) to ϕ and $\bar{\phi}$ gives

$$|a(\xi)|^2 + |b(\xi)|^2 = 1. \tag{2-14}$$

For sufficiently fast decaying potentials, the Jost functions ϕ and ψ are analytical in the upper half-plane [6] and from Eq. (2-8)

$$a(\zeta) = (\phi_1 \psi_2 - \phi_2 \psi_1)(x, \zeta). \tag{2-15}$$

Hence $a(\zeta)$ is also analytical in the upper half-plane. It is now possible to see that,

$$a(\zeta) \to 1 \quad as \quad |\zeta| \to \infty, \quad \text{Im } \zeta \geq 0. \tag{2-16}$$

In general $b(\zeta,t), \bar{b}(\zeta,t)$ are defined only on the real axis but if $q(x,t)$ and $r(x,t)$ have sufficient decay as $x \to \pm\infty$, the regions of analyticity can be extended (p.268 [6]).
The points $\zeta = \zeta_j$, j=1,...N, with $\text{Im}(\zeta) > 0$, in the upper half-plane where $a(\zeta) = 0$, correspond to the eigenvalues of the system. At these points,

$$\phi(x,\zeta_j) = b_j \psi(x,\zeta_j), \qquad j = 1,...,N. \tag{2-17}$$

where b_j will be termed as the norming constants throughout this report. However, it was found that some authors use different term for the same quantity. For real $q(x,t)$

$$\phi(x,-\xi) = \phi^*(x,\xi), \qquad \psi(x,-\xi) = \psi^*(x,\xi), \tag{2-18}$$

and consequently

$$a(\xi) = a^*(-\xi).$$

Continuing this in the upper half-plane,

$$a(\zeta) = a^*(-\zeta^*).$$

Hence the zeros of $a(\zeta)$ lie on the imaginary axis for real $q(x,t)$ [6]. It can be shown (p.63 [9]) that $a(\zeta)$ does not depend on time and

$$b(\zeta,t) = b(\zeta,0)e^{4i\zeta^2 t}, \qquad b_j(t) = b_j(0)e^{4i\zeta_j^2 t}. \tag{2-19}$$

Thus by associating the NSE with the eigenvalue problem Eq. (2-1) it is possible to reduce the evolution in time to just a phase change in the nonlinear Fourier domain.

2-2 Inverse Nonlinear Fourier Transform

The inverse NFT addresses the problem of reconstructing the potential $q(x,t)$ from the nonlinear Fourier spectrum. As the evolution of the nonlinear Fourier spectrum with time is known, it suffices to be able to reconstruct the potential $q(x)$ at a particular time instant. For the NSE equation, this was shown by Zakharov and Shabat (p.63 of [9]) but, a general method for a class of integrable evolution equations was given by Ablowitz et al. (p. 271 of [6]). The details of this method will not be mentioned here.

Another method of solution was developed by Hirota [10] where he assumed the solution to be formed by the interactions between several decaying plane waves. This method gives more insight into the physical meaning of the solution but is not numerically efficient (p.9 in [11]).

Neugebauer and Meinel [12] gave a systematic procedure to obtain the auto-Bäcklund transform for the AKNS class of equations and used it to compute the multi-soliton solutions. Lin [13] showed the evolution of scattering data under the classical Darboux transform and his work will be briefly mentioned here. The Darboux transform for integrable system has been explained in detail by Gu et al. in their book [3].

2-2-1 Brief Introduction to Bäcklund Transformations

Bäcklund transforms or Bäcklund transformations (named after the Swedish mathematician Albert Victor Bäcklund) relate partial differential equations and their solutions. A Bäcklund transform is typically a system of first order partial differential equations relating two functions, and often depending on an additional parameter [14].
A Bäcklund transform which relates solutions of the same equation is called an invariant Bäcklund transform or auto-Bäcklund transform. There is no systematic way of finding Bäcklund transforms in general, but there is a systematic way of finding auto-Bäcklund transforms for special classes of systems. The Darboux transform is a auto-Bäcklund transform with the classical Darboux transform being the most convenient form.

2-2-2 Classical Darboux Transform

Lin [13] showed that the solutions of $su(2)$ systems can be related by classical Darboux transformation (CDT). A $su(2)$ system is of the form,

$$su(2) = \left\{ \begin{pmatrix} \alpha & -\beta^* \\ \beta & \alpha^* \end{pmatrix} : \alpha, \beta \in \mathbb{C}, |\alpha|^2 + |\beta|^2 = 1 \right\}. \tag{2-20}$$

The Zakharov and Shabat eigenvalue problem Eq. (1-16) belongs to this class of systems.
Let

$$\Phi = \begin{pmatrix} v_1(x,t,\zeta) & w_1(x,t,\zeta) \\ v_2(x,t,\zeta) & w_2(x,t,\zeta) \end{pmatrix}, \tag{2-21}$$

be the eigenfunctions of the $su(2)$ system at $\zeta = \zeta_0$ and $q(x,t) = q_0$. Let its norming constant be b_0. Then by defining

$$\beta(x,t,\zeta_0,b_0) = \frac{v_2(x,t,\zeta_0) + b_0 w_2(x,t,\zeta_0)}{v_1(x,t,\zeta_0) + b_0 w_1(x,t,\zeta_0)}, \tag{2-22}$$

the Darboux matrix is then given by

$$D = \begin{bmatrix} \zeta & 0 \\ 0 & \zeta \end{bmatrix} + \begin{bmatrix} \frac{-i(\zeta_0^*|\beta|^2+\zeta_0)}{(1+|\beta|^2)} & \frac{-i(\zeta_0^*-\zeta_0)\beta^*}{(1+|\beta|^2)} \\ \frac{-i(\zeta_0-\zeta_0^*)\beta}{(1+|\beta|^2)} & \frac{-i(\zeta_0^*+\zeta_0|\beta|^2)}{(1+|\beta|^2)} \end{bmatrix}. \tag{2-23}$$

It can be proved that $\Phi' = D\Phi$ satisfies the $su(2)$ system with

$$q = q_0 + \frac{2\beta_x}{(1+|\beta|^2)}. \tag{2-24}$$

The transformation from $\{q_0, \Phi\}$ to $\{q, \Phi'\}$ is then known as the CDT.
If q_0 was a solution of NSE with $1/a_0(\zeta)$ as reflection coefficient, then,

- If ζ_0 is not a zero of $a_0(\zeta)$, the eigenvalue gets appended to solution.

$$a_1(\zeta) = \frac{(\zeta - \zeta_0)}{(\zeta - \zeta_0^*)} a_0(\zeta). \tag{2-25}$$

- If ζ_0 is a zero of $a_0(\zeta)$, the eigenvalue gets erased from the solution. The following change is seen to the scattering data.

$$a_1(\zeta) = \frac{(\zeta - \zeta_0^*)}{(\zeta - \zeta_0)} a_0(\zeta). \tag{2-26}$$

Let

$$\Phi_0 = \begin{pmatrix} e^{-i\zeta x} & 0 \\ 0 & e^{i\zeta x} \end{pmatrix}, \tag{2-27}$$

which satisfies the system Eq. (1-16) for $q = 0$ which is a trivial solution of the NSE. Hence by taking Φ_0 as the fundamental solution (also known as seed or vacuum solution), we can obtain several new solutions by successive application of CDT. All such solutions will be pure multi-solitons.
The number of eigenvalues added by a Darboux transformation is known as the degree of the Darboux transformation. The classical Darboux transform has degree one. The Darboux transformation has the important property of permutability (Theorem 1.13, p.29 in [3]). This means that not only a r degree Darboux transformation can be performed as r successive degree one Darboux transformations, the order of those r transformations is not fixed. This can be expressed by the diagram in Figure 2-1. It shows that starting from (P, Φ), both paths lead to the same solution.

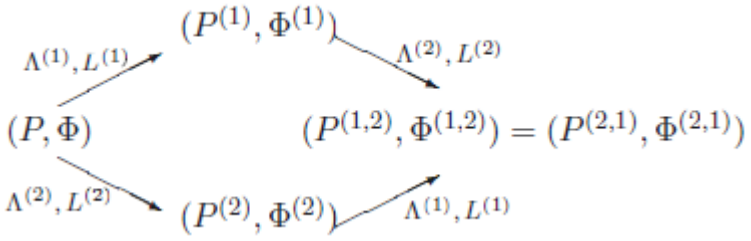

Figure 2-1: Permutability expressed as a Bianchi diagram, taken from p.29 of [3]

The CDT as described in [13] is not efficient for numerical implementation. Exploiting properties of norming constants allows for faster implementations such as Algorithm 2 in [15]. Permutability of CDT allows the addition of the eigenvalues in any order but the round-off errors can be minimized if the eigenvalues are added in the decreasing order of the magnitude of their imaginary parts [16]. Combining this idea with Algorithm 2 in [15] leads to a very fast and well-conditioned implementation of CDT.

Summary

Relating the NSE with the Zakharov-Shabat eigenvalue problem allows for systematic computation of the scattering data. It also reduces evolution of scattering data in time to a simple phase change. Inverse NFT can then be used to obtain the potential from the scattering data. The CDT is a special form of inverse NFT which is well suited for computing multi-soliton potentials. The ideas mentioned for continuous time NFT in this chapter can be extended to certain discrete evolution equations. This will be explored in detail in Chapter 3.

Chapter 3

Discrete Nonlinear Fourier transform

It is remarkable that the ideas developed in the preceding chapter also apply to certain types of discrete evolution equations. Flaschka [17] showed that the Toda lattice equation is related to a discretized Schrödinger eigenvalue problem. By employing inverse scattering analysis similar to that of Case and Kac [18] and Kac [19], he was able to solve the equation. Similar results were found by Manakov [20]. Motivated by these results, Ablowitz and Ladik [21] proposed a generalization for a discretized version of the eigenvalue problem of Zakharov and Shabat [9], as a basis for generating solvable discrete equations. Ablowitz and Ladik [8] later showed that starting from the same eigenvalue problem, a larger class of discrete evolution equations can be derived. Such a discrete eigenvalue problem not only helps solve discrete evolution equations, but also helps in formulating nonlinear Fourier transform algorithms which may be better suited for numerical implementation. In this chapter the work of Ablowitz and Ladik is mentioned briefly and then some other discretizations of the eigenvalue problem are derived. Some of the fast algorithms available in literature that utilize these discretizations for generating multi-solitons are discussed. Finally, the discrete Darboux transform is introduced.

3-1 Discretization of Eigenvalue Problem

The procedures mentioned in [21] and [8] will be paraphrased in this section.
A general linear differential-difference equation is given by,

$$U_{n_t} = -i\omega(E)U_n, \tag{3-1}$$

where E is the shift operator, $EU_n = U_{n+1}$. The dispersion relation in the discrete domain is given by $\omega(E)$. Eq. (3-1) is the discretized version of Eq. (1-13). The equation is discretized with respect to x alone and hence is known as a differential-difference equation. Taking $\omega(E) = (E + E^{-1} - 2)$ makes Eq. (3-1) equivalent to

$$iU_{n_t} = U_{n+1} + U_{n-1} - 2U_n. \tag{3-2}$$

This represents the linear part of the discrete nonlinear Schrödinger equation. As was shown in Chapter 2, the dispersion relation of the associated linearized problem plays a crucial role in deriving specific evolution equation.
To arrive at the discrete NSE we start with a scattering problem in the discrete domain:

$$\begin{aligned} V_{1_{n+1}} &= zV_{1_n} + Q_n(t)V_{2_n} + S_n(t)V_{2_{n+1}}, \\ V_{2_{n+1}} &= (1/z)V_{2_n} + R_n(t)V_{1_n} + T_n(t)V_{1_{n+1}}, \end{aligned} \tag{3-3}$$

where Q_n, R_n, S_n and T_n are the real or complex valued discrete potentials, $z \in \mathbb{C}$ is the eigenvalue in discrete domain and $V_n \in \mathbb{C}^2$ are the discrete eigenfunctions. The discrete step-size h is defined as $(x_{n+1} - x_n = h)$. The discrete eigenvalue z is defined as $z = e^{-i\zeta h}$. Taking the first order approximation, $z \sim 1 - i\zeta h$. The discrete potentials are given by $Q_n = q_n h, R_n = r_n h, S_n = s_n h$ and $T_n = t_n h$. The detailed derivation of the discrete eigenvalue problem Eq. (3-3) can be found on p.117 of [22]. The terms in Eq. (3-3) are hence analogous to the terms in Eq. (2-1).
The associated time dependence of the eigenfunction is given by,

$$\begin{aligned} V_{1_{n_t}} &= A_n V_{1_n} + B_n V_{2_n}, \\ V_{2_{n_t}} &= C_n V_{1_n} + D_n V_{2_n}. \end{aligned} \tag{3-4}$$

The integrability condition (also known as zero-curvature condition) is then given by $E(U_{n_t}) = (E(U_n))_t$ which corresponds to a specific nonlinear evolution equation for a certain set of functions $A_n, \ldots, D_n$ (depending in general on discrete potentials Q_n, R_n, S_n, T_n) with $\partial z/\partial t = 0$. Typically, the differential-difference nonlinear Schrödinger equation is given by (Eq. 1.7 in [8])

$$iU_{n_t} = U_{n+1} + U_{n-1} - 2U_n \pm U_n^* U_n (U_{n+1} + U_{n-1}) \tag{3-5}$$

where U_n^* is the complex conjugate of U_n.
To arrive at Eq. (3-5) it is sufficient to start with the simpler case $S_n = T_n = 0$ [8] and setting $(\partial/\partial t)(EV_{i_n}) = E(V_{i_{n_t}}), i = 1, 2$ in Eq. (3-3) and Eq. (3-4) leads to,

$$\begin{aligned} &z\Delta_n A_n + R_n B_{n+1} - Q_n C_n = 0, \\ &1/zB_{n+1} - zB_n + Q_n(A_{n+1} - D_n) = Q_{n_t}, \\ &zC_{n+1} - 1/zC_n - R_n(A_n - D_{n+1}) = R_{n_t}, \\ &1/z\Delta_n D_n + Q_n C_{n+1} - R_n B_n = 0, \end{aligned} \tag{3-6}$$

where $\Delta_n A_n = A_{n+1} - A_n$ etc. It can be shown that for sufficiently fast decaying potentials $Q_n, R_n, S_n, T_n \to 0$ as $|n| \to \infty$, $\lim_{n\to\infty}(A_n - D_n) = -i\omega(z^2)$ (Sec. 3 in [8]). The linearised version Eq. (3-2) of the nonlinear Schrödinger equation Eq. (3-5) has the dispersion relation $\omega(z^2) = z^2 + 1/z^2 - 2$. This is achieved by the following finite expansions in z for $A_n, \ldots, D_n$ [8].

$$\begin{aligned} A_n = A_n^{(2)} z^2 + A_n^{(0)}, \quad B_n = B_n^{(1)} z + B_n^{(-1)}/z, \\ C_n = C_n^{(1)} z + C_n^{(-1)}/z, \quad D_n = D_n^{(0)} + D_n^{(-2)}/z^2. \end{aligned} \tag{3-7}$$

Substituting these expansions into Eq. (3-6) and solving for the coefficients reveals that $\Delta_n A_n^{(-2)} = \Delta_n D_n^{(-2)} = 0$, $A_n^{(2)} = A_-^{(2)} = const$ and $D_n^{(-2)} = D_-^{(-2)} = const$. Solving further shows that,

$$\begin{aligned} A_n^{(0)} &= -R_{n-1} Q_n A_-^{(2)} + A_-^{(0)}, \\ D_n^{(0)} &= -Q_{n-1} R_n D_-^{(2)} + D_-^{(0)}. \end{aligned} \tag{3-8}$$

Then Q_n, R_n satisfy (p.1013 in [8])

$$\begin{aligned} R_{n_t} &= (1 - R_n Q_n)(R_{n+1} D_-^{(-2)} - R_{n-1} A_-^{(2)}) - R_n (A_-^{(0)} - D_-^{(0)}), \\ Q_{n_t} &= (1 - R_n Q_n)(Q_{n+1} A_-^{(2)} - Q_{n-1} D_-^{(-2)}) + Q_n (A_-^{(0)} - D_-^{(0)}). \end{aligned} \tag{3-9}$$

The solutions for $A_n, \ldots, D_n$ are summarized below

$$\begin{aligned} A_n &= A_-^{(2)}(z^2 - R_{n-1}Q_n) + A_-^{(0)}, \\ B_n &= A_-^{(2)} Q_n z + D_-^{(-2)} Q_{n-1} \frac{1}{z}, \\ C_n &= A_-^{(2)} R_{n-1} z + D_-^{(-2)} R_n \frac{1}{z}, \\ D_n &= D_-^{(0)} + D_-^{(-2)} \left(\frac{1}{z^2} - Q_{n-1} R_n \right). \end{aligned} \tag{3-10}$$

The nonlinear Schrödinger equation is obtained by taking $A_-^{(2)} = D_-^{(-2)*} = -i$, $A_-^{(0)} = D_-^{(0)*} = i$ and requiring that $R_n = \mp Q_n^*$. Then the coupled system Eq. (3-10) are mutually consistent leading to,

$$iQ_{n_t} = Q_{n+1} + Q_{n-1} - 2Q_n \pm Q_n Q_n^* (Q_{n+1} + Q_{n-1}), \tag{3-11}$$

which is the same as Eq. (3-5).
As mentioned earlier,

$$\lim_{n\to\infty} (A_n - D_n) = -i(z^2 + 1/z^2 - 2) = -i\omega(z^2). \tag{3-12}$$

Another choice of finite expansions in z for $A_n, \ldots, D_n$ can be found on p.599 of [21].

$$\begin{aligned} A_n &= A_n^{(1)} z + A_n^{(0)}, \quad B_n = B_n^{(0)} + B_n^{(-1)}/z, \\ C_n &= C_n^{(1)} z + C_n^{(0)}, \quad D_n = D_n^{(0)} + D_n^{(-1)}/z. \end{aligned} \tag{3-13}$$

Solving for $A_n, \ldots, D_n$ for a more general case of Eq. (3-6) results in,

$$\begin{aligned} A_n &= A_-^{(1)} z - T_{n-1} Q_n A_-^{(1)} - \sum_{-\infty}^{n-1} \frac{\Lambda_{Kt}}{\Lambda_K} + A_-^{(0)}, \\ B_n &= Q_n A_-^{(1)} + S_{n-1} D_-^{(-1)}/z, \\ C_n &= T_{n-1} A_-^{(1)} z + R_n D_-^{(-1)}, \\ D_n &= -R_n S_{n-1} D_-^{(-1)} - \sum_{-\infty}^{n-1} \frac{\Lambda_{Kt}}{\Lambda_K} + D_-^{(0)} + D_-^{(-1)}/z, \end{aligned} \tag{3-14}$$

where $\Lambda_n \equiv 1 - S_n T_n$. The time evolution of the potentials are then given by

$$\begin{aligned} R_{nt} &= (1 - R_n Q_n)(T_n D_-^{(-1)} - T_{n-1} A_-^{(-1)}), \\ S_{nt} &= (1 - S_n T_n)(Q_{n+1} A_-^{(1)} - Q_n D_-^{(-1)}), \\ Q_{nt} &= (1 - R_n Q_n)(S_n A_-^{(1)} - S_{n-1} D_-^{(-1)}), \\ T_{nt} &= (1 - S_n T_n)(R_{n+1} D_-^{(-1)} - R_n A_-^{(1)}), \end{aligned} \tag{3-15}$$

where $A_-^{(1)}, A_-^{(0)}, D_-^{(-1)}, D_-^{(0)}$ are all constants obtained as $n \to -\infty$. For convenience $A_-^{(0)} = D_-^{(0)}$ is chosen. Letting $R_n = \mp Q_n^*$, $S_n = \mp T_n^*$ and $D_-^{(-1)} = -A_-^{(1)} = i$ the above evolution equations Eq. (3-15) reduce to

$$\begin{aligned} R_{n_t} &= i(1 \pm R_n R_n^*)(\mp S_n^* \mp S_{n-1}^*), \\ S_{n_t} &= i(1 \pm S_n S_n^*)(\pm R_{n+1}^* \pm R_n^*). \end{aligned} \tag{3-16}$$

This is known as a discretized “second order in time nonlinear Schrödinger equation" [21].

3-1-1 Scattering Data in Discrete Domain

It is interesting to look at the scattering data and its time evolution for the discrete eigenvalue problem Eq. (3-3). The procedure is very similar to the one mentioned for continuous domain. Assuming that Q_n, S_n, R_n and T_n vanish sufficiently rapidly as $|n| \to \infty$. The asymptotic eigenfunctions of Eq. (3-3) are chosen to have the forms,

$$\begin{aligned} \phi_n &\sim \begin{pmatrix} 1 \\ 0 \end{pmatrix} z^n, \\ \bar{\phi}_n &\sim \begin{pmatrix} 0 \\ -1 \end{pmatrix} z^{-n}, \quad \text{as } n \to -\infty \\ \psi_n &\sim \begin{pmatrix} 0 \\ 1 \end{pmatrix} z^{-n}, \\ \bar{\psi}_n &\sim \begin{pmatrix} 1 \\ 0 \end{pmatrix} z^n, \quad \text{as } n \to +\infty. \end{aligned} \tag{3-17}$$

These are the Jost solutions equivalent to Eq. (2-10). For appropriately decaying potentials, $z^{-n}\phi, z^n\psi$ are analytic for $|z| > 1$, and $z^n\bar{\phi}, z^{-n}\bar{\psi}$ are analytic for $|z| < 1$. ϕ and ψ are the asymptotic forms of the eigenfunction v of Eq. (3-3) at z,

$$v = \begin{pmatrix} v_{1_n} \\ v_{2_n} \end{pmatrix}. \tag{3-18}$$

Therefore, when $Q_n = \mp R_n^*, T_n = \mp S_n^*$, the adjoint

$$\bar{v} = \begin{pmatrix} v_{2_n}^* \\ \mp v_{1_n}^* \end{pmatrix}, \tag{3-19}$$

is a solution at $z = 1/z^*$.
The Wronskian relation obeys the equation

$$W_{n+1} = \frac{1 - R_n Q_n}{1 - S_n T_n} W_n, \tag{3-20}$$

where $W_n(w, v) = (w_{1_n} v_{2_n} - w_{2_n} v_{1_n})$. This on the unit circle gives (p.600 in [21]),

$$\begin{aligned} W_n(\bar{\psi}, \psi) &= \prod_{n}^{\infty} \frac{1 - S_i T_i}{1 - R_i Q_i}, \\ W_n(\bar{\phi}, \phi) &= \prod_{-\infty}^{n-1} \frac{1 - R_i Q_i}{1 - S_i T_i}. \end{aligned} \tag{3-21}$$

For $T_i = -S_i^*, Q_i = -R_i^*$, Eq. (3-21) are positive definite hence $\{\bar{\psi}, \psi\}, \{\bar{\phi}, \phi\}$ are, respectively, linearly independent. Hence on the unit circle, using notation as used in [23],

$$\begin{aligned} \bar{\phi}_n(z,t) &= -\bar{a}^D(z,t)\psi_n + \bar{b}^D(z,t)\bar{\psi}_n, \\ \phi_n(z,t) &= a^D(z,t)\bar{\psi}_n + b^D(z,t)\psi_n, \end{aligned} \tag{3-22}$$

where $a^D, b^D, \bar{a}^D$ and $\bar{b}^D$ depend parametrically on time through the potentials. Substituting these in Eq. (3-21), on the unit circle,

$$a^D\bar{a}^D + b^D\bar{b}^D = \prod_{-\infty}^{n-1} \frac{1 - R_iQ_i}{1 - S_iT_i}, \tag{3-23}$$

and in the special case of $T_i = -S_i^*, Q_i = -R_i^*$

$$|a^D|^2 + |b^D|^2 = \prod_{-\infty}^{\infty} \frac{1 + |R_i|^2}{1 + |S_i|^2}, \tag{3-24}$$

since $\bar{a}^D = a^{D*}, \bar{b}^D = b^{D*}$.
Assuming that $\bar{a}^D(z)$ and $a^D(z)$ have finite number of simple zeros (z_k) inside and outside the unit circle, respectively [i.e., $|\bar{z}_k| < 1, \bar{a}^D(\bar{z}_k) = 0$ and $|z_k| > 1, a^D(z_k) = 0$], at these zeros,

$$\begin{aligned} \bar{\phi}_n(\bar{z}_k) &= \bar{b}_k^D\bar{\psi}_n(\bar{z}_k) \equiv \bar{b}_k^D\bar{\psi}_{n,k} = \bar{\phi}_{n,k}, \\ \phi_n(z_k) &= b_k^D\psi_n(z_k) \equiv b_k^D\psi_{n,k} = \phi_{n,k}, \end{aligned} \tag{3-25}$$

where $\bar{z}_k = 1/z_k^*$, $\bar{b}_k = b_k^{D*}$.
The time dependence of the scattering coefficients for the dispersion relation $\omega(z^2) = z^2 + 1/z^2 - 2$ is given by (p.222 in [23]),

$$\begin{aligned} \bar{a}^D(t) &= \bar{a}_0^D, \\ \bar{b}^D(t) &= \bar{b}_0^D \exp\left(i\frac{(z^2 + 1/z^2 - 2)t}{\Delta x^2}\right), \\ \bar{b}_k^D &= \bar{b}_{k,0}^D \exp\left(i\frac{(\bar{z}_k^2 + 1/\bar{z}_k^2 - 2)t}{\Delta x^2}\right), \end{aligned} \tag{3-26}$$

where $\Delta x = h$ is the step-size.
The discrete eigenvalue problem Eq. (3-3) has scattering data analogous to the continuous eigenvalue problem. The similarities between the continuous and discrete scattering problems makes it interesting to look at other discretizations of the Zakharov-Shabat problem. The procedure followed by Vaibhav in [4] is mentioned here. For ease of reading, the derivation starts by compactly representing the Zakharov-Shabat Eq. (2-1) problem as

$$\begin{aligned} v_x &= -i\zeta\sigma_3 v + Uv, \\ v_t &= 2i\zeta^2\sigma_3 v + [-2\zeta U + i\sigma_3(U^2 - U_x)]v, \end{aligned} \tag{3-27}$$

where

$$U = \begin{pmatrix} 0 & q(x,t) \\ r(x,t) & 0 \end{pmatrix}, \quad r(x,t) = -q^*(x,t), \tag{3-28}$$

and

$$\sigma_3 = \begin{pmatrix} 1 & 0 \\ 0 & -1 \end{pmatrix}. \tag{3-29}$$

The spectral domain-approach will be used to obtain couple of other discrete scattering problems. The first step is to apply the transformation $\tilde{q} = e^{i\sigma_3\zeta x}v$ so that Eq. (3-27) becomes

$$\partial_x[e^{i\sigma_3\zeta x}v] = e^{i\sigma_3\zeta x}Ue^{-i\sigma_3\zeta x}[e^{i\sigma_3\zeta x}v], \tag{3-30}$$

or,

$$\begin{aligned} &\tilde{v}_x = \tilde{U}\tilde{v}, \\ &\tilde{U} = e^{i\sigma_3\zeta x}Ue^{-i\sigma_3\zeta x} = \begin{pmatrix} 0 & qe^{2i\zeta x} \\ re^{-2i\zeta x} & 0 \end{pmatrix}. \end{aligned} \tag{3-31}$$

The linear-step methods [24] can be applied to Eq. (3-31) to obtain a recurrence relation. The discretizations obtained are known as exponential integrators based on linear one-step methods. One of the advantages of Eq. (3-31) is that the "vacuum" solution obtained from the discrete problem is exact.

Trapezoidal scheme

For the discretization scheme, an equispaced grid is defined by $x_n = L_0 + nh$, $n = -N, -N+1, \ldots, N$, with $x_{-N} = L_1$, $x_N = L_2$ and L_0 is midpoint between L_1 and L_2. The grid spacing (step-size) is h and let $z = e^{i\zeta h}$. For the potential sampled on the grid, set $q_n = q(x_n, t)$, $r_n = r(x_n, t)$ where the time dependence is suppressed. Using the same convention, $U_n = U(x_n, t)$ and $\tilde{U}_n = \tilde{U}(x_n, t)$. The discretization of Eq. (3-31) using the trapezoidal rule gives

$$\begin{aligned} \tilde{V}_{n+1} &= \left(I - \frac{h}{2}\tilde{U}_{n+1}\right)^{-1}\left(I + \frac{h}{2}\tilde{U}_n\right)\tilde{V}_n \\ V_{n+1} &= \left(I - \frac{h}{2}U_{n+1}\right)^{-1} e^{-i\sigma_3\zeta h}\left(I + \frac{h}{2}U_n\right)V_n. \end{aligned} \tag{3-32}$$

Setting $2Q_n = hq_n, 2R_n = hr_n$ and $\Theta_n = 1 - Q_nR_n$, the discrete one step scheme can be stated as:

$$V_{n+1} = \frac{1}{\Theta_n}\begin{pmatrix} z^{-1} + zQ_{n+1}R_n & zQ_{n+1} + Q_nz^{-1} \\ R_{n+1}z^{-1} + zR_n & R_{n+1}Q_nz^{-1} + z \end{pmatrix} V_n. \tag{3-33}$$

Split-Magnus Integrator

Applying the Magnus method with one-point Gaussian quadrature ([25]-[26]) to the Zakharov-Shabat problem in Eq. (3-27),

$$V_{n+1} = e^{-i\zeta\sigma_3 h + U_{n+1/2}h}v_n \tag{3-34}$$

The exponential operator can be computed exactly as

$$e^{-i\zeta\sigma_3 h + U_{n+1/2}h} = \begin{pmatrix} \cosh(\Gamma) - \frac{i\zeta h}{\Gamma}sinh(\Gamma) & \frac{Q_{n+1/2}}{\Gamma}sinh(\Gamma) \\ \frac{R_{n+1/2}}{\Gamma}sinh(\Gamma) & \cosh(\Gamma) + \frac{i\zeta h}{\Gamma}sinh(\Gamma) \end{pmatrix}, \tag{3-35}$$

where $\Gamma = \sqrt{Q_{n+1/2}R_{n+1/2} - \zeta^2 h^2}$, $Q_{n+1/2} = hq(x_n + h/2, t)$ and $R_{n+1/2} = hr(x_n + h/2, t)$. This is the Magnus integrator with one-point Gauss quadrature. This method is also referred to as the exponential mid-point rule and has order two. It has been shown to be consistent and stable [4]. It retains the *su(2)* structure and is specially suited for highly oscillatory problems. It has been used by several authors to solve forward scattering problems[27],[28]. Applying Strang-type splitting [29] to the exponential,

$$e^{-i\zeta\sigma_3 h + U_{n+1/2}h} = e^{-i\zeta\sigma_3 h/2} e^{U_{n+1/2}h} e^{-i\zeta\sigma_3 h/2} + \mathcal{O}(h^3). \tag{3-36}$$

The order of the approximation is determined by applying the Baker-Campbell-Hausdroff (BCH) formula to the exponential operators ([30], Chapter 4). Setting $\Gamma = \sqrt{Q_{n+1/2}R_{n+1/2}}$,

$$\begin{aligned} e^{U_{n+1/2}h} &= \begin{pmatrix} \cosh(\Gamma) & Q_{n+1/2}\frac{sinh(\Gamma)}{\Gamma} \\ R_{n+1/2}\frac{sinh(\Gamma)}{\Gamma} & \cosh(\Gamma) \end{pmatrix} \\ &= \frac{1}{\sqrt{1 - tanh^2\Gamma}} \begin{pmatrix} 1 & Q_{n+1/2}\frac{tanh(\Gamma)}{\Gamma} \\ R_{n+1/2}\frac{tanh(\Gamma)}{\Gamma} & 1 \end{pmatrix} \\ &= \frac{1}{\sqrt{1 - \Gamma^2}} \begin{pmatrix} 1 & Q_{n+1/2} \\ R_{n+1/2} & 1 \end{pmatrix} + \mathcal{O}(h^3). \end{aligned} \tag{3-37}$$

Hence the discretization scheme works out to be

$$V_{n+1} = \frac{1}{\Theta_{n+1/2}^{1/2}} \begin{pmatrix} z^{-1} & Q_{n+1/2} \\ R_{n+1/2} & z \end{pmatrix} V_n, \tag{3-38}$$

where $\Theta_{n+1/2}^{1/2} = (1 - Q_{n+1/2}R_{n+1/2}) > 0$. The integration scheme obtained is referred to as the Split-Magnus (SM) method.

Properties of scattering data

The scattering data has two helpful properties. These are given more elaborately as Remark II.1 and II.2 in [4].

Conjugation and reflection

The inverse scattering problem for the right-sided profile can be transformed to that of a left-sided profile in the following way: putting $y = -x$, we have

$$\begin{aligned} v_y(-y;\zeta) &= i\zeta\sigma_3 v(-y;\zeta) - U(-y)v(-y;\zeta) \\ w_y &= -i\zeta\sigma_3 w + U^*(-y)w, \end{aligned} \tag{3-39}$$

where $w(y) = \sigma_1 v(-y;\zeta)$. The new system with the potential $U^*(-y)$ will have the same discrete eigenvalues but the norming constants change as $B_k = 1/b_k$. Therefore, an implementation for the case of left-sided profile is sufficient to solve problems of general nature encountered in forward and inverse NFT.

Translation

The whole potential can be translated on account of the translational properties of the discrete spectrum. Considering the transformation $x = y + x_0$ corresponding to translation of potential by x_0, the new potential $U(y + x_0)$ has the same discrete eigenvalues, however, the norming constants change as $B_k = b_k e^{-2i\zeta_k x_0}$.

Based on the discretizations of the eigenvalue problem, various algorithms for forward and inverse NFT have been published. Some methods are superior than others either in robustness or computational speed or both. Yousefi and Kschischang have consolidated some of the algorithms in [31] and [11]. In [31] they cover most of the standard forward NFT algorithms and in [11] they cover inverse NFT. In their paper [32], Wahls and Poor proposed fast NFTs and specifically discussed the NFT with respect to the NSE. They made use of the Ablowitz-Ladik dicretization but their approach has been adapted for other discretizations as well.
The inverse NFT involves two steps. First is the computation of the scattering coefficients from the nonlinear Fourier spectrum and the second step is the retrieval of the potential from the scattering coefficients. Layer peeling algorithm has been applied in various fields for inverting nonlinear spectrum. Brenne and Skaar [33] applied conventional layer peeling to the NSE. Wahls and Poor in [34] applied layer peeling specifically to the Ablowitz-Ladik discretization. They concluded that the layer peeling algorithm was the computational bottleneck and hence they proposed the fast layer peeling algorithm (Figure 3-1) in [35] based on the work of McClary [36]. Currently layer peeling is the most computationally efficient method for computing the potential from the scattering coefficients. In [35], Wahls and Poor, proposed and demonstrated a method to compute the discrete polynomial representation of the eigenfunctions directly from the nonlinear Fourier spectrum. Their approach is currently the fastest algorithm in literature for generating multi-solitons with a floating point operations complexity (FLOPS) of $\mathcal{O}(N \log^2 N)$ for N samples. However, their approach does not give precise control over the norming constants. Combining the advantages of CDT and layer-peeling, Vaibhav has proposed a new approach in [4]. For the case of multi-solitons, this algorithm has a FLOPS complexity of $\mathcal{O}(N(K + \log^2 N))$ for K eigenvalues and N samples. The CDT is a continuous algorithm while layer peeling is a discrete algorithm. This makes the calculation of the scattering coefficients the computational bottleneck. The discrete Darboux which is analogous to CDT was first studied with the hope that it will help circumvent the bottleneck. However, a slightly different approach was finally used to propose a new algorithm as will be seen in Chapter 4.

3-2 Discrete Darboux Transform

Ablowitz and Ladik and others before them showed that the inverse scattering problem for nonlinear differential-difference equations that can be derived using the scheme mentioned in Section 3-1, can be solved. The details for the same can be found under Section 3 in [8]. The current study is focused on the multi-soliton case and as shown in Section 2-2, the inverse problem for multi-solitons can be solved efficiently using the Darboux transform. Xianguo [37] in 1989 derived the Darboux transformation for the discrete Ablowitz-Ladik eigenvalue problem Eq. (3-3). The same is introduced in this section.

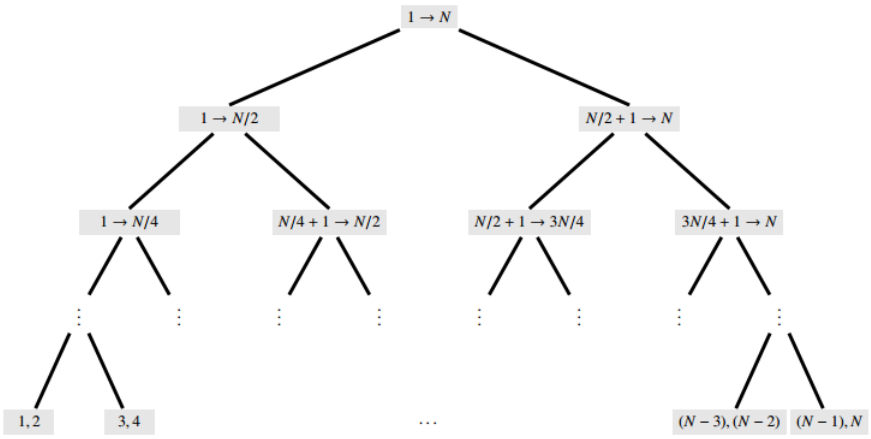

Figure 3-1: The figure shows the binary-tree structure obtained as a result of applying a divide-and-conquer strategy to the conventional layer-peeling method. The node label depicts the range of indices of the layers ordered from left to right in the computational domain, taken from p.72 of [4]

The eigenvalue problem Eq. (3-3) scaled by a factor $(1 - S_n T_n)$ can be compactly represented as,

$$V_{n+1} = L_n V_n, \quad L_n = \begin{bmatrix} z + R_n S_n & Q_n + z^{-1} S_n \\ R_n + z T_n & z^{-1} + Q_n T_n \end{bmatrix}. \tag{3-40}$$

The time dependence of the eigenfunction V_n is given by substituting Eq. (3-14) in Eq. (3-4) and can be written as,

$$V_{n_t} = N_n V_n, \quad N_n = \begin{bmatrix} A_-^{(1)} z - A_-^{(1)} T_{n-1} Q_n & A_-^{(1)} Q_n + D_-^{(-1)} z^{-1} S_{n-1} \\ A_-^{(1)} z T_{n-1} + D_-^{(-1)} R_n & D_-^{(-1)} z^{-1} - D_-^{(-1)} R_n S_{n-1} \end{bmatrix}. \tag{3-41}$$

The compatibility condition then gives the evolution equation,

$$L_{n_t} = N_{n+1} L_n - L_n N_n, \tag{3-42}$$

which is equivalent to equations Eq. (3-15). This becomes the discrete NSE Eq. (3-16) for

$$R_n = \mp Q_n^*, \quad S_n = \mp T_n^*, \quad D_-^{(-1)} = -A_-^{(1)} = i. \tag{3-43}$$

Let

$$V_n = \begin{bmatrix} v_{1_n} & w_{1_n} \\ v_{2_n} & w_{2_n} \end{bmatrix}, \tag{3-44}$$

be a fundamental matrix of solutions to Eq. (3-40). Then let the Darboux matrix in the discrete domain be M_n which gives the linear transformation $V_n \to V_n'$:

$$V_n' = M_n V_n, \quad M_n = \begin{bmatrix} A_n & B_n \\ C_n & D_n \end{bmatrix} = \begin{bmatrix} z^k + \sum_{j=-k}^{k-1} A_n^{(j)} z^j & \sum_{j=-k}^{k-1} B_n^{(j)} z^j \\ \sum_{j=-(k-1)}^{k} C_n^{(j)} z^j & z^{-k} + \sum_{j=-(k-1)}^{k} D_n^{(j)} z^j \end{bmatrix}. \tag{3-45}$$

The choice of structure of M_n is based on the eigenvalue problem Eq. (3-40). The ' indicates the terms after a Darboux update.

Let $z_i(z_i \neq z_j, i \neq j)$, $b_i(b_i \neq 0)(i = 1, 2, ..., 4k)$ be $8k$ parameters. Let $z_i(i = 1, 2, ..., 4k)$ be the roots of the $4k - th$ order polynomial $z^{2k}\mathbf{det}M_n$. Then at $z = z_i$, the columns vectors of V'_n will be linearly independent. Let its dependent coefficients be $b_i(i = 1, 2, ..., 4k)$, then from the definition Eq. (3-45),

$$\begin{aligned} \sum_{j=-k}^{k-1} (A_n^{(j)} + B_n^{(j)}\alpha_i^{-1}(n))z_i^j = -z_i^k, \\ \sum_{j=-(k-1)}^{k} (D_n^{(j)} + C_n^{(j)}\alpha_i(n))z_i^j = -z_i^{-k}, \end{aligned} \tag{3-46}$$

where

$$\alpha_i(n) = \frac{v_{1_n}(z_i) - b_i w_{1_n}(z_i)}{v_{2_n}(z_i) - b_i w_{2_n}(z_i)}. \tag{3-47}$$

The formulation of the discrete Darboux transform is very similar to the continuous case. The definition of α_i in the discrete domain is analogous to the definition of β in the continuous domain (Eq. (2-22)). For appropriately chosen $8k$ parameters and corresponding eigenfunctions V_n, the system of equations Eq. (3-46) has a solution which allows calculation of M_n. Suppose v'_n is any column of V'_n. Then from definition of the Darboux matrix,

$$v'_n = M_n v_n, \tag{3-48}$$

from which Eq. (3-40) is transformed into an eigenvalue problem of v'_n in the case $z \neq z_i$ as

$$v'_{n+1} = M_{n+1}L_n M_n^{-1} v'_n = L'_n v'_n, \tag{3-49}$$

where

$$L'_n = M_{n+1}L_n M_n^{-1}. \tag{3-50}$$

Requiring L'_n to have the same form as L_n

$$L'_n \triangleq M_{n+1}L_n M^{-1} = \begin{bmatrix} z + R'_n S'_n & Q'_n + z^{-1}S'_n \\ R'_n + zT'_n & z^{-1} + Q'_n T'_n \end{bmatrix}, \tag{3-51}$$

the transformation formulae from old potentials into new ones are then given by (Eq. 2.10 in [37]):

$$\begin{aligned} Q'_n = \frac{1}{D_n^{(k)}}Q_n - \frac{B_n^{(k-1)}}{D_n^{(k)}}, \quad R'_n = \frac{1}{A_n^{(-k)}}R_n - \frac{C_n^{(-k+1)}}{A_n^{(-k)}}, \\ S'_n = A_{n+1}^{(-k)}S_n + B_{n+1}^{(-k)}, \quad T'_n = D_{n+1}^{(k)}T_n + C_{n+1}^{(k)}. \end{aligned} \tag{3-52}$$

For the trivial solution $R_n = -Q_n^* = 0$ and $S_n = -T_n^* = 0$ of Eq. (3-40), the fundamental solution matrix can be chosen as:

$$V_n = \begin{bmatrix} z^n & 0 \\ 0 & -z^{-n} \end{bmatrix} \tag{3-53}$$

Again the analogy between the discrete and continuous domain is clear when comparing the seed solution Eq. (3-53) and Eq. (2-27). The discrete Darboux transform also displays the property of permutability. Hence starting from the seed solution Eq. (3-53), the multi-soliton solution can be obtained through repeated degree one discrete Darboux transforms.

Summary

In this chapter the NFT was extended to discrete evolution equations through association with the discrete eigenvalue problem. The procedure to arrive at various discrete evolution equations and scattering data in discrete domain was mentioned. Analogies were drawn at each step between the continuous and discrete time NFTs. Some of the current fast algorithms were mentioned and finally the discrete Darboux transform was introduced. In Chapter 4, the discrete Darboux transform will be extended to other discretizations and a new fast inverse NFT algorithm will be proposed.

Chapter 4

Discrete Darboux Evolution Algorithm (DDE)

The existence of exactly solvable discrete evolution equations is interesting in itself but the ease with which the continuous domain techniques extend to the discrete domain is fascinating. Although the discrete Darboux transform (DDT) discussed in Chapter 3 is very useful in finding multi-soliton solutions of discrete evolution equations, for the case of the NSE, it has no advantages over CDT. However a new approach for generating multi-solitons based on DDT will be proposed in this chapter.
In Section 4-1 the new approach is demonstrated first for the Ablowitz-Ladik discretization and then extended to other discretizations. Later, in Section 4-2 computational complexities of the algorithms are compared.

4-1 Derivation of DDE

To understand the motivation for the new approach, it helps to look again at the schematic representation of the classical Darboux transform shown in Figure 4-1. In CDT, at each sample point the computationally expensive Darboux transform is carried out with the only difference being the information regarding position of the sample. For K eigenvalues the FLOPS complexity at each sample point is $\mathcal{O}(K^2)$, which means the overall complexity is $\mathcal{O}(K^2N)$ for N sample points. Instead, if some transformation could be used to transform the Darboux matrix at some point x_n to the Darboux matrix at x_{n-1}, the potential can be computed more efficiently. Unfortunately such a transformation is not trivial in case of the continuous Darboux transform. Discretizing the eigenvalue problem helps in realizing such a transformation.
The discrete time NFT is defined using the discrete eigenvalue problem Eq. (3-40),

$$V_{n+1} = L_n V_n. \tag{4-1}$$

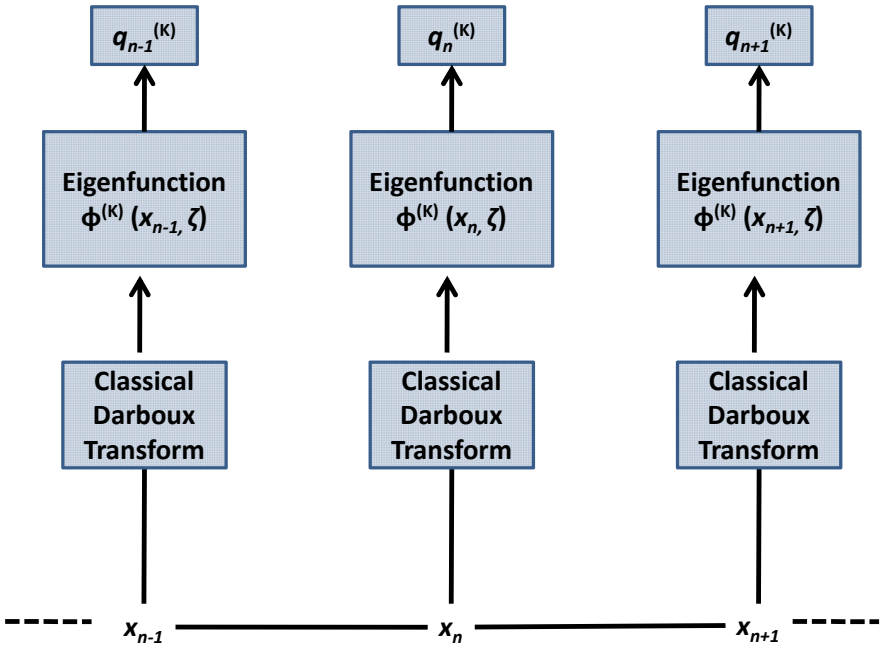

Figure 4-1: Schematic representation of CDT.

Again let M_n be the discrete Darboux matrix as defined in Eq. (3-45). Starting from the seed solution Eq. (3-53), after solving for the coefficients of M_n the eigenfunction can be updated (addition of eigenvalues) as

$$V'_n = M_n V_n. \tag{4-2}$$

Eq. (3-49) can be written as,

$$V'_{n+1} = M_{n+1} V_{n+1} = L'_n M_n V_n, \tag{4-3}$$

where L'_n is again required to have the same form as L_n,

$$L'_n = \begin{bmatrix} z + R'_n S'_n & Q'_n + z^{-1} S'_n \\ R'_n + z T'_n & z^{-1} + Q'_n T'_n \end{bmatrix}. \tag{4-4}$$

For the case of multi-solitons, the seed solution V_n at any point n is to be trivially known. Hence, if all the updated potentials Q'_n,R'_n,T'_n and S'_n can be computed from M_n alone, Eq. (4-3) can then be used to compute the Darboux matrix M_{n+1}. Such a procedure can then be repeated to compute the potential at all points to the right of the arbitrary starting point x_n. The complete algorithm will have three parts.

1. The discrete part of the continuous-time nonlinear Fourier spectrum is transformed according to the chosen discrete eigenvalue problem.
2. Discrete Darboux transform is used to compute the discrete eigenfunctions V'_n at one sample point.
3. The potential at all the sample points is computed by alternating between potential update and eigenfunction update.

The complete procedure can be schematically represented as shown in Figure 4-2. The details of the steps will be discussed in the following subsections. This procedure is based on the assumption that Q'_n,R'_n,T'_n and S'_n can be computed from M_n alone. This is not obvious from Eq. (3-52). To derive the update equations for the potential, substitute

$$M_{n+1} = \begin{bmatrix} A_{n+1} & B_{n+1} \\ C_{n+1} & D_{n+1} \end{bmatrix} = \begin{bmatrix} z^k + \sum_{j=-k}^{k-1} A_{n+1}^{(j)} z^j & \sum_{j=-k}^{k-1} B_{n+1}^{(j)} z^j \\ \sum_{j=-(k-1)}^{k} C_{n+1}^{(j)} z^j & z^{-k} + \sum_{j=-(k-1)}^{k} D_{n+1}^{(j)} z^j \end{bmatrix}, \tag{4-5}$$

in Eq. (4-3). Also substituting V_n and V_{n+1} from Eq. (3-53) in Eq. (4-3) gives

$$\begin{bmatrix} A_{n+1}z^{n+1} & -B_{n+1}z^{-(n+1)} \\ C_{n+1}z^{n+1} & -D_{n+1}z^{-(n+1)} \end{bmatrix} = \begin{bmatrix} z + R'_n S'_n & Q'_n + z^{-1}S'_n \\ R'_n + zT'_n & z^{-1} + Q'_n T'_n \end{bmatrix} \begin{bmatrix} A_n z^n & -B_n z^{-n} \\ C_n z^n & -D_n z^{-n} \end{bmatrix} \tag{4-6}$$

Solving the system of equations Eq. (4-6) for Q'_n, R'_n, S_n and T'_n, it is found that,

$$\begin{aligned} R'_n &= \frac{-C_n^{(-k+1)}}{A_n^{(-k)}}, \\ Q'_n &= -(R'_n)^*, \\ T'_n &= \frac{-C_n^{(-k+2)} - R'_n A_n^{(-k+1)}}{A_n^{(-k)} + Q'_n C_n^{(-k+1)}}, \\ S'_n &= -(T'_n)^*. \end{aligned} \tag{4-7}$$

and,

$$\begin{aligned} T'_n &= C_{n+1}^{(k)}, \\ S'_n &= -(T'_n)^*, \\ R'_n &= \frac{C_{n+1}^{(k-1)} - T'_n A_{n+1}^{(k-1)}}{1 - T'_{n-} S'_n}, \\ Q'_n &= -(R'_n)^*. \end{aligned} \tag{4-8}$$

Comparing Eq. (4-7) and Eq. (3-52) reveals that the update equation is the same for R'_n starting from null potential $R_n = 0$. In Eq. (4-7), T'_n depends only on the coefficients of M_n. Similarly comparing Eq. (4-8) and Eq. (3-52) reveals that the update equation is the same for T'_n starting from null potential $T_n = 0$. Again in Eq. (4-8), R'_n depends only on the coefficients of M_{n+1}. The Q'_n and S'_n terms can be easily computed due to symmetry (Eq. (3-43)) from R'_n and T'_n respectively.
The implication of these relations is that, starting at any sample point x_n, using Eq. (4-7)

the updated potentials at that point can be computed (Potential update). The updated eigenfunction V'_{n+1} at the next sample point x_{n+1}, can then be computed using the relation $V'_{n+1} = L'_n V'_n$ (Eigenfunction update). By alternating between the potential update and eigenfunction update, the potential can be computed at all grid points x_{n+1}, x_{n+2}, ... right of the starting point x_n. Similar to the forward case, starting from x_n, using Eq. (4-8) the updated potentials can be computed at the point x_{n-1} (Potential update). The relation $V'_{n-1} = L'^{-1}_{n-1} V'_n$, where L'^{-1}_{n-1} is the inverse of the matrix L'_{n-1}, then gives the updated eigenfunction V'_{n-1} (Eigenfunction update). The procedure can then be repeated to obtain the potential at all grid points x_{n-1}, x_{n-2}, ... left of the starting point x_n. The algorithm can be visualized as Figure 4-2.

Later, in Section 4-2, a complexity analysis will reveal that this scheme requires less FLOPS

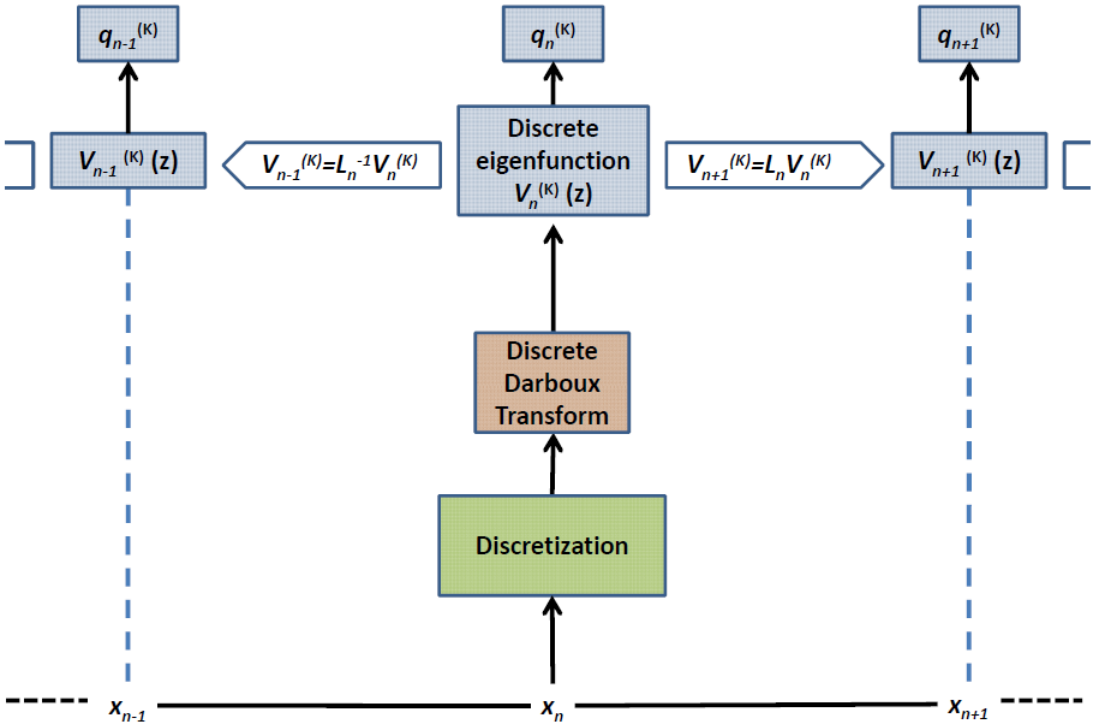

Figure 4-2: Schematic representation of proposed algorithm.

than classic Darboux. The lower complexity comes with a cost of slightly higher error which will be discussed in Chapter 5. The scheme shown in Figure 4-2 will be referred to as the discrete Darboux evolution (DDE) scheme from here on.

Other Discretizations

It is interesting to explore the approach further by applying it to the other discretizations mentioned in Section 3-1-1. The complete derivation is repeated for the case of the Split-Magnus discretization(SM) Eq. (3-38) for sake of clarity. The first step is to find the appropriate discrete Darboux matrix. Taking a hint from the structure used in [38], the discrete Darboux

matrix M_n of degree k is chosen to be

$$V_n' = M_n V_n, \quad M_n = \begin{bmatrix} A_n & B_n \\ C_n & D_n \end{bmatrix} = \begin{bmatrix} z^{-k} + \sum\limits_{j=\{-k+2,-k+4,\ldots,k\}} a_n^j z^j & \sum\limits_{j=\{-k+1,-k+3,\ldots,k-1\}} b_n^j z^j \\ \sum\limits_{j=\{-k+1,-k+3,\ldots,k-1\}} c_n^j z^j & z^k + \sum\limits_{j=\{-k,-k+2,\ldots,k-2\}} d_n^j z^j \end{bmatrix}, \tag{4-9}$$

where V_n' is the updated eigenfunction. The eigenfunction is chosen as,

$$V_n = \begin{bmatrix} \phi_{n,1} & \psi_{n,1} \\ \phi_{n,2} & \psi_{n,2} \end{bmatrix}, \tag{4-10}$$

where ϕ_n and ψ_n are the Jost solutions. For a null potential, i.e. $Q_n = R_n = 0$, the Jost solutions can be solved exactly and these can be used as the seed solutions:

$$\phi_n = \begin{bmatrix} z^{-n} \\ 0 \end{bmatrix}, \quad \psi_n = \begin{bmatrix} 0 \\ z^n \end{bmatrix}. \tag{4-11}$$

Substituting V_n in Eq. (4-9) leads to

$$\begin{bmatrix} \phi_{n,1}' & \psi_{n,1}' \\ \phi_{n,2}' & \psi_{n,2}' \end{bmatrix} = \begin{bmatrix} z^{-k} + \sum\limits_{j=\{-k+2,-k+4,\ldots,k\}} a_n^j z^j & \sum\limits_{j=\{-k+1,-k+3,\ldots,k-1\}} b_n^j z^j \\ \sum\limits_{j=\{-k+1,-k+3,\ldots,k-1\}} c_n^j z^j & z^k + \sum\limits_{j=\{-k,-k+2,\ldots,k-2\}} d_n^j z^j \end{bmatrix} \begin{bmatrix} \phi_{n,1} & \psi_{n,1} \\ \phi_{n,2} & \psi_{n,2} \end{bmatrix}. \tag{4-12}$$

The columns of the updated eigenfunction V_n' are linearly dependent whenever $z = z_i$ is an eigenvalue, i.e. $\phi_n' = b_i \psi_n'$ (see Section 3-1-1), where b_i is the norming constant. Let

$$\alpha_{n,i} = \frac{\phi_{n,2}(z_i) - b_i \psi_{n,2}(z_i)}{\phi_{n,1}(z_i) - b_i \psi_{n,1}(z_i)}, \qquad i = 1, 2, \ldots, 2k. \tag{4-13}$$

Rewriting $\phi_n' = b_i \psi_n'$ using the expressions from Eq. (4-12) gives

$$\begin{aligned} &\left(z^{-k} + \sum_{j=\{-k+2,-k+4,\ldots,k\}} a_n^j z^j\right)\phi_{n,1} + \left(\sum_{j=\{-k+1,-k+3,\ldots,k-1\}} b_n^j z^j\right)\phi_{n,2} \\ &\quad = b_i\left(\left(z^{-k} + \sum_{j=\{-k+2,-k+4,\ldots,k\}} a_n^j z^j\right)\psi_{n,1} + \left(\sum_{j=\{-k+1,-k+3,\ldots,k-1\}} b_n^j z^j\right)\psi_{n,2}\right), \end{aligned} \tag{4-14}$$

$$\begin{aligned} &\left(\sum_{j=\{-k+1,-k+3,\ldots,k-1\}} c_n^j z^j\right)\phi_{n,1} + \left(z^k + \sum_{j=\{-k,-k+2,\ldots,k-2\}} d_n^j z^j\right)\phi_{n,2} \\ &\quad = b_i\left(\left(\sum_{j=\{-k+1,-k+3,\ldots,k-1\}} c_n^j z^j\right)\psi_{n,1} + \left(z^k + \sum_{j=\{-k,-k+2,\ldots,k-2\}} d_n^j z^j\right)\psi_{n,2}\right). \end{aligned} \tag{4-15}$$

Eq. (4-14) and Eq. (4-15) can be rearranged to give

$$\left(z^{-k} + \sum_{j=\{-k+2,-k+4,\ldots,k\}} a_n^j z^j\right)\left(\phi_{n,1} - b_i\psi_{n,1}\right) + \left(\sum_{j=\{-k+1,-k+3,\ldots,k-1\}} b_n^j z^j\right)\left(\phi_{n,2} - b_i\psi_{n,2}\right) = 0, \tag{4-16}$$

$$\left(\sum_{j=\{-k+1,-k+3,\ldots,k-1\}} c_n^j z^j\right)\left(\phi_{n,1}-b_i\psi_{n,1}\right)+\left(z^k+\sum_{j=\{-k,-k+2,\ldots,k-2\}} d_n^j z^j\right)\left(\phi_{n,2}-b_i\psi_{n,2}\right)=0. \tag{4-17}$$

Using the definition of $\alpha_{n,i}$ from Eq. (4-13), simplifying Eq. (4-16) and Eq. (4-17) results in the following equations,

$$\begin{aligned}\sum_{j=\{-k+2,-k+4,\ldots,k\}} a_n^j z_i^j + \alpha_{n,i}\sum_{j=\{-k+1,-k+3,\ldots,k-1\}} b_n^j z_i^j &= -z_i^{-k}\\ \frac{1}{\alpha_{n,i}}\sum_{j=\{-k+1,-k+3,\ldots,k-1\}} c_n^j z_i^j + \sum_{j=\{-k,-k+2,\ldots,k-2\}} d_n^j z_i^j &= -z_i^k\end{aligned} \tag{4-18}$$

The Darboux coefficients could in principle be calculated by solving Eq. (4-18) using z_i, $1/z_i^*$, b_i and $-1/b_i^*$ for $i = 1,\ldots,k$. However, owing to permutability of Darboux transform (see Section 2-2-2), the higher order Darboux matrix is more easily obtained by repetitive degree one Darboux updates. In degree one case, the matrix M_n in Eq. (4-9) reduces to

$$M_n = \begin{bmatrix} z^{-1}+a_n^1 z & b_n^0 \\ c_n^0 & z+d_n^{-1}z^{-1}\end{bmatrix}. \tag{4-19}$$

Using Eq. (4-18) the coefficients a_n^1, b_n^0, c_n^0 and d_n^{-1} can be expressed in terms of $\alpha_{n,i}$ as follows,

$$\begin{aligned} a_n^1 &= \frac{\alpha_{n,2}z_2-\alpha_{n,1}z_1}{z_1z_2(\alpha_{n,1}z_2-\alpha_{n,2}z_1)},\\ b_n^0 &= \frac{z_1^2-z_2^2}{z_1z_2(\alpha_{n,1}z_2-\alpha_{n,2}z_1)},\\ c_n^0 &= \frac{\alpha_{n,1}\alpha_{n,2}(z_1^2-z_2^2)}{(\alpha_{n,1}z_2-\alpha_{n,2}z_1)},\\ d_n^{-1} &= \frac{z_1z_2(\alpha_{n,2}z_2-\alpha_{n,1}z_1)}{(\alpha_{n,1}z_2-\alpha_{n,2}z_1)}.\end{aligned} \tag{4-20}$$

The updated potentials $Q'_{n+1/2}$ and $R'_{n+1/2}$ can be computed from these coefficients. The scaled discrete eigenvalue problem Eq. (3-38) after an update,

$$L'_n = \begin{pmatrix} z^{-1} & Q'_{n+1/2} \\ R'_{n+1/2} & z\end{pmatrix}, \tag{4-21}$$

satisfies $V'_{n+1} = L'_nV'_n$. However, V'_{n+1} can also be found by (see Section 3-2)

$$V'_{n+1} = M_{n+1}V_{n+1}, \tag{4-22}$$

where

$$M_{n+1} = \begin{bmatrix} z^{-k}+\sum_{j=\{-k+2,-k+4,\ldots,k\}} a_{n+1}^j z^j & \sum_{j=\{-k+1,-k+3,\ldots,k-1\}} b_{n+1}^j z^j \\ \sum_{j=\{-k+1,-k+3,\ldots,k-1\}} c_{n+1}^j z^j & z^k+\sum_{j=\{-k,-k+2,\ldots,k-2\}} d_{n+1}^j z^j\end{bmatrix}. \tag{4-23}$$

Hence,

$$M_{n+1}V_{n+1} = L'_nM_nV_n. \tag{4-24}$$

Substituting the seed solutions from equation Eq. (4-11) for the degree one Darboux matrix Eq. (4-19), Eq. (4-24) gives

$$\begin{aligned}
&\begin{bmatrix} z^{-n-2}+a_{n+1}^{1}z^{-n} & b_{n+1}^{0}z^{n+1} \\ c_{n+1}^{0}z^{-n-1} & z^{n+2}+d_{n+1}^{-1}z^{n} \end{bmatrix} \\
&\qquad = \begin{pmatrix} z^{-1} & Q'_{n+1/2} \\ R'_{n+1/2} & z \end{pmatrix} \begin{bmatrix} z^{-n-1}+a_{n}^{1}z^{-n+1} & b_{n}^{0}z^{n} \\ c_{n}^{0}z^{-n} & z^{n+1}+d_{n}^{-1}z^{n-1} \end{bmatrix} \\
&= \begin{bmatrix} z^{-n-2}+(a_{n}^{1}+Q'_{n+1/2}c_{n}^{0})z^{-n} & Q'_{n+1/2}z^{n+1}+(b_{n}^{0}+Q'_{n+1/2}d_{n}^{-1})z^{n-1} \\ R'_{n+1/2}z^{-n-1}+(R'_{n+1/2}a_{n}^{1}+c_{n}^{0})z^{-n+1} & z^{n+2}+(R'_{n+1/2}b_{n}^{0}+d_{n}^{-1})z^{n} \end{bmatrix}. \quad (4\text{-}25)
\end{aligned}$$

Equating the coefficients of z^{n+1}, z^{-n-1}, z^{n-1} and z^{-n+1} yields

$$\begin{aligned}
Q'_{n+1/2} &= b_{n+1}^{0}, \quad R'_{n+1/2} = c_{n+1}^{0}, \\
Q'_{n+1/2} &= \frac{-b_{n}^{0}}{d_{n}^{-1}}, \quad R'_{n+1/2} = \frac{-c_{n}^{0}}{a_{n}^{1}}.
\end{aligned} \quad (4\text{-}26)$$

Similarly, substituting the seed solutions from equation Eq. (4-11) and the degree k Darboux matrix Eq. (4-9) in Eq. (4-24) and equating the coefficients of z^{n+k} yields

$$Q'_{n+1/2} = b_{n+1}^{(k-1)}, \quad (4\text{-}27)$$

whereas equating coefficients of z^{-n-k} gives,

$$R'_{n+1/2} = c_{n+1}^{(-k+1)}. \quad (4\text{-}28)$$

Similarly equating the coefficients of z^{n-k} yields,

$$Q'_{n+1/2} = \frac{-b_{n}^{(-k+1)}}{d_{n}^{(-k)}}, \quad (4\text{-}29)$$

while from z^{-n+k} gives,

$$R'_{n+1/2} = \frac{-c_{n}^{(k-1)}}{a_{n}^{(k)}}. \quad (4\text{-}30)$$

For the first case i.e. computing the potential at $x_{n+1/2}$ using the Darboux coefficients at x_{n+1}, the relation

$$V'_{n} = L_{n}^{'-1}V'_{n+1}, \quad L_{n}^{'-1} = \frac{1}{(1-Q'_{n+1/2}R'_{n+1/2})}\begin{pmatrix} z & -Q'_{n+1/2} \\ -R'_{n+1/2} & z^{-1} \end{pmatrix} \quad (4\text{-}31)$$

can be used for the eigenfunction update. For the second case i.e. computing the potential at $x_{n+1/2}$ using the Darboux coefficients at x_{n}, the relation,

$$V'_{n+1} = L'_{n}V'_{n}, \quad L'_{n} = \begin{pmatrix} z^{-1} & Q'_{n+1/2} \\ R'_{n+1/2} & z \end{pmatrix}. \quad (4\text{-}32)$$

can be used. The potential at all the grid points can be computed by alternating between the potential update and eigenfunction update.

Following the same set of steps as in the case of the Ablowitz-Ladik discretization, it was possible to arrive at the potential update and eigenfunction update equations for the Split-Magnus discretization. The procedure can be extended similarly to other discretizations. The structure of the discrete Darboux matrix is crucial for arriving at the appropriate potential update equations. For the trapezoidal discretization (TR) Eq. (3-33), the degree one Darboux matrix should be chosen as

$$M_n = \begin{bmatrix} a_n z + z^{-1} & -z + b_n z^{-1} \\ c_n z + z^{-1} & z + d_n z^{-1} \end{bmatrix}, \tag{4-33}$$

The coefficients a_n, b_n, c_n and d_n can be found by solving a system of equations similar to Eq. (4-20). Starting again with the recurrence relation,

$$M_{n+1} V_{n+1} = L'_n M_n V_n, \tag{4-34}$$

and comparing the powers of z yields,

$$\begin{aligned} R'_{n+1} &= \frac{C_{n+1}^{-k}}{A_{n+1}^{-k}}, & R'_n &= \frac{\mathcal{X}}{1 + \sqrt{1 + |\mathcal{X}|^2}}, \\ Q'_{n+1} &= -(R'_{n+1})^*, & Q'_n &= -(R'_n)^*, \end{aligned} \tag{4-35}$$

where

$$\mathcal{X} = \frac{C_{n+1}^{-k+2} - R'_{n+1} A_{n+1}^{-k+2}}{A_{n+1}^{-k} - Q'_{n+1} C_{n+1}^{-k}} \tag{4-36}$$

The equations Eq. (4-35) can be used to compute the potential at all points left of the arbitrary starting point x_n. Alternative to finding potential update equations for the points to the right of x_n, the reflection property (Section 3-1-1) can be used. By repeating the procedure used for the points left of x_n with new norming constants $b_r = 1/b$, the potential can be computed at all points right of x_n for the original norming constants b. Such an alternative scheme requires the DDT to be performed twice which adds small complexity to the overall fast scheme.

The scheme derived above is now summarized as an algorithm. Owing to the symmetry property $R_n = -Q_n^*$ of the NSE, it suffices to compute either the Q_n or the R_n. This immediately halves the number of computations required by the algorithm. For the numerical implementation, the first step is to define an equidistant grid of 2N+1 points $x_n, n = -N, -N+1, ..., N$, over the support $[x_{-N}, x_N] = [L_1, L_2]$. The computation of the Darboux coefficients is typically well conditioned at $n = 0$ and hence it is chosen as the starting point.

The fast scheme independent of the underlying discretization can be summarized as follows.

DDE

Input: Eigenvalues ζ_k, norming constants b_k (Eq. (2-17)), step-size h (Section 3-1) and number of samples N
Output: $Q_n \approxeq hq(nh)$, where Q_n is the discrete potential and $q(x)$ is the continuous potential (Section 3-1)

- Transform the eigenvalues according to the chosen discretization. Ex. $z = e^{-i\zeta h}$ for Ablowitz-Ladik discretization (Section 3-1).
- Find the discrete eigenfunction V'_n (Ex. Eq. (3-45)) at $n = 0$ using discrete Darboux transform.
- For $n = 0, \cdots, N$ do:
  - $Q'_n = f(V'_n)$, where $f(V'_n)$ is a relation specific to the discretization. Ex. Eq. (4-7) for Ablowitz-Ladik discretization.
  - $R'_n = -Q'^{*}_n$
  - $V'_{n+1} = L'_n V'_n$, where L_n is the discrete eigenvalue problem. Ex. Eq. (3-40) for the Ablowitz-Ladik discrerization.
- For $n = 0, \cdots, -N$ do:
  - $Q'_{n-1} = g(V'_n)$, where $g(V'_n)$ is a relation specific to the discretization. Ex. Eq. (4-8) for Ablowitz-Ladik discretization.
  - $R'_{n-1} = -Q'^{*}_{n-1}$
  - $V'_{n-1} = L'^{-1}_{n-1} V'_n$

The DDE scheme specific to the Split-Magnus discretization is given in Appendix B.

4-2 Complexity Analysis

An efficient implementation of the classical Darboux transform (Algorithm 2 in [15]) and the DDE scheme derived in the previous section were implemented in MATLAB. Each of the elementary operations, addition, subtraction, multiplication, division and complex conjugation are assumed to require one floating point operation (FLOP). The FLOPS required for higher operations such as matrix manipulations follow directly from the elementary operations. Through manual counting, for K eigenvalues and N samples, the CDT algorithm requires $NK(15 + 11K)/2$ FLOPS. For the DDE algorithm with Split-Magnus discretization (DDE-SM in Appendix B), the discrete Darboux transform requires $35K^2 + 17K - 36$ FLOPS while the fast computation of the potential requires $N(20K + 19)$ FLOPS. Therefore, the DDE-SM algorithm requires a total of $17K + 19N + 35K^2 + 20KN - 36$ FLOPS. The

DDE algorithm thus has a computational complexity of $\mathcal{O}(KN)$ while CDT has $\mathcal{O}(K^2N)$. Both Ablowitz-Ladik and Trapezoidal discretizations have longer execution times compared to the Split-Magnus discretization due to the higher number of FLOPS involved at each sample point.

Summary

A new scheme for fast computation of multi-solitons based on discrete Darboux transform was proposed. The relevant equations specific to different discretizations were derived. Simple FLOPS analysis shows that the algorithm has a complexity of $\mathcal{O}(KN)$. This claim will be proved using numerical tests in Chapter 5.

Chapter 5

Analysis and Modifications of DDE

Several tests were carried out to evaluate the performance of the DDE algorithm proposed in the previous chapter. Various observations and results from those tests are presented in Section 5-1. In Section 5-2 the effect of limited precision on the algorithms is discussed. Finally in Section 5-3, based on the insights from the multi-precision study, two modifications are proposed.

5-1 Error and Run-Time Analysis

The performance of CDT and DDE algorithm with different discretizations will be compared in the following using the analytically known example of the secant-hyperbolic potential $q(x) = A\,\mathrm{sech}(x)$ [39]. For integer values of A, $A\,\mathrm{sech}(x)$ is a multi-soliton with the eigenvalues ζ_k,

$$\zeta_k = i(\tilde{A} - k), k = 1, 2, \ldots, K, \tag{5-1}$$

where K is the largest integer smaller than $\tilde{A} = (A + 1/2)$. The corresponding norming constants are given by $b_k = (-1)^k$. The relative L^2 error is used as the measure of accuracy and is defined as,

$$\text{rel. } L^2\text{-error} = \frac{\|q_{actual} - q\|^2}{\|q_{actual}\|^2} \tag{5-2}$$

For low number of eigenvalues ($K < 10$), the CDT can compute the multi-soliton potential with very small errors (rel. L^2-error$<10^{-15}$) and the computed potential can be assumed to be the actual potential. Hence, the error in the potential computed by CDT is not presented in this section. For Figure 5-1, Figure 5-3 and Figure 5-2, the support chosen was [-10,10]. Figure 5-1 shows the error in the potential computed by DDE with different discretizations for two eigenvalues. Figure 5-3 shows the error in the potential computed by DDE with different discretizations for eight eigenvalues. In Figure 5-1 and Figure 5-3 it can be observed that the error decreases as a function of the step-size. This is true for all algorithms employing discrete eigenvalue problems. DDE algorithm with Ablowitz-Ladik being a first order method shows

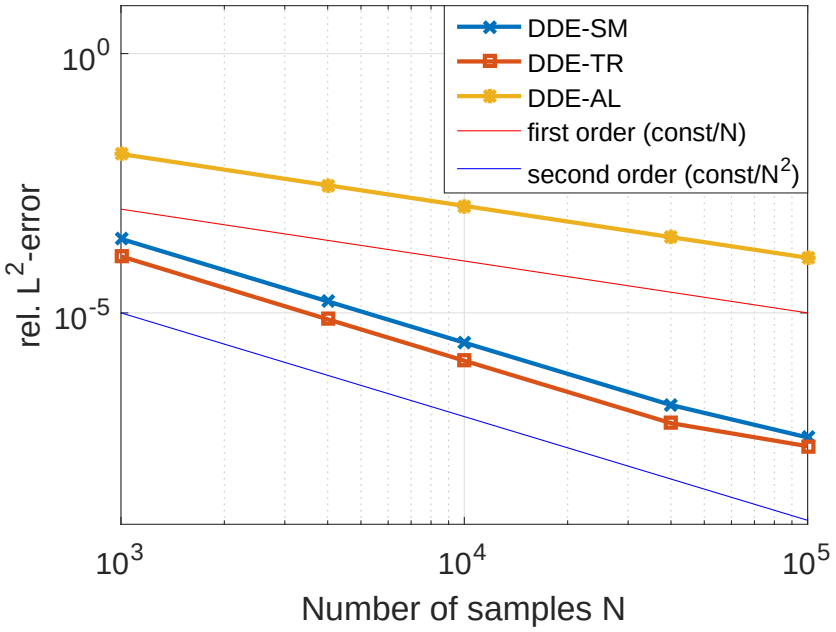

Figure 5-1: Error in constructed potential $2\,\mathrm{sech}(x)$

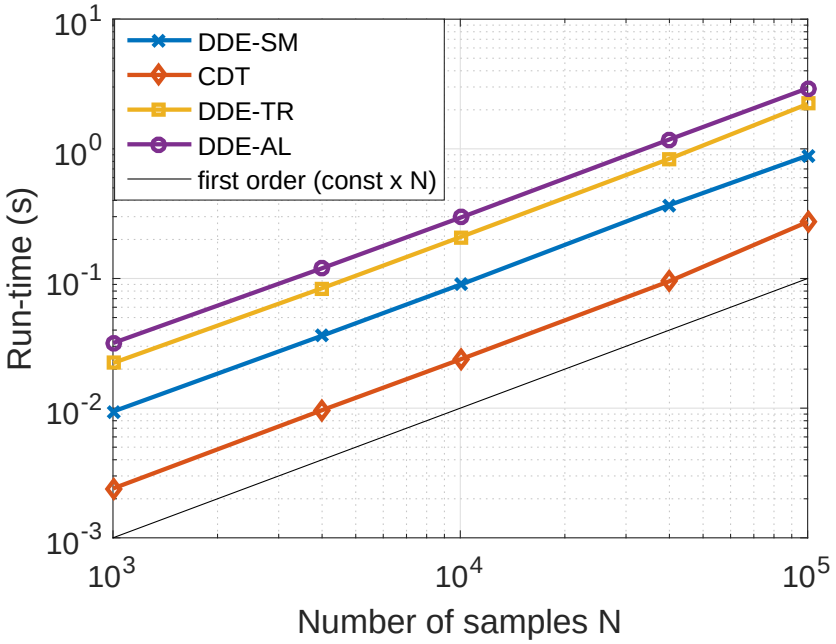

Figure 5-2: Run-time for construction of $2\,\mathrm{sech}(x)$ potential

first order behaviour ($p = 1$). This means that if the error for N_1 samples is e_1, then the error for N_2 samples is given by $e_2 = e_1(N_1/N_2)^p$ where p is the order of convergence. The Split-Magnus and Trapezoidal discretizations show second order behaviour ($p = 2$). The error using the Trapezoidal discretization is significantly lower than Ablowitz-Ladik method as is

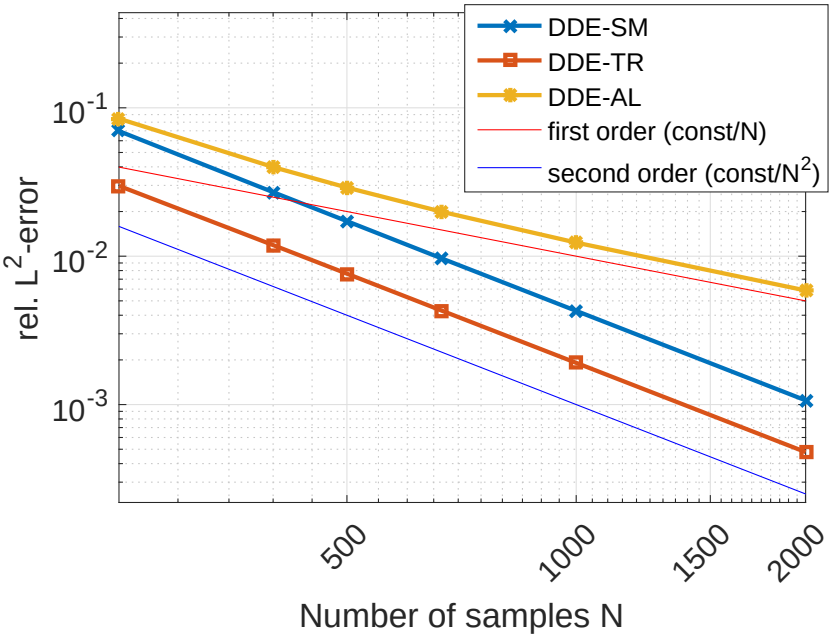

Figure 5-3: Error in constructed potential $8\,\mathrm{sech}(x)$

expected from a higher order method. The algorithm has linear complexity in the number of samples as can be seen in Figure 5-2. For Figure 5-4 and Figure 5-5, the $\mathrm{sech}(x)$ potential was

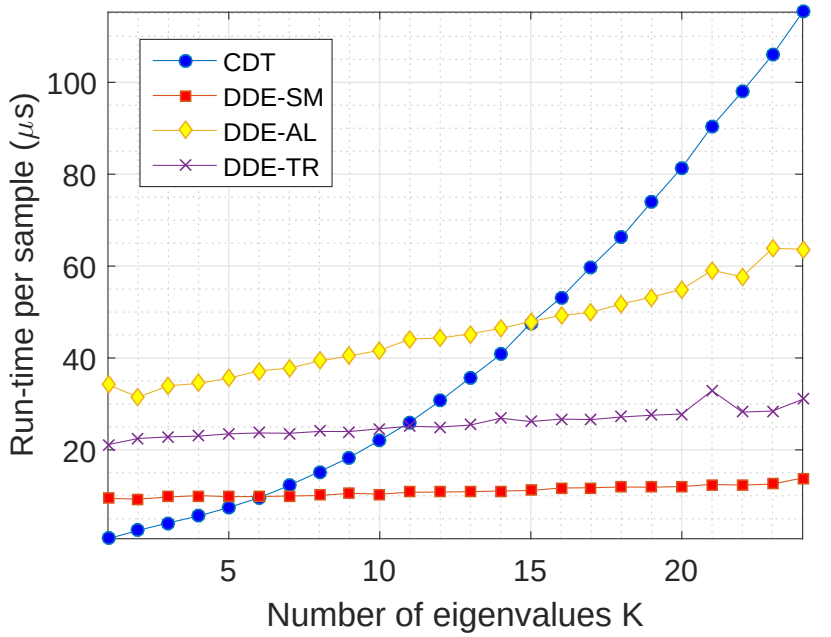

Figure 5-4: Run-times for different number of eigenvalues

used with support of [-10,10] and step-size 0.02. Figure 5-4 shows the comparison between

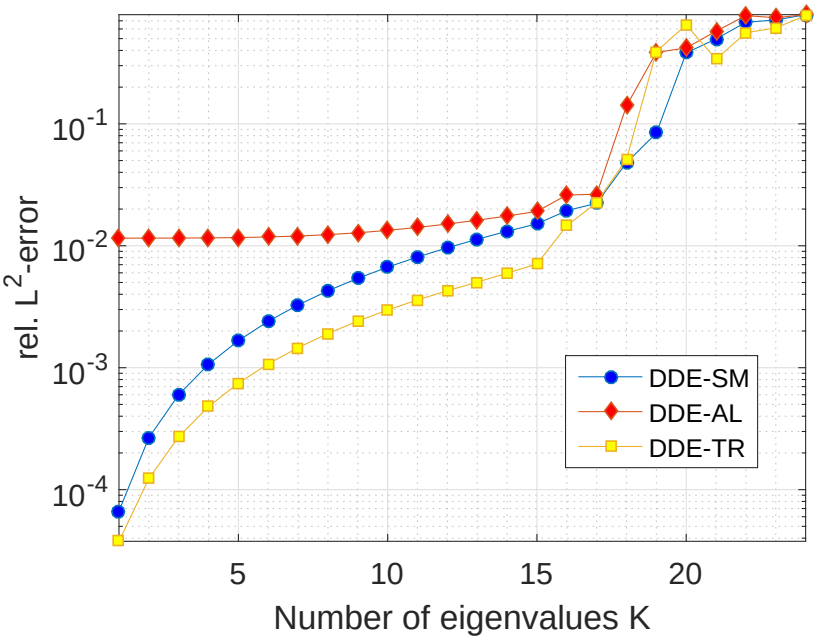

Figure 5-5: Variation of error with number of eigenvalues

the speeds of the algorithms. Figure 5-5 shows the error in the computed potential as a function of the number of eigenvalues. As foreseen from the complexity analysis in Section 4-2, the DDE algorithm has linear complexity in number of eigenvalues. The error increases with increasing number of eigenvalues which is seen in Figure 5-5. The error of second order methods increases steeply compared to the first order method. In Figure 5-5, for more than 16 eigenvalues the error is significant. During further tests it was observed that the algorithm breaks-down in the limit $h \to 0$. An example of failure to construct the potential can be seen in Figure 5-6. The step-size h for which the DDE algorithm fails to compute the potential is a function of the number of eigenvalues as will be revealed in the next section. To understand this better, simple perturbation experiments were carried out.

5-1-1 Perturbation Experiment

In order to investigate different possible sources of error which cause the failure, experiments have been carried out. The first possible source were the round-off errors in the eigenfunction computed at $n = 0$. To quantify the effects, test cases of hyperbolic-secant signal for which DDE could construct the potential were used. Increasing amount of error E_{max} was added to the computed eigenfunctions till a failure of the algorithm was confirmed visually. Such an experiment was carried out for increasing number of eigenvalues and decreasing step-size h. Close inspection of the observations led to the empirical relationship for the error E_{max} which leads to failure of the algorithm.

$$E_{max} = 10^{-4-k\log_{10}(\frac{0.1}{h})}, \tag{5-3}$$

where h is the step-size and k is the number of eigenvalues. Eq. (5-3) is valid only for a fixed support of [-10,10]. Working in a limited precision environment introduces the round-off

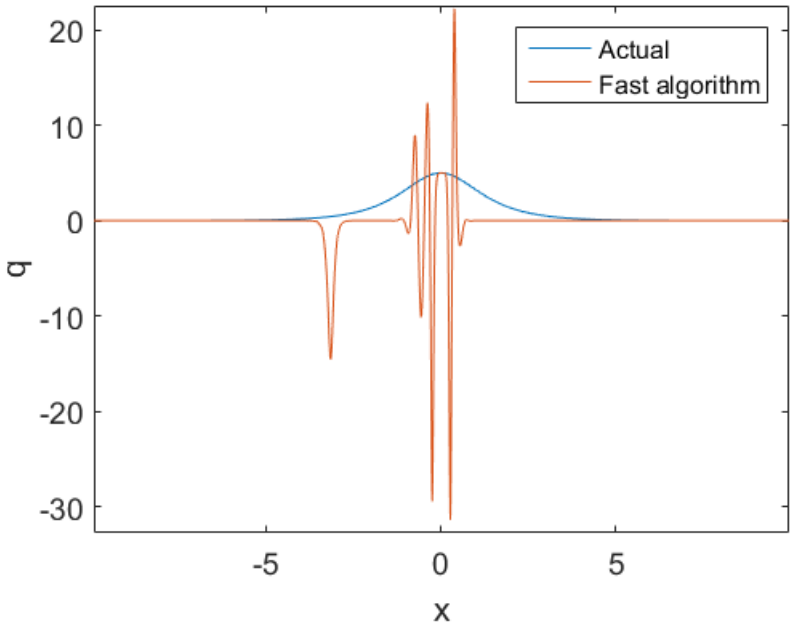

Figure 5-6: $5\,\mathrm{sech}(x)$ with step size of 0.0001.

errors which are equivalent to the error added externally for the tests. Hence using Eq. (5-3) an estimate for the machine precision required to prevent failure can be determined. The machine precision (ϵ) required to compute a multi-soliton potential for a given number of eigenvalues with a particular step-size is visualized in Figure 5-7. Figure 5-7 is specific for the sech(x) potential over a support of [-10,10].

Further experiments showed that in a limited precision environment (Eq. (4-1)),

$$V'_{n+1} \approxeq L'_n V'_n. \tag{5-4}$$

Thus, at each sample point errors are introduced eventually causing failure. The magnitude of error increases with increasing number of eigenvalues. Hence, the relation Eq. (5-3) does not tell the whole story. The required precision depends on the number of samples rather than the step-size. For a fixed support, step-size and number of samples are related and this led to the relation Eq. (5-3).

To estimate the limits, the step-size was set to $h = 0.0001$ and the number of samples of the DDE-SM algorithm that are correctly ($|q_{DDT} - q| < 0.001$) computed was recorded. As mentioned earlier, the error depends on the number of eigenvalues and hence the number of correctly computed samples decreases steeply Figure 5-8. It should be noted that Figure 5-8 gives only the trend and not the exact values as they also depend on the discrete spectrum and the step-size.

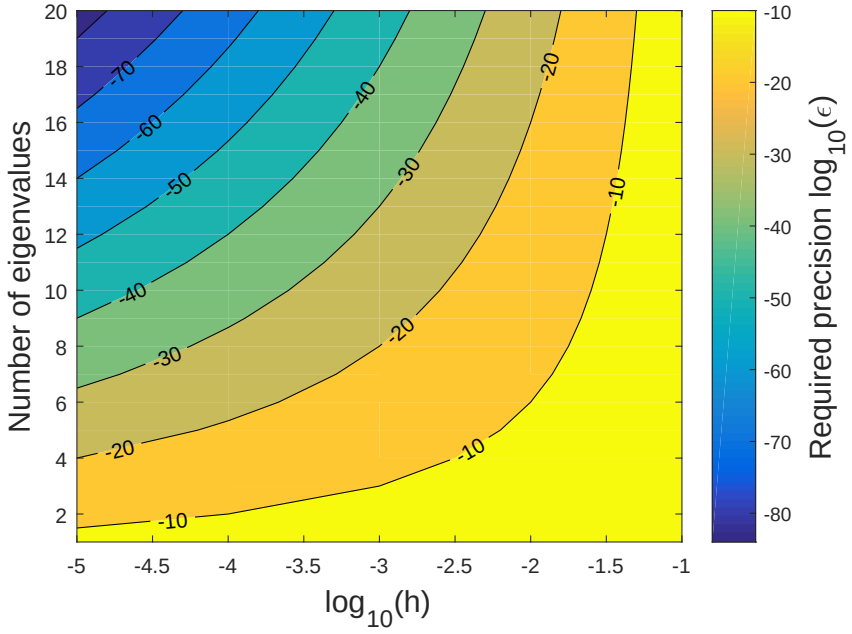

Figure 5-7: Eq. (5-3) plotted for varying number of eigenvalues and step-sizes.

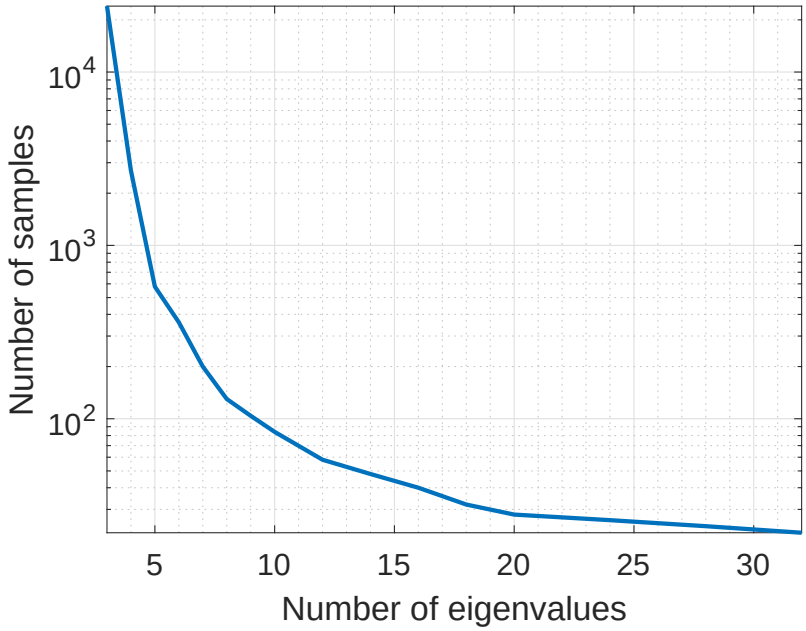

Figure 5-8: Number of correctly computed samples as a function of number of eigenvalues.

The error in the potential constructed by CDT although small, is also a function of the number of eigenvalues. This can be seen in Figure 5-9. Further experiments show that the error does not depend significantly on the number of samples. No studies of CDT under varying precision were found in literature. This was the motivation to study both CDT and the DDE algorithm under varying precision.

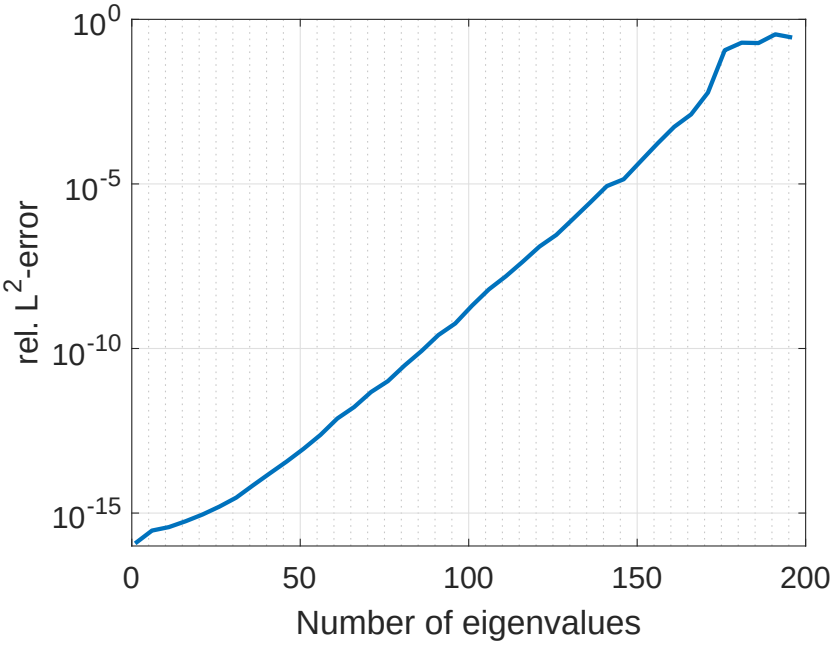

Figure 5-9: Error in the potential constructed using CDT

5-2 Study of Limited Precision Effects

To study behaviour under different precisions, both the CDT and the DDE algorithm were implemented in Julia language. Julia uses the GNU MPFR library to implement arbitrary precision arithmetic very efficiently. The Split-Magnus discretization was used. As the behaviour of DDE algorithm for all the discretizations is comparable in standard double machine precision, the observations for the SM discretization can be extended to other discretizations. The algorithms were tested for increasing number eigenvalues for varying precision. The potential computed by the CDT with 256 bit precision was chosen as the ideal solution. The algorithms were run for precisions of 16, 32, 64 and 128 bits. The support was fixed to [-25, 25] with 5001 samples.
The discrete spectrum used in [4] will be utilized for the tests. This will allow for comparison of DDE scheme with the algorithm published in [4]. A sequence of angles was defined as $\theta_j = \theta_0 + (j-1)\Delta\theta, j = 1, 2, \ldots, J$ with $\Delta\theta = (\pi - 2\theta_0)/(J-1)$. Then the eigenvalues for the numerical experiment were chosen as

$$\zeta_{j+J(l-1)} = le^{i\theta_j}, l = 1, 2, \ldots, L, j = 1, 2, \ldots, J.$$

The norming constants are chosen as

$$b_j = e^{i\pi(j-1)/(LJ-1)}, j = 1, 2, \ldots, LJ.$$

For the tests $\theta_0 = \pi/3, J = 4$ and $L = 19$. Then the sequence of discrete spectra considered is defined as

$$\mathfrak{S} = \{(\zeta_k, b_k), k = 1, 2, \ldots, K\}, K = 4, 8, \ldots, 76.$$

The test was done for a maximum of 64 eigenvalues. Using the error data for 128 bit and

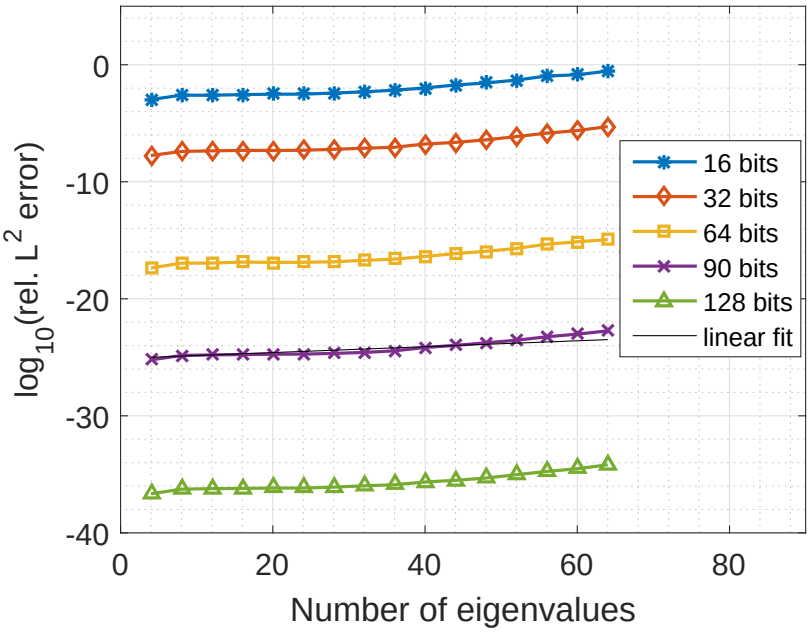

Figure 5-10: The relative L^2 error of the CDT algorithm is plotted against number of eigenvalues for varying precision.

32 bit runs, a linear fit between the $\log_{10}$(rel. L^2-error), number of eigenvalues and working precision was obtained. In figure 5-10 this fit was used to estimate the error for precision of 90 bits and was plotted against the actual error. The simple linear function describes the error well for arbitrary precision and number of eigenvalues. Such a relation is independent of the step-size. For standard double machine precision, the CDT algorithm can compute potentials with more than 50 eigenvalues with low errors ($< 10^{-10}$).

The error in the computed potential for algorithms based on the discrete eigenvalue problem has two components. One is due to the discretization and cannot be avoided, while the other is due to finite-precision and is implementation-specific. Comparing the potential computed by DDE with that of the the CDT gives the combined error which is shown in 5-11. Unlike the case of CDT, the error is primarily a function of the step-size in presence of sufficient precision. Thus, to isolate the implementation-specific error, the solution computed by discrete Darboux transform (DDT) for the Split-Magnus discretization using 256 bit precision was taken as the actual solution instead of CDT (Figure 5-12). The error seen in Figure 5-12 is the result of error introduced at each sample point Eq. (5-4). The trend in the error is similar to the case of CDT, but the dependence on precision is much more pronounced i.e. limited precision affects

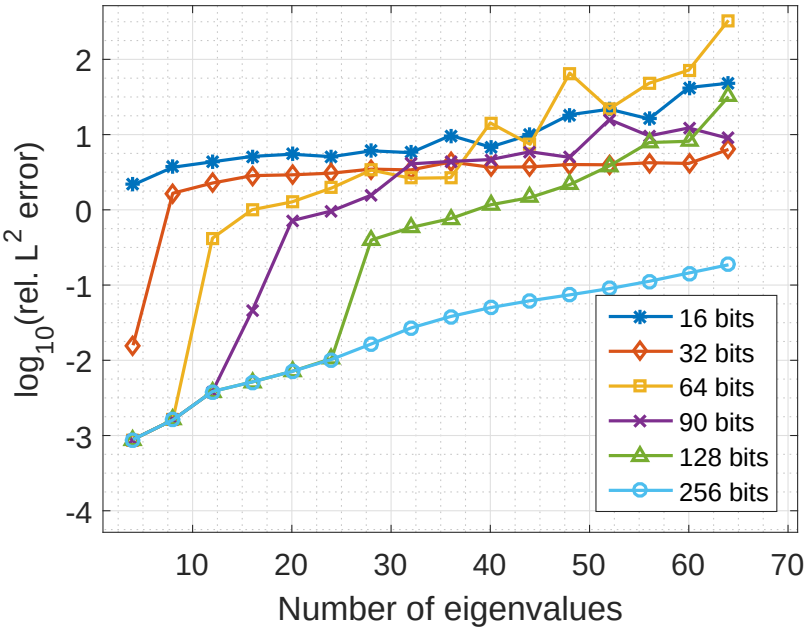

Figure 5-11: The relative L^2 error of DDE-SM algorithm compared with CDT is plotted against number of eigenvalues for varying precision.

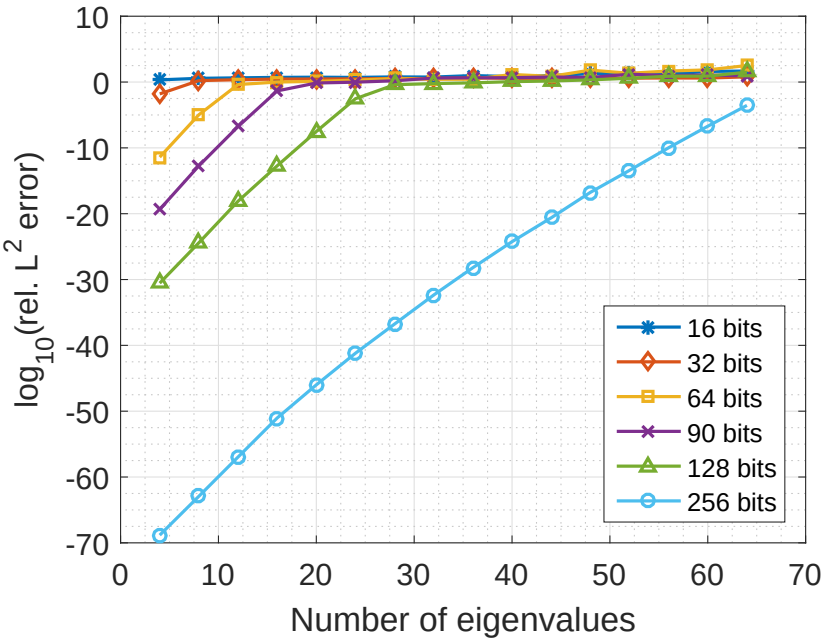

Figure 5-12: The relative L^2 error DDE-SM algorithm compared with DDT is plotted against number of eigenvalues for varying precision.

the fast algorithm much more than CDT and DDT. Other data from the multi-precision runs is documented in Appendix A.

5-3 Modifications of DDE Algorithm

In this section two modifications to the DDE scheme are introduced which can compute the potential as $h \to 0$ without breaking down. These modifications are engineering solutions rather than improvements based on additional mathematical theory. Both the modifications allow the algorithm to achieve slightly different goals which will become clearer in the following subsections.

5-3-1 Modification 1

It is assumed that the computational domain of the potential is known a priori. With some abuse of notation this domain is termed as the support of the potential. Figure 5-7 provides an estimate for the minimum step-size h^k_{min} at which the algorithm can correctly reconstruct the potential with the support [-10,10]. The error in the computed potential is a function of the step-size and using the minimum step-size h^k_{min} will yield the least error. This information can be used by scaling the support and eigenvalues. Let $\mathfrak{S}$ be the set of eigenvalues, h_o be the chosen step-size and [LL,LR] be the support. Let q_o be the corresponding potential. Let $\mathcal{S}$ denote the scaling factor,

$$\mathcal{S} = |LR - LL|/20. \tag{5-5}$$

The scaled set of eigenvalues will be $\mathfrak{S}_s = \mathcal{S}\mathfrak{S}$ and scaled step-size $h_s = h_o/\mathcal{S}$. The new potential q_s is related to the original potential q_o as $q_o(x) = q_s(x/\mathcal{S})/\mathcal{S}$. The norming constants $\mathfrak{B}$ remain invariant under the scaling [48].
For step-size h_s lower than h^k_{min}, the idea is to reconstruct the potential using multiple staggered runs with step-size h^k_{min}. The modified algorithm can be divided into three main sections.

1. **Determination of number of runs**
   The number of runs required to reconstruct a potential with step-size h_s approximately using step-size of h^k_{min} is given by $\mathcal{F} = \left\lfloor h^k_{min}/h_s \right\rfloor$. $\lfloor x \rfloor$ means the floor of x, i.e. the largest integer less than or equal to x. An array $\mathfrak{C}$ is then defined as $\mathfrak{C}_k = -\lfloor \mathcal{F}/2 \rfloor + (k-1)$, $k = 1, 2..., \mathcal{F}$.

2. **Multiple runs with step-size h^k_{min}**
   The fast algorithm needs to be run $\mathcal{F}$ times with grids shifted by h_s. Such translation is achieved by changing the norming constants (see Section 3-1-1) as follows

   $$b_k = \mathfrak{B}_k e^{(2i\mathfrak{S}_k \mathfrak{C}_j h_o)},$$

   where $\mathfrak{S}_k$ denotes the k^{th} element of $\mathfrak{S}$ and $\mathfrak{C}_j$ is the j^{th} element of $\mathfrak{C}$.

3. **Interweaving of potentials**
   The potentials generated from all the runs are interweaved to obtain a single potential corresponding to the step-size h_s.

For the purpose of demonstration the example of $12\,\mathrm{sech}(x)$ potential with a step-size $h_o = 0.01$ and support of [-10,10] is chosen. Hence the scaling factor $\mathcal{S} = 1$ and $h_s = h_o$. From

Figure 5-7, h^k_{min} is taken as 0.05, hence $\mathcal{F} = \left\lfloor h^k_{min}/h \right\rfloor$=5. In Figure 5-13, the subplot P1 shows all the runs resulting in the multi-soliton. Interweaving the data from the five individual runs with step-size $h^k_{min} = 0.05$ results in the potential with step-size $h_s = 0.01$. This can be seen in subplot P2. It is important to note that this modification only allows for fast

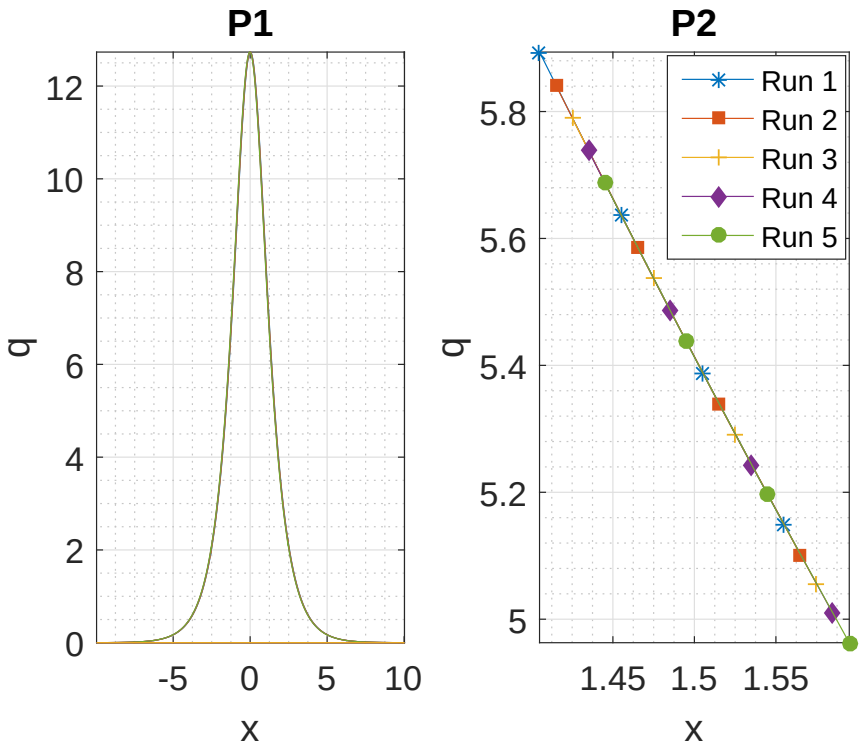

Figure 5-13: Potentials from all the runs are interweaved.

computation of a potential with higher number of samples while the error is more or less constant and is a function of the step-size h^k_{min}. This is seen in Figure 5-14, which shows the error in reconstruction of $8\,\mathrm{sech}(x)$ potential over a support of [-10,10]. The base step-size h^k_{min} is 0.01 which corresponds to only 2001 samples over the support [-10,10].

The modified algorithm referred to as Mod1 can be summarized as,

Mod1

Input: Eigenvalues $\mathfrak{S}$, norming constants $\mathfrak{B}$ (Eq. (2-17)), step-size h_o (Section 3-1) and support [LL,LR]
Output: $Q_n \approxeq h_o q(nh_o)$, where Q_n is the discrete potential and $q(x)$ is the continuous potential (Section 3-1)

- Compute the scaling factor $\mathcal{S} = |LR - LL|/20$ (Eq. (5-5)).
- Compute the scaled parameters as $\mathfrak{S}_s = \mathcal{S}\mathfrak{S}$ and $h_s = h_o/\mathcal{S}$.
- Look-up h^k_{min} from Figure 5-7.
- Calculate number of required iterations $\mathcal{F} = \left\lfloor h^k_{min}/h_s \right\rfloor$ and let $\mathfrak{C}_k = -\lfloor \mathcal{F}/2 \rfloor + (k-1)$, $k = 1, 2, \ldots, \mathcal{F}$. The number of samples per run $N = \mathcal{F}20/h^k_{min}$.
- Transform the scaled eigenvalues $\mathfrak{S}_s$ according to the chosen discrete eigenvalue problem and step-size h^k_{min}. Ex. $z = e^{-i\zeta h}$ for Ablowitz-Ladik discretization (Section 3-1).
- For j = 1 to $\mathcal{F}$ do:
  - $b_k = \mathfrak{B}_k e^{(2i\mathfrak{S}_k \mathfrak{C}_j h_o)}$, where subscript k denotes the k^{th} element.
  - Find the discrete eigenfunction V'_n (Ex. Eq. (3-45)) at $n = 0$ using discrete Darboux transform.
  - For $n = 0, 1, \ldots, N$ do:
    - $Q^{j'}_n = f(V'_n)$, where $f(V'_n)$ is a relation specific to the discretization. Ex. Eq. (4-7) for Ablowitz-Ladik discretization.
    - $R^{j'}_n = -Q^{j'*}_n$
    - $V'_{n+1} = L'_n V'_n$, where L_n is the discrete eigenvalue problem. Ex. Eq. (3-40) for the Ablowitz-Ladik discrerization.
  - For $n = 0, -1, \ldots, -N$ do:
    - $Q^{j'}_{n-1} = g(V'_n)$, where $g(V'_n)$ is a relation specific to the discretization. Ex. Eq. (4-8) for Ablowitz-Ladik discretization.
    - $R^{j'}_{n-1} = -Q^{j'*}_{n-1}$
    - $V'_{n-1} = L'^{-1}_{n-1} V'_n$
- Interweave and scale $Q^{1'}_n$ to $Q^{\mathcal{F}'}_n$ by defining vector $Q_n = \frac{1}{\mathcal{S}}(Q^{1'}_1, Q^{2'}_1, \ldots, Q^{\mathcal{F}'}_1, Q^{1'}_2, Q^{2'}_2, \ldots, Q^{\mathcal{F}'}_2, \ldots, Q^{1'}_n, Q^{2'}_n, \ldots, Q^{\mathcal{F}'}_n)$

The Mod1 scheme specific to the Split-Magnus discretization is given as Mod1-SM in Appendix B.

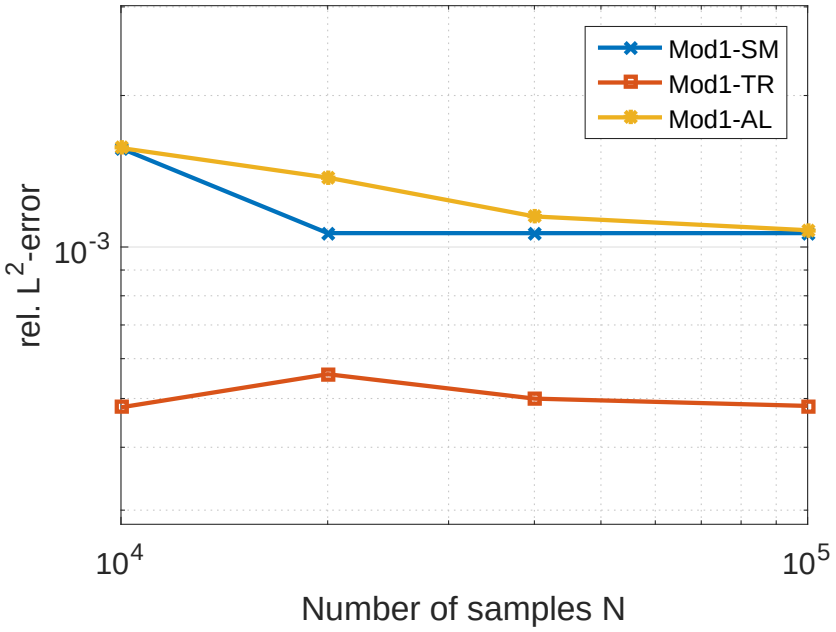

Figure 5-14: Error in potential constructed by modified algorithm

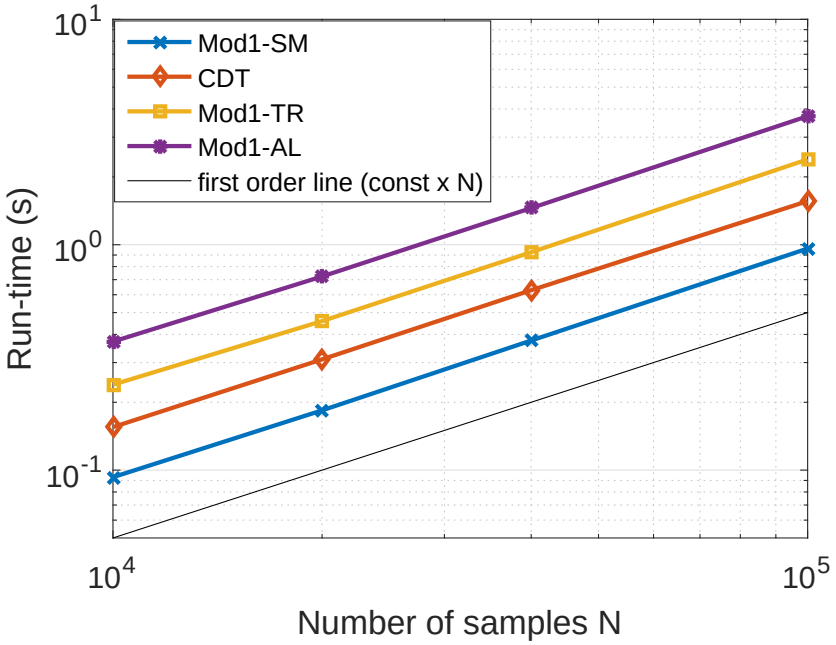

Figure 5-15: Run-times of modified algorithm

Through manual counting it can be seen that each iteration of the modified algorithm with Split-Magnus discretization (Mod1-SM) requires $17K+19N/\mathcal{F}+35K^2+20KN/\mathcal{F}-36$ FLOPS. Hence the total FLOPS complexity of Mod1-SM is found to be $17K\mathcal{F} + 19N + 35K^2\mathcal{F} + 20KN - 36\mathcal{F}$. For the cases in consideration $K < N$ and $F < N$ and hence the modified

algorithm also has a FLOPS complexity of $\mathcal{O}(KN)$. The linear complexity in N can be seen in Figure 5-15. For the modified algorithm, due to the overhead of computing the discrete Darboux matrix for each run, the hidden constant in the $\mathcal{O}(KN)$ increases. For Figure 5-16 and Figure 5-17 the hyperbolic-secant potential was computed over a support of [-10,10] and step-size $h = 0.01$. In Figure 5-16 the comparison in the run-times of the modified algorithm for the different discretizations can be seen. While in Figure 5-17 the relative error in the computed potentials is shown. In Figure 5-16 a jump in the run-times is observable after eight eigenvalues. This is the point at which the modified algorithm starts to use multiple runs ($\mathcal{F} > 1$) for the chosen step size of 0.01. The significant increase in the run-time of Mod1-AL can be attributed to naive implementation of the underlying discrete Darboux transform. The error also increases after eight eigenvalues but is still acceptable.

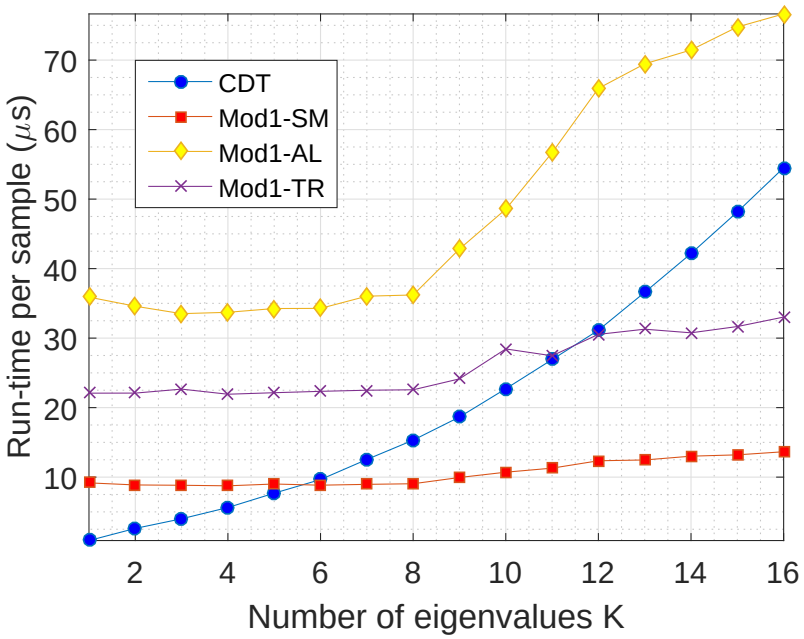

Figure 5-16: Averaged run-times of modified algorithm for increasing number of eigenvalues

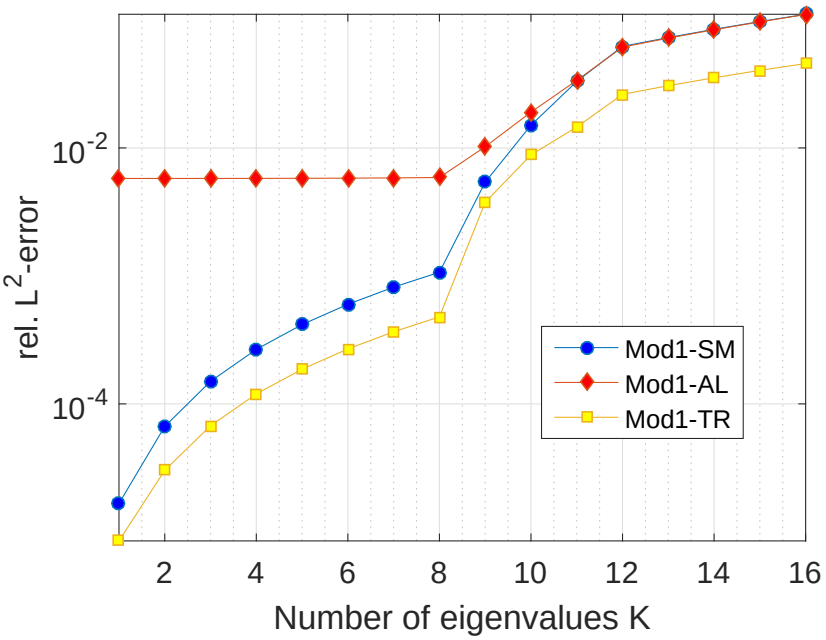

Figure 5-17: Variation of error of modified algorithm with number of eigenvalues

5-3-2 Modification 2

The modification mentioned in Section 5-3-1 allows fast computation of the potential but is limited in the base step-size which ultimately leads to a lower bound on the achievable error. The goal of Modification 2 is to find a fast algorithm that is not limited in error. To motivate this approach it helps to look at the propagation of error in the discrete Darboux coefficients obtained from the DDE algorithm compared to the conventional discrete Darboux transform. For a set of 12 eigenvalues as defined in Section 5-2, the actual potential and the

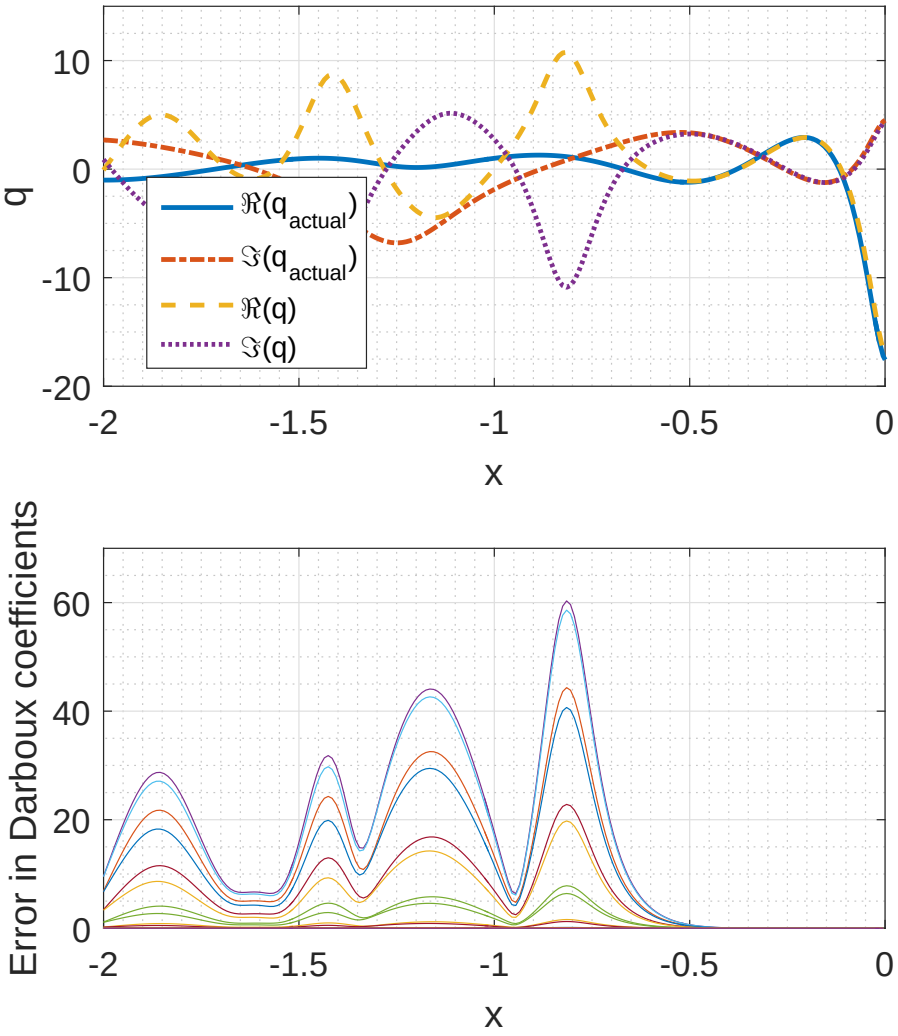

Figure 5-18: Error in Darboux coefficients (B_n in Eq. (4-9))

one constructed by the DDE-SM algorithm are plotted in the top subplot of Figure 5-18. The fast algorithm is successful at reconstructing the potential only upto to $x = -0.5$ starting from $x = 0$. The error in the Darboux coefficients (B_n in Eq. (4-9))is plotted in the lower subplot of Figure 5-18. As explained in Section 5-1-1, the DDE algorithm accumulates round-off

errors which eventually leads to failure. If the coefficients can be corrected before the errors become significant, the DDE algorithm can still be used to compute the complete potential. This observation motivated a multi-start approach. In the DDE scheme described in Section 4-1, the discrete Darboux transform is performed at only one point $n = 0$. In the multi-start approach it will be performed at M points ($M < N$), where N is the total number of samples. The DDE scheme will then be used to compute the samples between these M points. The number of such seed points M depends on the number and location of eigenvalues, norming constants and step-size. By performing tests on multiple sets of eigenvalues, $M = KN/500$ was chosen as a conservative value for N samples and K eigenvalues. The algorithm can be summarized as,

---

Mod2

Input: Eigenvalues $\mathfrak{S}$, norming constants $\mathfrak{B}$ (Eq. (2-17)), step-size h (Section 3-1) and support [LL,LR]
Output: $Q_n \approxeq hq(nh)$, where Q_n is the discrete potential and $q(x)$ is the continuous potential (Section 3-1)

- Transform the eigenvalues $\mathfrak{S}$ according to the chosen discrete eigenvalue problem and step-size h. Ex. $z = e^{-i\zeta h}$ for Ablowitz-Ladik discretization (Section 3-1).
- Total number of samples $N = |LR - LL|/h$. Define $N_{max} = \lceil 250/K \rceil$. Number of required seed points $M = \lceil KN/500 \rceil$, where $\lceil x \rceil$ means the ceiling of x, i.e. the smallest integer larger than or equal to x.
- Let l be the location of M seed points. $l_j = LL + (250h/K) + j - 1, j = 1, 2, \ldots, M$.
- For $j = 1$ to M do:
  - Translate the norming constants $b_k = \mathfrak{B}_k e^{2i\mathfrak{S}_k l_j}$.
  - Find the discrete eigenfunction V'_n (Ex. Eq. (3-45)) at $n = 0$ using discrete Darboux transform.
  - For $n = 0, 1, \ldots, N_{max}$ do:
    - $Q_n^{j'} = f(V'_n)$, where $f(V'_n)$ is a relation specific to the discretization. Ex. Eq. (4-7) for Ablowitz-Ladik discretization.
    - $R_n^{j'} = -Q_n^{j'*}$
    - $V'_{n+1} = L'_n V'_n$, where L_n is the discrete eigenvalue problem. Ex. Eq. (3-40) for the Ablowitz-Ladik discrerization.
  - For $n = 0, -1, \ldots, -N_{max}$ do:
    - $Q_{n-1}^{j'} = g(V'_n)$, where $g(V'_n)$ is a relation specific to the discretization. Ex. Eq. (4-8) for Ablowitz-Ladik discretization.
    - $R_{n-1}^{j'} = -Q_{n-1}^{j'*}$
    - $V'_{n-1} = L'^{-1}_{n-1} V'_n$

- Combine Q_n^1 to Q_n^M by defining vector

$$Q_n = (Q^1_{-N_{max}}, Q^1_{-N_{max}+1}, \ldots, Q^1_{N_{max}}, Q^2_{-N_{max}}, Q^2_{-N_{max}+1}, \ldots, Q^2_{N_{max}}, \ldots \\ \ldots, Q^M_{-N_{max}}, Q^M_{-N_{max}+1}, \ldots, Q^M_{N_{max}})$$

Analysis of a particular implementation using Split-Magnus discretization (Mod2-SM in Appendix B) shows FLOPS complexity of $19N - 36M + 35K^2M + 17KM + 20KN$. Substituting the choice of $M = KN/500$ gives a FLOPS complexity of $19N - \frac{9964}{500}KN + \frac{35}{500}K^3N + \frac{17}{500}K^2N$ which in $\mathcal{O}$ notation is $\mathcal{O}(K^3N)$ The error and run-time tests were conducted using $q(x) =$

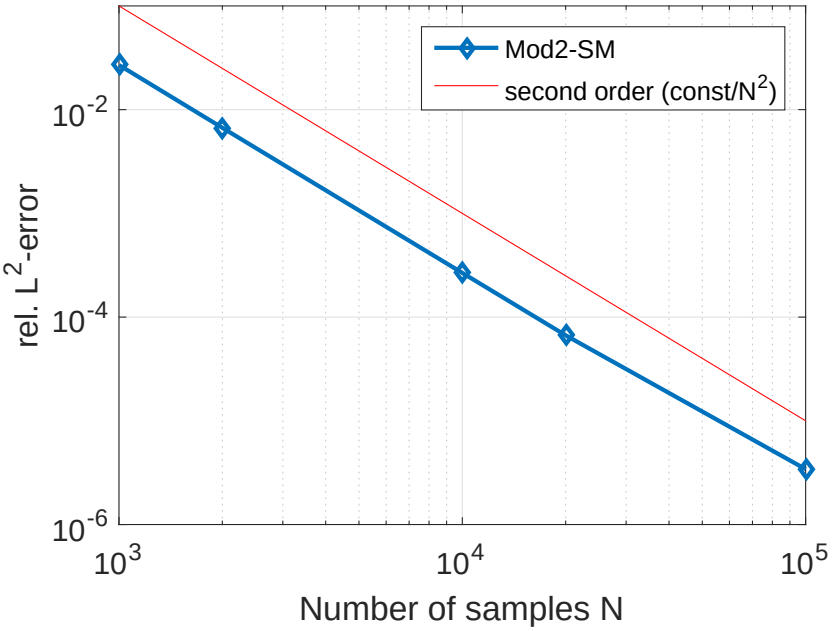

Figure 5-19: Error of modified algorithm for $20\,\mathrm{sech}(x)$ potential

$20\,\mathrm{sech}(x)$ potential which corresponds to 20 eigenvalues (Section 5-1). For Figure 5-20 and Figure 5-19 the support was chosen to be $[-10, 10]$. Figure 5-19 shows the error in the potential computed by Mod2-SM algorithm. Figure 5-20 shows the run-times of CDT and Mod2-SM algorithms. The error shows second order behaviour unlike the case of Mod1-SM (Figure 5-14). Hence the Mod2 algorithm achieves the goal of being a fast algorithm that is not limited in error. The run-time is linear in N (Figure 5-20) as expected from the FLOPS analysis for the choice of $M = KN/500$. The complexity may not remain linear if some other choice of M is used. For Figure 5-21 the hyperbolic-secant potential was used with a step-size $h = 0.01$ over a support of $[-10, 10]$. The run-time is not linear in K anymore as seen in Figure 5-21.

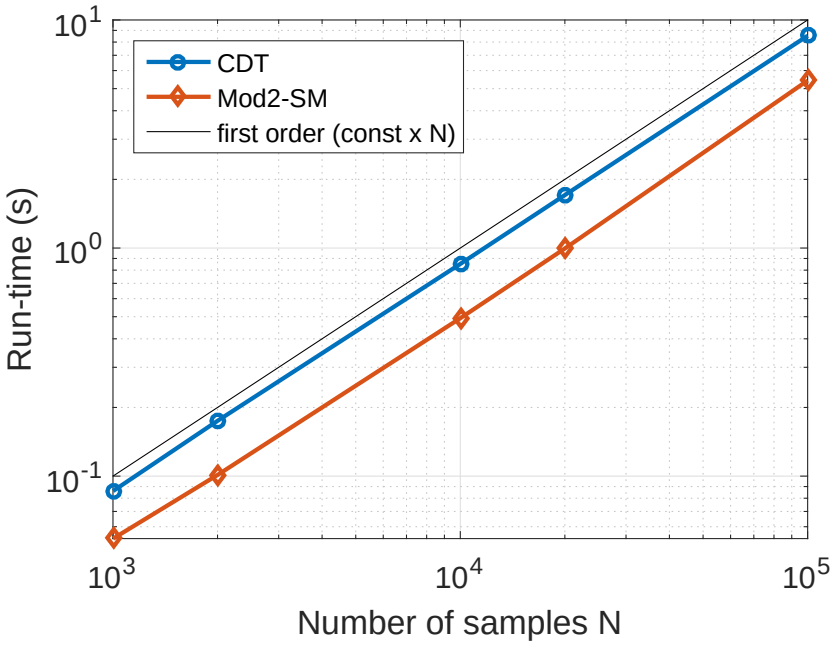

Figure 5-20: Run-times of modified algorithm for $20\,\mathrm{sech}(x)$ potential

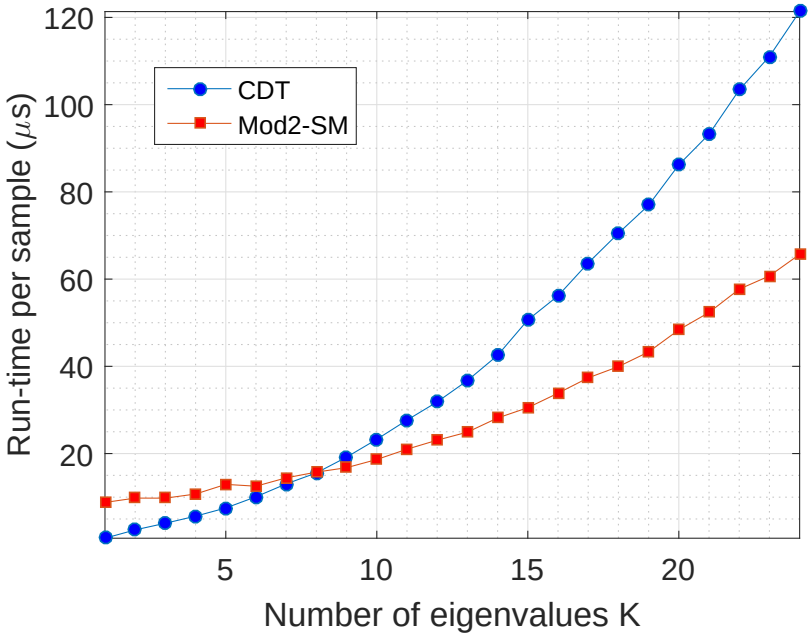

Figure 5-21: Run-times of modified algorithm for different number of eigenvalues

5-4 Comparison of Algorithms

In this section the DDE, Mod1 and Mod2 algorithms are compared against CDT for a numerical example taken from literature. Their advantages and disadvantages when compared to the algorithm in [4] are discussed.

For comparing the algorithms proposed in this report, the discrete spectrum from the experiment conducted in [40] was chosen. The set of seven eigenvalues is given by,

$$\mathfrak{S} = (0.45i - 0.6, 0.3i - 0.4, 0.45i - 0.2, 0.3i, 0.45i + 0.2, 0.3i + 0.4, 0.45i + 0.6). \tag{5-6}$$

The spectral amplitude of each eigenvalue in $\mathfrak{S}$, has Quadrature Phase Shift Keying (QPSK) constellation, $q_d(\mathfrak{S}_k) = |q_d(\mathfrak{S}_k)| \exp\{i\frac{\pi}{2}j\}$ with,

$$\ln(|q_d(\mathfrak{S}_k)|) = (11.85, 7.06, 7.69, 3.81, 1.93, -0.62, -5.43). \tag{5-7}$$

QPSK is a form of Phase Shift Keying in which two bits are modulated at once, selecting one of four possible carrier phase shifts (0, 90, 180, or 270 degrees). The phase shifts correspond to $j = 0, 1, 2, 3$. The data was arbitrarily chosen as the set $D = (3, 2, 0, 1, 0, 3, 1)$. The spectral amplitudes are then found to be,

$$\begin{aligned} q_d = (&-25.73\text{x}10^{-12} - 140.08\text{x}10^{3}i, -1.16\text{x}10^{3} + 142.60\text{x}10^{-15}i, 2.19\text{x}10^{3}, \\ &2.76\text{x}10^{-15} + 45.15i, 6.89, -98.82\text{x}10^{-18} - 537.94\text{x}10^{-3}i, 268.39\text{x}10^{-21} + 4.38\text{x}10^{-3}i). \end{aligned}$$

The norming constants are then given by [9],

$$b_k = \frac{q_d(\mathfrak{S}_k)}{\mathfrak{S}_k - \mathfrak{S}_k^*} \prod_{j=1,2,\ldots,7, j\neq k} \frac{\mathfrak{S}_k - \mathfrak{S}_j}{\mathfrak{S}_k - \mathfrak{S}_j^*} \tag{5-8}$$

The set of norming constants,

$$\begin{aligned} \mathfrak{B} = (&1.45\text{x}10^{3} + 5.45\text{x}10^{3}i, 18.90 - 42.53i, 17.73 - 1.34i, 995.90\text{x}10^{-3} + 134.83\text{x}10^{-18}i, \\ &- 55.87\text{x}10^{-3} - 4.23\text{x}10^{-3}i, 19.65\text{x}10^{-3} - 8.73\text{x}10^{-3}i - 45.30\text{x}10^{-6} + 170.45\text{x}10^{-6}i). \end{aligned}$$

The support was chosen to be $[-22, 22]$. In experimental setups the number of samples is limited by the speed of the digital-to-analog converter (DAC). In [40] a DAC capable of 88GSa/s ($88\text{x}10^9$ samples per second) was used. They also mention that the multi-soliton signal scales down to 2ns on their setup. This would mean that the multi-soliton signal would have only 176 samples. CDT was used to compute the potential in [40].

Error and run-time tests were performed for a wide range of number of samples to compare the performance of DDE-SM, Mod1-SM and Mod2-SM with CDT. It should be noted that the results presented in this thesis are from specific implementations of all the algorithms in MATLAB. The error in the potential computed by each algorithm can be seen in Figure 5-22. To better visualize the difference in run-times, the run-time per sample is plotted in Figure 5-23. All the three algorithms have very similar errors for less than 10^3 samples. For higher number of samples the DDE-SM algorithm fails to compute the potential correctly and this leads to the diverging error seen in Figure 5-22. For the Mod1-SM algorithm the error remains constant once the base step-size gets fixed. The error continues to decrease as a function of number of samples for Mod2-SM.

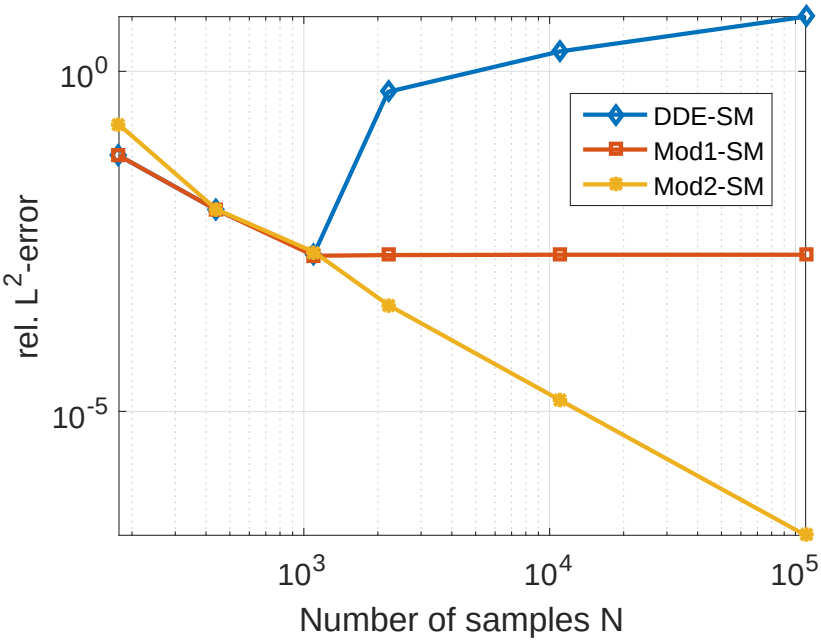

Figure 5-22: Variation of error of modified algorithm with number of eigenvalues

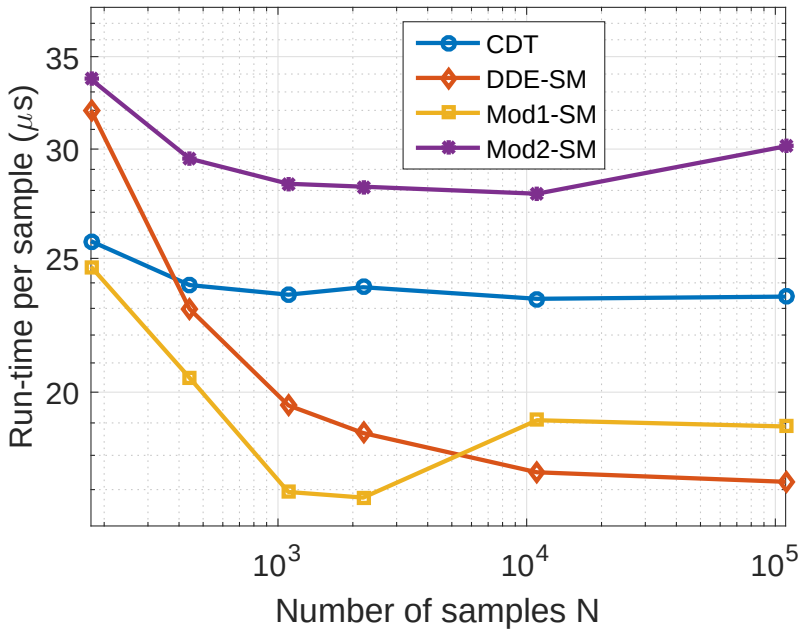

Figure 5-23: Variation of error of modified algorithm with number of eigenvalues

The run-time per sample of CDT is almost constant as expected from the scheme Figure 4-1. DDE-SM is slower (higher run-time per sample) than CDT for low number of samples but becomes faster (lower run-time per sample) for more than 500 samples. Mod1-SM has run-times very comparable to CDT at low number of samples and becomes faster as the

number of samples increases. The cross-over around $5x10^3$ samples between the run-times of DDE-SM and Mod1-SM is the result of overhead from multiple runs required by the Mod1 scheme (Section 5-3-1). For seven eigenvalues, Mod2-SM is slower than CDT for any number of samples. However for more than eight eigenvalues Mod2-SM is found to be faster than CDT for more than 1000 samples (Figure 5-21).

5-4-1 Comparison with Current State-of-the-Art Algorithm

The algorithm reported in [4] is currently the fastest algorithm in literature for generating multi-solitons with accurate control over norming constants. The algorithm will be referred to as FDT in the following discussion. FDT has a FLOPS complexity of $\mathcal{O}(N(K+\log^2 N))$. FDT could not be implemented in MATLAB for comparison due to time constraints. However, a qualitative comparison can still be done by assuming that the implementation of CDT used in [4] is the same as the one used in this thesis (Algorithm 2 in [15]). Such an assumption allows for a relative comparison of run-times irrespective of the computing environment (MATLAB in this thesis and C in [4]) and specific computing power. It is fair only to compare the results for Mod2 with the results in [4] as the other schemes DDE and Mod1 have some limitations on achievable error. For ease of reading, Figure 5-24a, Figure 5-25a and Figure 5-26a have been taken from [4]. Figure 5-24a shows the error for different variants of FDT for 20 eigenvalues. In Figure 5-25a the run-times per sample for 20 eigenvalues can be seen. In Figure 5-26a the run-time per sample as a function of number of eigenvalues is plotted.

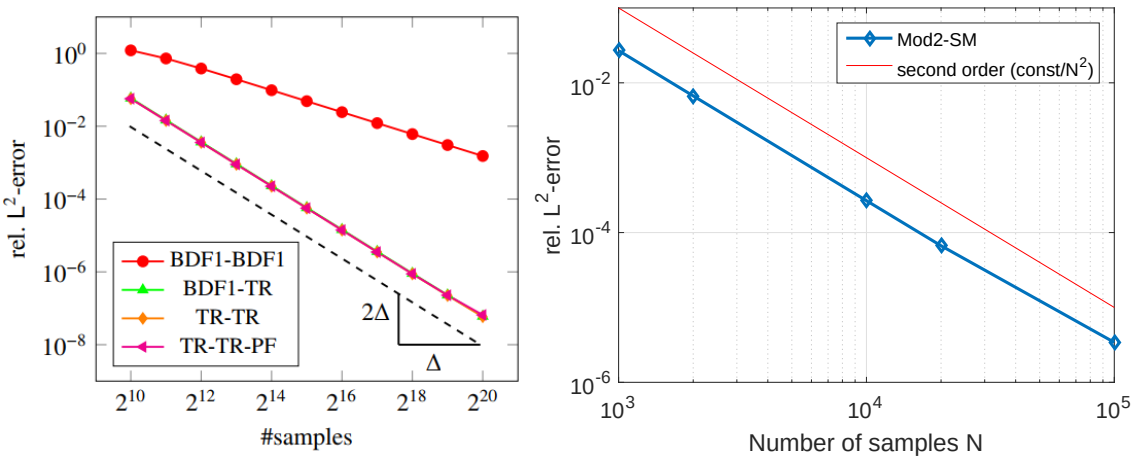

Figure 5-24: (a) Convergence analysis of FDT algorithm for multi-solitons (20 eigenvalues), taken from Figure 8.c in [4]. (b) Error of Mod-SM for 20 eigenvalues (Figure 5-19)

The fastest variant of FDT i.e. TR-TR-PF and Mod2-SM will be compared. From Figure 5-24 it can be seen that the errors achieved by Mod2-SM and FDT are very similar. The FDT algorithm is faster than CDT for less than 2^{14} samples (Figure 5-25a) while Mod2-SM is always faster than CDT (Figure 5-25b). In Figure 5-26a, FDT is faster than CDT for more than 20 eigenvalues while from Figure 5-26b it can be seen that Mod2-SM is faster than CDT

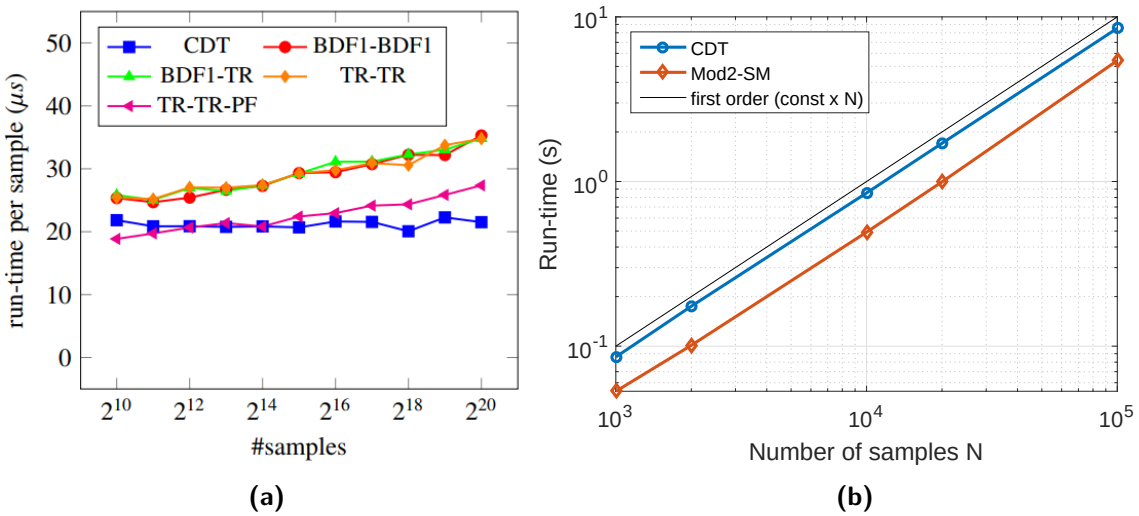

Figure 5-25: (a) Run-time behaviour of FDT algorithm for multi-solitons (20 eigenvalues), taken from Figure 8.f in [4]. (b) Run-time of Mod-SM for 20 eigenvalues (Figure 5-20)

for more than 8 eigenvalues. Hence from such a relative comparison it can be concluded that Mod2-SM is potentially faster than FDT for generating multi-solitons although more thorough run-time tests on same platform are needed for conclusive proof. It is important to point out that FDT will be faster than Mod2-SM after certain number of eigenvalues. The author in [4] has demonstrated multi-soliton generation for 32 eigenvalues but does not mention an upper bound on the number of eigenvalues that FDT can handle. Mod2-SM has been tested for generating $3x10^5$ samples over a support of [-15,15] for 76 eigenvalues using the discrete spectrum defined in Section 5-2 (Figure 5-27).

In conclusion, CDT was found to be faster than other multi-soliton generation algorithms for low number of eigenvalues (K<4). DDE can be used for fast computation of multi-soliton potentials with acceptable errors when number of samples required is low ($N < 500$). Mod1 scheme is useful for applications which do not have hard requirements on error. Mod2 scheme can be used for generating large number of samples of multi-solitons with high number of eigenvalues. It was shown to be potentially faster than other algorithms currently available in literature.

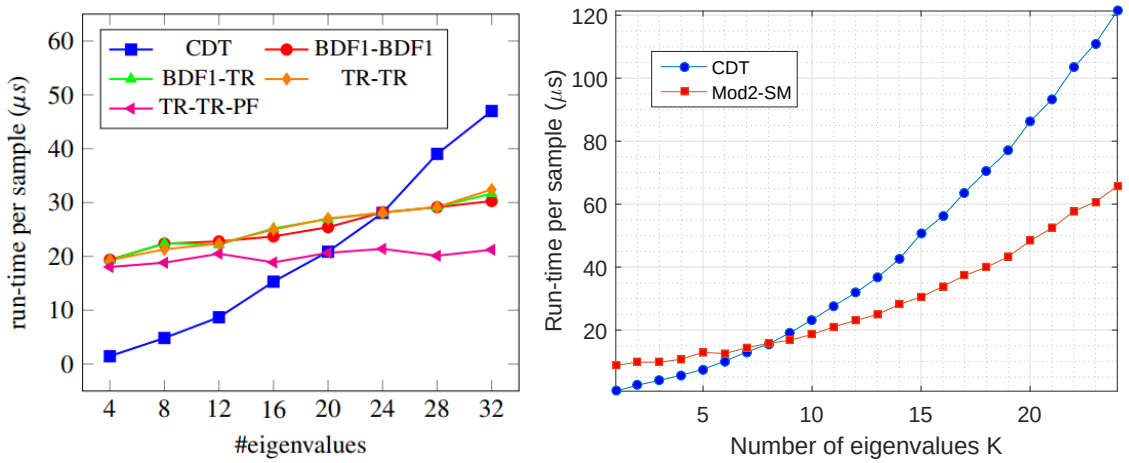

Figure 5-26: (a) Run-time of FDT algorithm for multi-solitons as a function of number of eigenvalues (2^{12} samples), taken from Figure 9.a in [4]. (b) Run-time of Mod-SM for 20 eigenvalues (Figure 5-20)

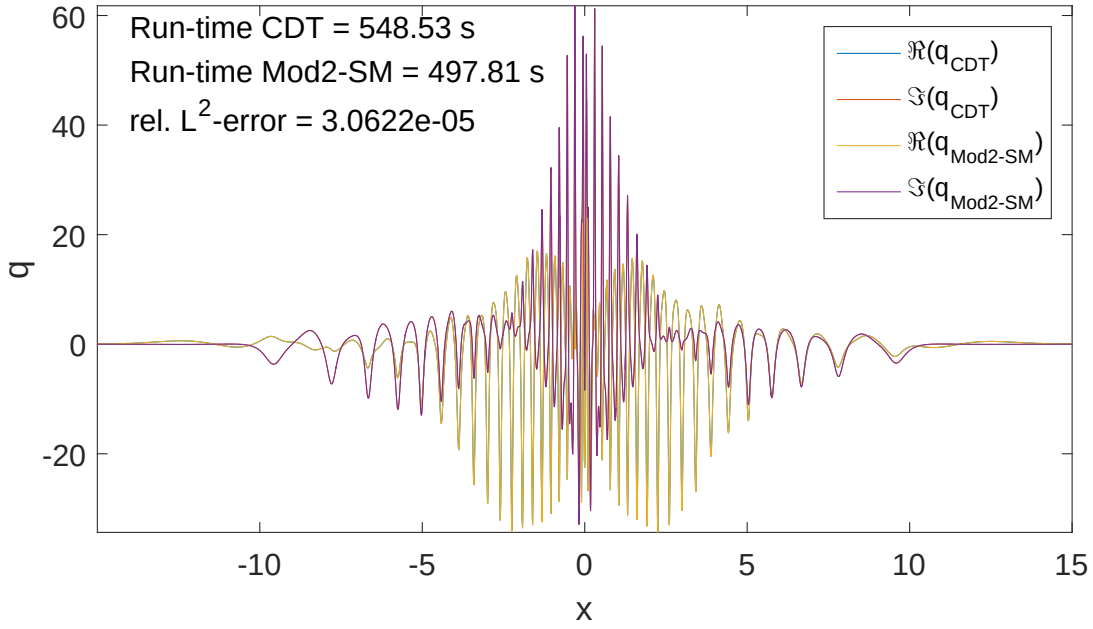

Figure 5-27: Potentials computed by CDT and Mod2-SM for 76 eigenvalues

Chapter 6

Conclusion and Future Work

Fast algorithms for inverse nonlinear Fourier transforms (NFT) are essential in making NFT based fiber-optic communications systems a reality. The use of discrete time methods for deriving such fast algorithms has already been demonstrated in literature. One such discrete time method is the discrete Darboux transform (DDT). It is an inverse NFT algorithm for computing multi-soliton solutions of discrete evolution equations. Exploiting properties of multi-solitons using the discrete Darboux transform led to an algorithm with a FLOPS complexity of $\mathcal{O}(KN)$ for K eigenvalues in the discrete part of the NFT and N samples. The algorithm is based on the evolution of the discrete Darboux matrix over the samples and is hence referred to as the discrete Darboux evolution (DDE) scheme. Error and run-time tests were conducted for the DDE by comparison with an efficient implementation of classical Darboux transform (CDT). It was shown to have acceptable errors while having run-time linear in K and N. The working precision of the underlying floating point number format however imposes some restrictions. The effects of working precision on the CDT, DDT and DDE were studied by implementing the algorithms in Julia language. It was found that the error in the potential computed by CDT is a simple function of the working precision and number of eigenvalues. For DDT and DDE, the error is primarily a function of step-size when the working precision is sufficient. The DDE scheme was found to have higher dependence on precision compared to DDT. Two modifications of DDE were introduced to overcome the restrictions arising from limited precision. The first modification (Mod1) uses the idea of building the potential in multiple runs instead of a single one. Mod1 can be used for fast computation of the potential but the approach leads to a lower bound on the achievable error. The second modification (Mod2) tries to overcome the limitation on error by using a multi-start approach instead of the single-start approach used by DDE. The error in the computed potential is shown to be comparable with algorithms currently found in literature. The run-time does not remain linear in K due to the additional computation time required for multiple starts.

The CDT was found to be faster than other multi-soliton generation algorithms for low number of eigenvalues (K<4). DDE can be used for fast computation of multi-soliton potentials with acceptable errors when number of samples required is low ($N < 500$). Mod1 is useful for

applications which do not have hard requirements on error. Mod2 can be used for generating large number of samples of multi-solitons with high number of eigenvalues. In a qualitative comparison it was shown to be potentially faster than the algorithm in [4] till 24 eigenvalues.

The modifications described in Chapter 5 may be extended further in the future. The ideal approach would be to either find an estimate for the errors in the Darboux coefficients at each sample point or measure the errors between two sample points and track their evolution. The error estimates could then be used to correct Darboux coefficients which might allow for computation of large number of samples without significant additional cost. In the multi-start approach of Mod2 (Section 5-3-2), the choice of the seed points can be made dynamic. An easily computable parameter should be used to measure the error in the Darboux coefficients and the coefficients should be corrected when the errors become significant. Such an algorithm will not have to rely upon a lookup table and can therefore work for any number and set of eigenvalues. The algorithm in [4] may be improved further by using the discrete Darboux transform instead of CDT. The discrete eigenfunctions can be used to efficiently compute the scattering coefficients and fast layer-peeling can then be used to compute the potential. Working completely in a discrete environment will perhaps help reduce the complexity.

Appendix A

The data on the maximum absolute errors collected during the multi-precision study is plotted here.

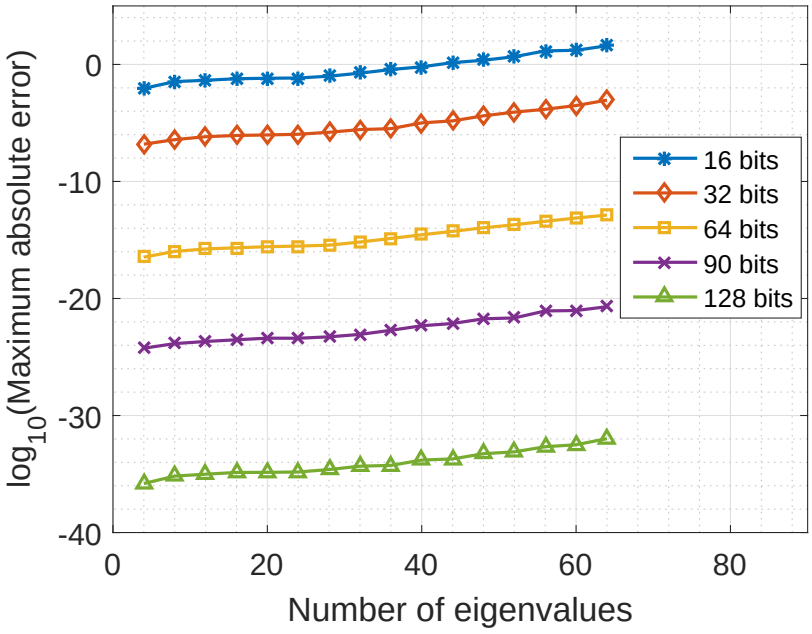

Figure A-1: The maximum absolute error of CDT algorithm is plotted against number of eigenvalues for varying precision.

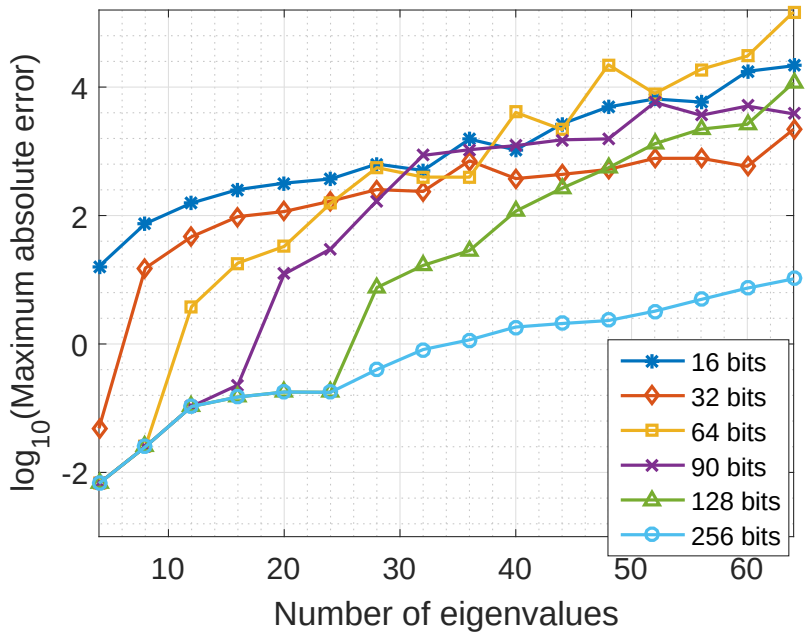

Figure A-2: The maximum absolute error of DDE-SM algorithm compared to CDT is plotted against number of eigenvalues for varying precision.

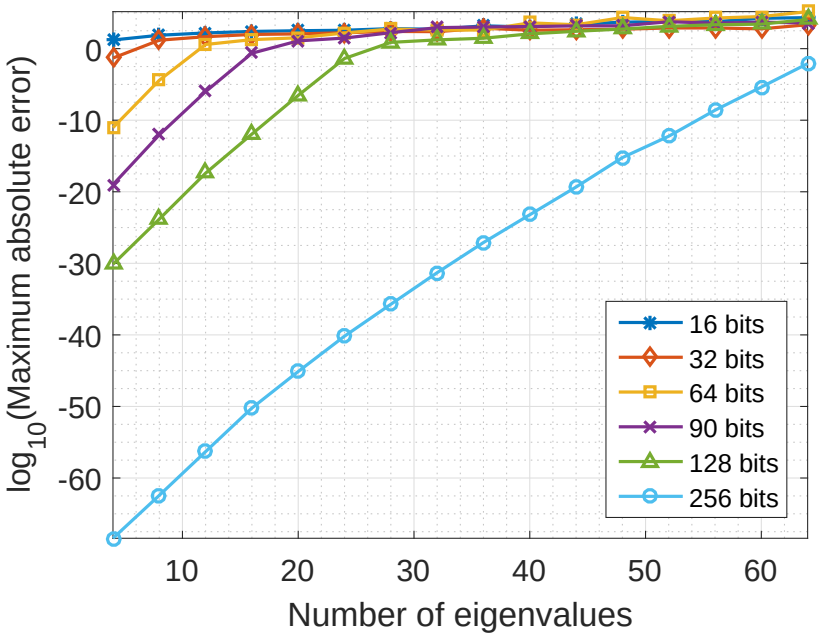

Figure A-3: The maximum absolute error of DDE-SM algorithm compared to DDT is plotted against number of eigenvalues for varying precision.

Appendix B

Pseudocode

Specific implementations of the DDE, Mod1 and Mod2 algorithms with the Split-Magnus discretization are mentioned here.

DDE-SM

Input: Eigenvalues ζ_k, norming constants b_k (Eq. (2-17)), step-size h (Section 3-1-1) and number of samples N
Output: $Q_n \approxeq hq(nh)$, where Q_n is the discrete potential and $q(x)$ is the continuous potential (Section 3-1-1)

- Arrange eigenvalues in decreasing order of magnitude of their imaginary parts.
- Transform the eigenvalues $z = e^{i\zeta h}$ (Section 3-1-1).
- For $j = 1, \ldots, K$ do:
  - Let $z_a = z_j$, $z_b = 1/z_j^*$, $\beta_a = -b_j$ and $\beta_b = 1/b_j^*$
  - $a_n = \frac{(\beta_b z_b - \beta_a z_a)}{(z_a z_b(\beta_a z_b - \beta_b z_a))}$, $\quad b_n = \frac{(z_a^2 - z_b^2)}{(z_a z_b(\beta_a z_b - \beta_b z_a))}$, $c_n = -b_n^*$ and $d_n = a_n^*$ (Eq. (4-20))
  - For $k = j+1, \cdots, K$ do:
    - $b_k = \frac{-(c_n - b_k(z_k + d_n/z_k)}{(a_n z_k + 1/z_k - b_k b_n)}$ (Darboux transform)
  - If j=1

$$M_0 = \begin{bmatrix} z^{-1} + a_n^1 z & b_n^0 \\ c_n^0 & z + d_n^{-1} z^{-1} \end{bmatrix} \quad \text{Eq. (4-19).}$$

    else

$$M = \begin{bmatrix} z^{-1} + a_n^1 z & b_n^0 \\ c_n^0 & z + d_n^{-1} z^{-1} \end{bmatrix}, \quad M_0 = M M_0.$$

- $V_0' = M_0 V_0$ (Eq. (4-9))

- For $n = 0, 1, \ldots, N$ do:
  - $Q'_{n+1/2} = \frac{-b_n^{(-K+1)}}{d_n^{(-K)}}$ (Eq. (4-29))
  - $R'_{n+1/2} = -Q'^{*}_{n+1/2}$
  - $V'_{n+1} = L'_n V'_n$ (Eq. (4-32))
- For $n = 0, -1, \ldots, -N$ do:
  - $Q'_{n+1/2} = b_{n+1}^{(K-1)}$ (Eq. (4-27))
  - $R'_{n+1/2} = -Q'^{*}_{n+1/2}$
  - $V'_{n-1} = L'^{-1}_{n-1} V'_n$ (Eq. (4-31))

Mod1-SM

Input: Eigenvalues $\mathfrak{S}$, norming constants $\mathfrak{B}$ (Eq. (2-17)), step-size h_o (Section 3-1) and support [LL,LR]
Output: $Q_n \approxeq h_o q(nh_o)$, where Q_n is the discrete potential and $q(x)$ is the continuous potential (Section 3-1-1)

- Arrange eigenvalues in decreasing order of magnitude of their imaginary parts.
- Compute the scaling factor $\mathcal{S} = |LR - LL|/20$ (Eq. (5-5)).
- Compute the scaled parameters as $\mathfrak{S}_s = \mathcal{S}\mathfrak{S}$ and $h_s = h_o/\mathcal{S}$.
- Look-up h^k_{min} from Figure 5-7.
- Calculate number of required iterations $\mathcal{F} = \left\lfloor h^k_{min}/h_s \right\rfloor$ and let $\mathfrak{C}_k = -\lfloor \mathcal{F}/2 \rfloor + (k-1)$, $k = 1, 2, \ldots, \mathcal{F}$. The number of samples per run $N = \mathcal{F}20/h^k_{min}$.
- Transform the eigenvalues $z = e^{i\zeta h}$ (Section 3-1-1).
- For f = 1 to $\mathcal{F}$ do:
  - $b_k = \mathfrak{B}_k e^{(2i\mathfrak{S}_k \mathfrak{C}_f h_o)}$, where subscript k denotes the k^{th} element.
  - For $j = 1, \ldots, K$ do:
    - Let $z_a = z_j$, $z_b = 1/z_j^*$, $\beta_a = -b_j$ and $\beta_b = 1/b_j^*$
    - $a_n = \frac{(\beta_b z_b - \beta_a z_a)}{(z_a z_b(\beta_a z_b - \beta_b z_a))}$, $b_n = \frac{(z_a^2 - z_b^2)}{(z_a z_b(\beta_a z_b - \beta_b z_a))}$, $c_n = -b_n^*$ and $d_n = a_n^*$ (Eq. (4-20))
    - For $k = j+1, \ldots, K$ do:
      - $b_k = \frac{-(c_n - b_k(z_k + d_n/z_k)}{(a_n z_k + 1/z_k - b_k b_n)}$ (Darboux transform)

* If j=1

$$M_0 = \begin{bmatrix} z^{-1} + a_n^1 z & b_n^0 \\ c_n^0 & z + d_n^{-1} z^{-1} \end{bmatrix} \quad \text{Eq. (4-19).}$$

else

$$M = \begin{bmatrix} z^{-1} + a_n^1 z & b_n^0 \\ c_n^0 & z + d_n^{-1} z^{-1} \end{bmatrix}, \quad M_0 = M M_0.$$

- $V_0' = M_0 V_0$ (Eq. (4-9))
- For $n = 0, 1, \ldots, N$ do:
  - $Q_{n+1/2}^{f'} = \frac{-b_n^{(-K+1)}}{d_n^{(-K)}}$ (Eq. (4-29))
  - $R_{n+1/2}^{f'} = -Q_{n+1/2}^{f'*}$
  - $V_{n+1}' = L_n' V_n'$ (Eq. (4-32))
- For $n = 0, -1, \ldots, -N$ do:
  - $Q_{n+1/2}^{f'} = b_{n+1}^{(K-1)}$ (Eq. (4-27))
  - $R_{n+1/2}^{f'} = -Q_{n+1/2}^{f'*}$
  - $V_{n-1}' = L_{n-1}^{'-1} V_n'$ (Eq. (4-31))

- Interweave and scale $Q_n^{1'}$ to $Q_n^{\mathcal{F}'}$ by defining vector $Q_n = \frac{1}{\mathcal{S}}(Q_1^{1'}, Q_1^{2'}, \ldots, Q_1^{\mathcal{F}'}, Q_2^{1'}, Q_2^{2'}, \ldots, Q_2^{\mathcal{F}'}, \ldots, Q_n^{1'}, Q_n^{2'}, \ldots, Q_n^{\mathcal{F}'})$

Mod2-SM

Input: Eigenvalues $\mathfrak{S}$, norming constants $\mathfrak{B}$ (Eq. (2-17)), step-size h (Section 3-1) and support [LL,LR]
Output: $Q_n \approxeq hq(nh)$, where Q_n is the discrete potential and $q(x)$ is the continuous potential (Section 3-1)

- Arrange eigenvalues in decreasing order of magnitude of their imaginary parts.
- Transform the eigenvalues $z = e^{i\zeta h}$ (Section 3-1-1).
- Total number of samples $N = |LR - LL|/h$. Define $N_{max} = \lceil 250/K \rceil$. Number of required seed points $M = \lceil KN/500 \rceil$, where $\lceil \rceil$ denotes rounding up to nearest integer.
- Let l be the location of M seed points. $l_j = LL + (250h/K) + j - 1, j = 1, 2, \ldots, M$.
- For $f = 1$ to M do:
  - Translate the norming constants $b_k = \mathfrak{B}_k e^{2i\mathfrak{S}_k l_f}$.
  - For $j = 1, \ldots, K$ do:
    - Let $z_a = z_j$, $z_b = 1/z_j^*$, $\beta_a = -b_j$ and $\beta_b = 1/b_j^*$

* $a_n = \frac{(\beta_b z_b - \beta_a z_a)}{(z_a z_b(\beta_a z_b - \beta_b z_a))}$, $b_n = \frac{(z_a^2 - z_b^2)}{(z_a z_b(\beta_a z_b - \beta_b z_a))}$, $c_n = -b_n^*$ and $d_n = a_n^*$ (Eq. (4-20))
* For $k = j+1, \ldots, K$ do:
  · $b_k = \frac{-(c_n - b_k(z_k + d_n/z_k)}{(a_n z_k + 1/z_k - b_k b_n)}$ (Darboux transform)
* If j=1

$$M_0 = \begin{bmatrix} z^{-1} + a_n^1 z & b_n^0 \\ c_n^0 & z + d_n^{-1} z^{-1} \end{bmatrix} \quad \text{Eq. (4-19).}$$

else

$$M = \begin{bmatrix} z^{-1} + a_n^1 z & b_n^0 \\ c_n^0 & z + d_n^{-1} z^{-1} \end{bmatrix}, \quad M_0 = M M_0.$$

– $V_0' = M_0 V_0$ (Eq. (4-9))
– For $n = 0, 1, \ldots, N_{max}$ do:
  * $Q_{n+1/2}^{f'} = \frac{-b_n^{(-K+1)}}{d_n^{(-K)}}$ (Eq. (4-29))
  * $R_{n+1/2}^{f'} = -Q_{n+1/2}^{f'*}$
  * $V_{n+1}' = L_n' V_n'$ (Eq. (4-32))
– For $n = 0, -1, \ldots, -N_{max}$ do:
  * $Q_{n+1/2}^{f'} = b_{n+1}^{(K-1)}$ (Eq. (4-27))
  * $R_{n+1/2}^{f'} = -Q_{n+1/2}^{f'*}$
  * $V_{n-1}' = L_{n-1}^{'-1} V_n'$ (Eq. (4-31))

- Combine Q_n^1 to Q_n^M by defining vector

$$Q_n = (Q_{-N_{max}}^1, Q_{-N_{max}+1}^1, \ldots, Q_{N_{max}}^1, Q_{-N_{max}}^2, Q_{-N_{max}+1}^2, \ldots, Q_{N_{max}}^2, \ldots \\ \ldots, Q_{-N_{max}}^M, Q_{-N_{max}+1}^M, \ldots, Q_{N_{max}}^M)$$

Animations

In this section some interesting animations are presented. Such animations add the dimension of time which makes understanding complex processes easier. The animations can be controlled using the control options below each one. Pressing ▷ begins the animation. They have been tested and found to be working correctly using Adobe Acrobat Reader.

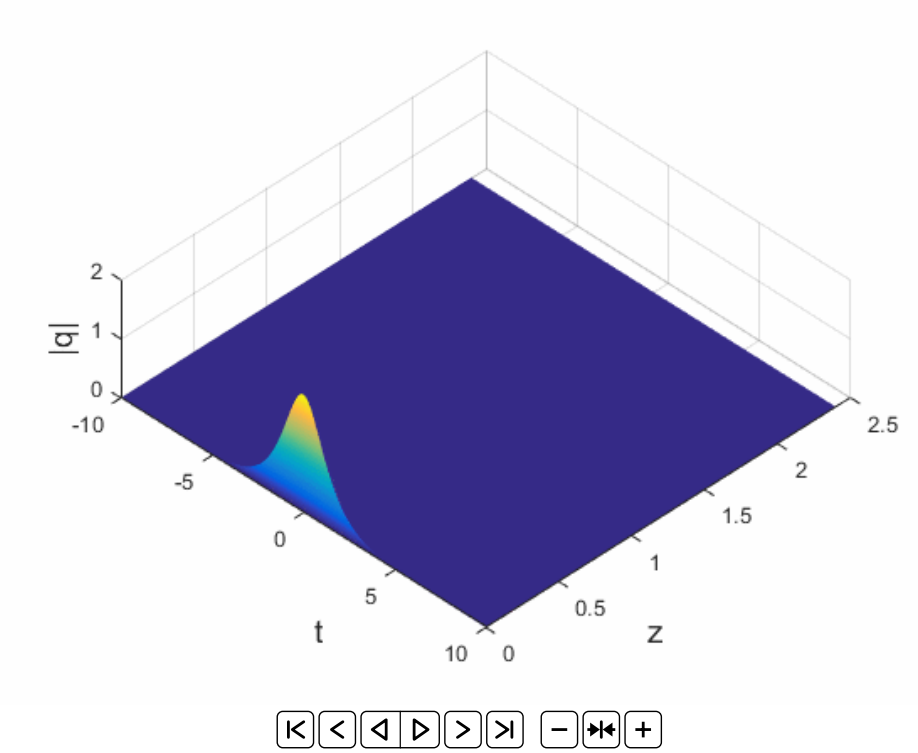

Figure B-1: Propogation of breather solution formed by interaction of two solitons moving at the same phase velocity

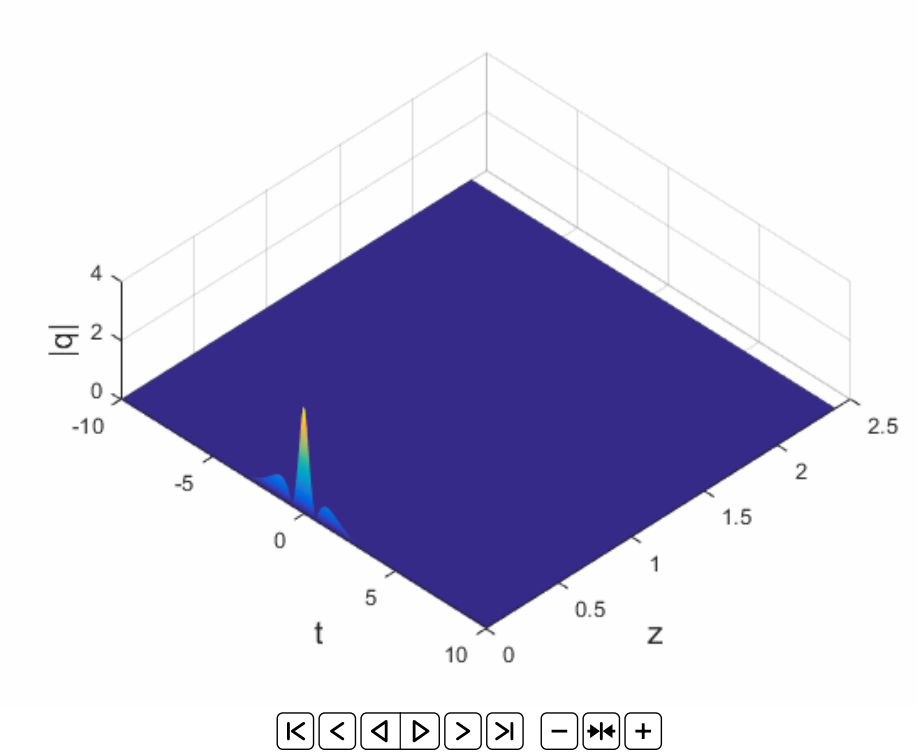

Figure B-2: A multi-soliton splits into two individual solitons as it propagates through the fiber

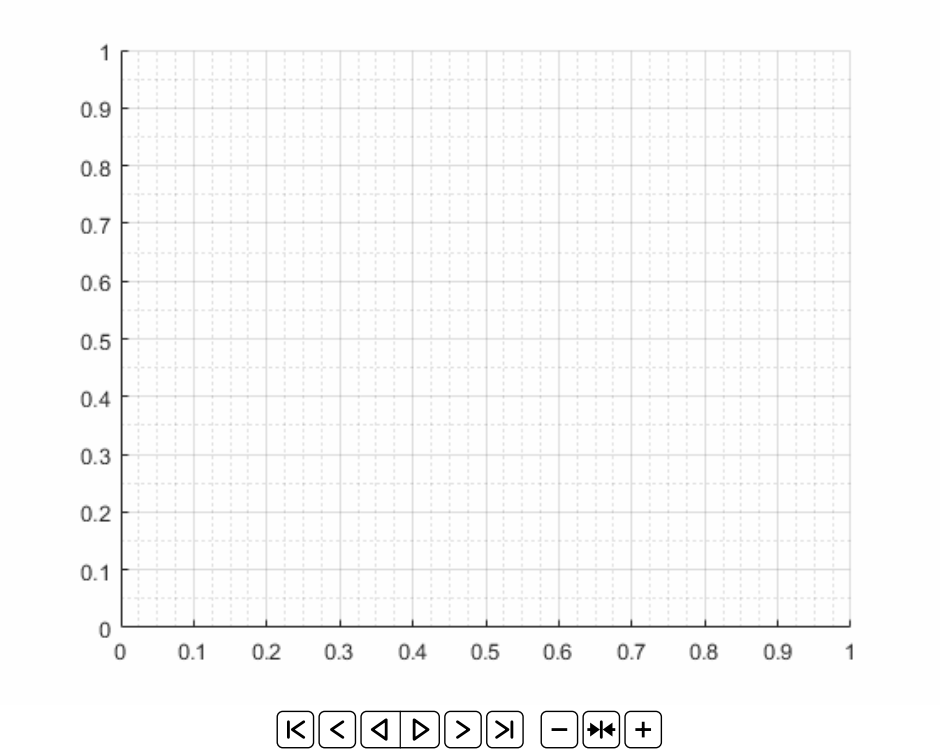

Figure B-3: Visual representation of the DDE scheme generating $2\,\mathrm{sech}(x)$ signal

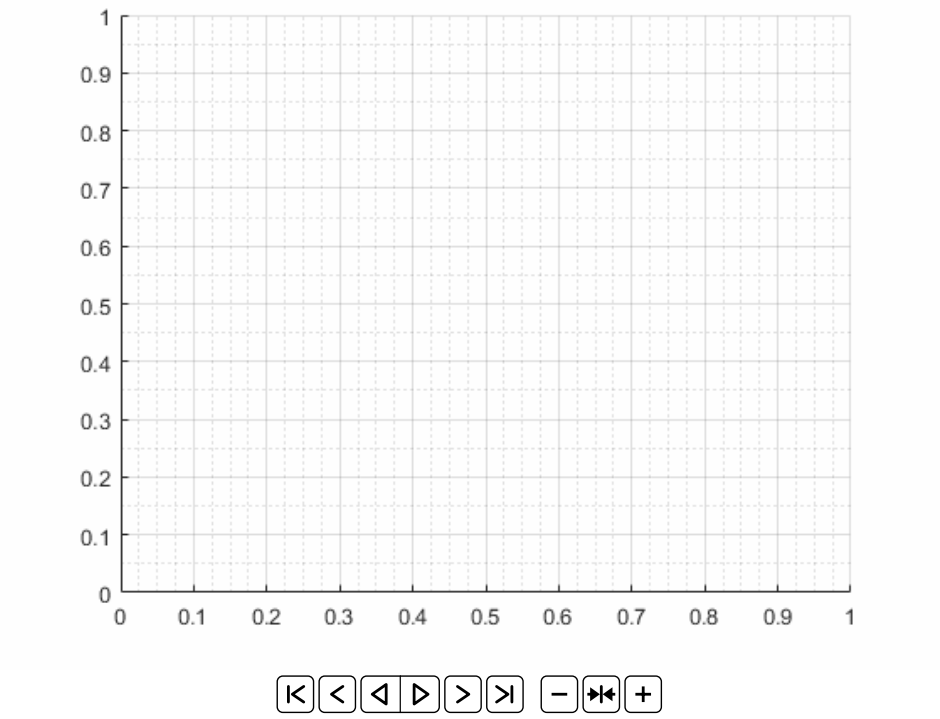

Figure B-4: Visual representation of failure of the DDE scheme while generating $12\,\mathrm{sech}(x)$ signal

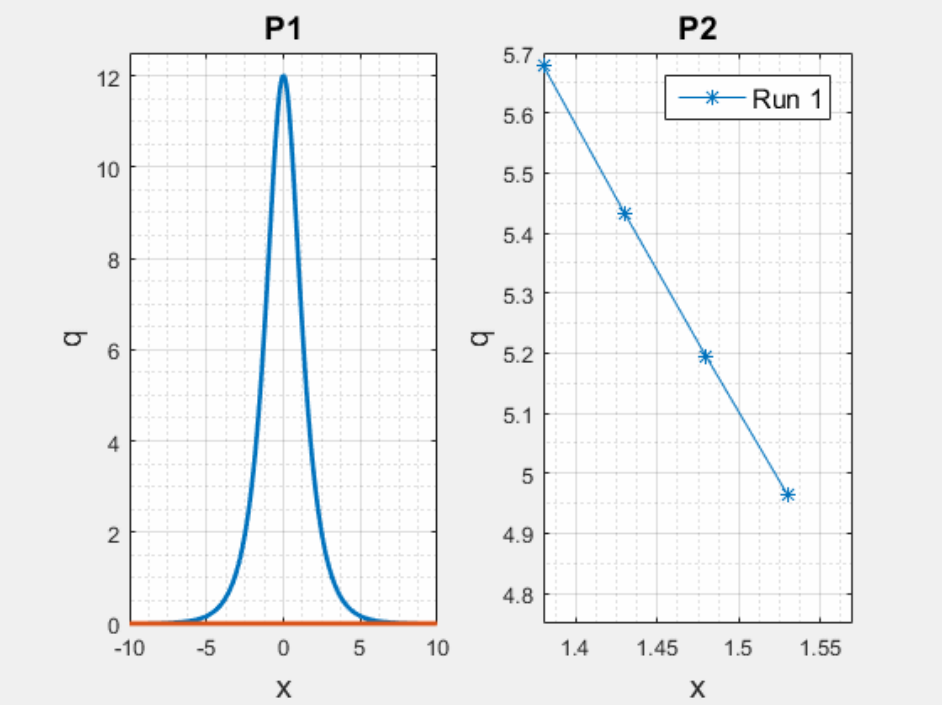

Figure B-5: Visual representation of the Mod1 scheme generating $12\,\mathrm{sech}(x)$ signal

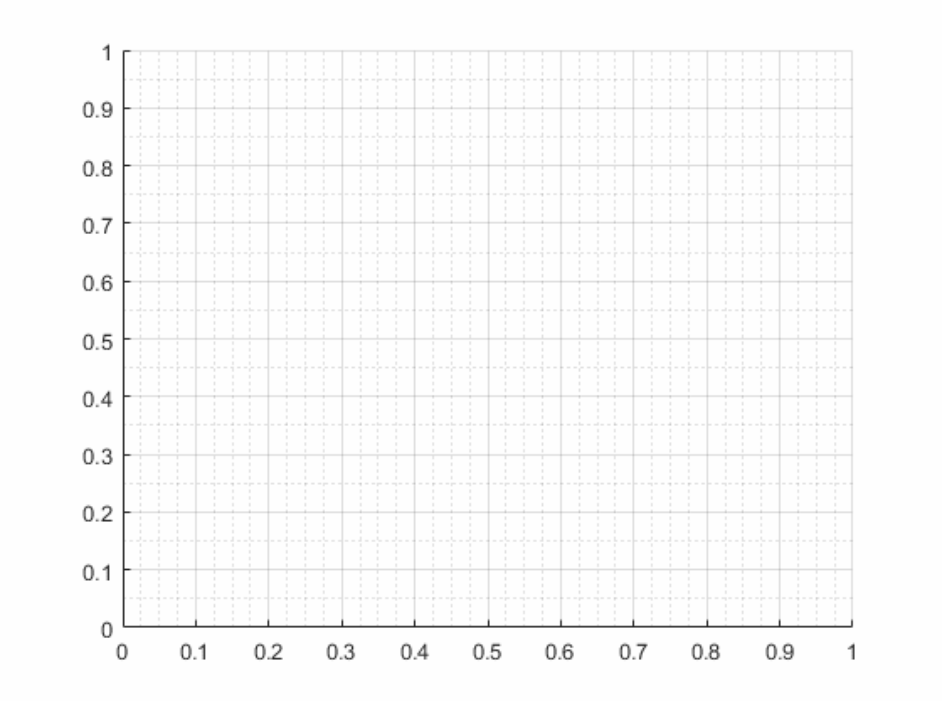

Figure B-6: Visual representation of the Mod2 scheme generating $12\,\mathrm{sech}(x)$ signal

Bibliography

[1] "Soliton(optics)." https://en.wikipedia.org/wiki/Soliton_(optics). Accessed: 01-05-2017.

[2] P. Krtner, "Nonlinear Pulse Propagation." https://ocw.mit.edu/courses/electrical-engineering-and-computer-science/6-977-ultrafast-optics-spring-2005/lecture-notes/chapter3.pdf, 2016. Accessed: 01-02-2017.

[3] C. Gu, H. Hu, and Z. Zhou, *Darboux Transformations in Integrable Systems*, ch. "1+1 Dimensional Integrable Systems". Dordrecht: Springer, 2005.

[4] V. Vaibhav, "Fast Inverse Nonlinear Fourier Transformation using Exponential One-Step Methods, Part I: Darboux Transformation." Preprint: https://arxiv.org/abs/1704.00951, 2017. Accessed: 18-04-2017.

[5] S. Desbruslais, "Inverse Scattering Transform for Soliton Transmission Analysis," *Optical Fiber Technology*, vol. 2, no. 4, pp. 319–342, 1996.

[6] M. J. Ablowitz, D. J. Kaup, A. C. Newell, and S. Harvey, "The Inverse Scattering Transform-Fourier Analysis for Nonlinear Problems," *Studies in Applied Mathematics*, vol. 53, no. 4, pp. 249–315, 1974.

[7] C. Gardner and et al, "Method for Solving the Korteweg-de Vries Equation," *Phys. Rev. Lett.*, vol. 19, pp. 1095–1097, 1967.

[8] M. J. Ablowitz and J. F. Ladik, "Nonlinear Differential-Difference Equations and Fourier Analysis ," *J. Math. Phys.*, vol. 17, no. 6, p. 1011, 1976.

[9] V. Zakharov and A. Shabat, "Exact Theory of Two-Dimensional Self-Focusing and One-Dimensional Self-Modulation of Waves in Nonlinear Media," *Soviet Physics JETP*, vol. 34, p. 62, January 1972.

[10] R. Hirota, *The Direct Method in Soliton Theory*. Cambridge, U.K.: Cambridge University Press, 2004.

[11] M. Yousefi and F. Kschischang, "Information Transmission Using the Nonlinear Fourier Transform, Part III: Spectrum Modulation," *IEEE Transactions on Information Theory*, vol. 60, no. 7, pp. 4346–4369, 2014.

[12] G. Neugebauer and R. Meinel, "General N-Soliton Solution of the AKNS Class on Arbitrary Background," *Physics Letters A*, vol. 100, no. 9, pp. 467–470, 1984.

[13] J. Lin, "Evolution of the Scattering Data under the Classical Darboux Transform for su(2) Soliton Systems," *Acta Mathematicae Applicatae Sinica*, vol. 6, no. 4, pp. 308–316, 1990.

[14] "Bäcklund transform." https://en.wikipedia.org/wiki/B%C3%A4cklund_transform. Accessed: 01-05-2017.

[15] V. Aref, "Control and Detection of Discrete Spectral Amplitudes in Nonlinear Fourier Spectrum." Preprint: https://arxiv.org/abs/1605.06328v1, 2017. Accessed: 18-04-2017.

[16] V. Vaibhav and S. Wahls, "Multipoint Newton-type Nonlinear Fourier Transform for Detecting Multi-Solitons," in *Optical Fiber Communication Conference*, p. W2A.34, Optical Society of America, 2016.

[17] H. Flaschka, "On the Toda Lattice. II: Inverse-Scattering Solution," *Progress of Theoretical Physics*, vol. 51, no. 3, pp. 703–716, 1974.

[18] K. M. Case and M. Kac, "A Discrete Version of the Inverse Scattering Problem," *Journal of Mathematical Physics*, vol. 14, no. 5, pp. 594–603, 1973.

[19] K. M. Case, "On Discrete Inverse Scattering Problems. II," *Journal of Mathematical Physics*, vol. 14, no. 7, pp. 916–920, 1973.

[20] S. Manakov, "Complete Integrability and Stochastization of Discrete Dynamic Systems," *Soviet Physics JETP*, vol. 40, p. 269, January 1975.

[21] M. J. Ablowitz and J. F. Ladik, " Nonlinear Differential-Difference Equations ," *J. Math. Phys.*, vol. 17, no. 6, p. 598, 1975.

[22] M. Ablowitz and H. Segur, "IST in Other Settings," in *Solitons and the Inverse Scattering Transform*, SIAM, 1981.

[23] M. J. Ablowitz and J. F. Ladik, "A Nonlinear Difference Scheme and Inverse Scattering," *Studies in Applied Mathematics*, vol. 55, no. 3, pp. 213–229, 1976.

[24] W. Gautschi, *Numerical Analysis*. Boston: Birkhäuser, 2012.

[25] W. Magnus, "On the Exponential Solution of Differential Equations for a Linear Operator," *Communications on Pure and Applied Mathematics*, vol. 7, no. 4, pp. 649–673, 1954.

[26] M. Hochbruck and C. Lubich, "On Magnus Integrators for Time-Dependent Schrödinger Equations," *SIAM Journal on Numerical Analysis*, vol. 41, no. 3, pp. 945–963, 2003.

[27] G. Boffetta and A. R. Osborne, "Computation of the Direct Scattering Transform for the Nonlinear Schrödinger Equation," *Journal of Computational Physics*, vol. 102, no. 2, pp. 252–264, 1992.

[28] S. Burtsev, R. Camassa, and I. Timofeyev, "Numerical Algorithms for the Direct Spectral Transform with Applications to Nonlinear Schrödinger Type Systems," *Journal of Computational Physics*, vol. 147, no. 1, pp. 166–186, 1998.

[29] G. Strang, "On the Construction and Comparison of Difference Schemes," *SIAM Journal on Numerical Analysis*, vol. 5, no. 3, pp. 506–517, 1968.

[30] E. Hairer, C. Lubich, and G. Wanner, *Geometric Numerical Integration: Structure-Preserving Algorithms for Ordinary Differential Equations*. Springer Series in Computational Mathematics, Verlag Berlin Heidelberg: Springer, 2nd ed., 2006.

[31] M. Yousefi and F. Kschischang, "Information Transmission Using the Nonlinear Fourier Transform, Part II: Numerical Methods," *IEEE Transactions on Information Theory*, vol. 60, no. 7, pp. 4329–4345, 2014.

[32] S. Wahls and H. V. Poor, "Introducing the Fast Nonlinear Fourier Transform," in *2013 IEEE International Conference on Acoustics, Speech and Signal Processing*, pp. 5780–5784, May 2013.

[33] J. K. Brenne and J. Skaar, "Design of Grating-Assisted Codirectional Couplers With Discrete Inverse-Scattering Algorithms," *Journal of Lightwave Technology*, vol. 21, no. 1, pp. 254–263, 2003.

[34] S. Wahls and H. V. Poor, "Inverse Nonlinear Fourier Transforms Via Interpolation: The Ablowitz-Ladik Case," in *Proc. Int. Symp. Math. Theory Networks Systems (MTNS)*, (Groningen. The Netherlands), pp. 1848–1855, July 2014.

[35] S. Wahls and H. V. Poor, "Fast Inverse Nonlinear Fourier Transform for Generating Multi-Solitons in Optical Fiber," in *2015 IEEE International Symposium on Information Theory (ISIT)*, pp. 1676–1680, June 2015.

[36] W. K. McClary, "Fast Seismic Inversion," *Geophysics*, vol. 48, pp. 1371–1372, October 1983.

[37] G. Xianguo, "Darboux Transformation of the Discrete Ablowitz-Ladik Eigenvalue Problem," *Acta Math. Sci.*, vol. 9, pp. 21–6, 1989.

[38] R. Guo and X. Zhao, "Discrete Hirota Equation: Discrete Darboux Transformation and New Discrete Soliton Solutions," *Nonlinear Dynamics*, vol. 84, pp. 1901–1907, 2016.

[39] J. Satsuma and N. Yajima, "B. Initial Value Problems of One-Dimensional Self-Modulation of Nonlinear Waves in Dispersive Media," *Progress of Theoretical Physics Supplement*, vol. 55, pp. 284–306, 1974.

[40] H. Buelow, V. Aref, and W. Idler, "Transmission of Waveforms Determined by 7 Eigenvalues with PSK-Modulated Spectral Amplitudes," in *European Conference on Optical Communications (ECOC)*, pp. 412–414, 2016.

[41] A. Hasegawa and T. Nyu, "Eigenvalue Communication," *Journal of Lightwave Technology*, vol. 11, no. 3, pp. 395–399, 1993.

[42] S. Hari *et al.*, "Multieigenvalue Communication," *Journal of Lightwave Technology*, vol. 34, no. 13, pp. 3110–3117, 2016.

[43] M. Yousefi and F. Kschischang, "Information Transmission Using the Nonlinear Fourier Transform, Part I: Mathematical Tools," *IEEE Transactions on Information Theory*, vol. 60, no. 7, pp. 4312–4328, 2014.

[44] P. D. Lax, "Integrals of Nonlinear Equations of Evolution and Solitary Waves," *Comm. Pure Appl. Math.*, vol. 21, pp. 467–490, 1968.

[45] A. Iserles and S. Nørsett, "On the Solution of Linear Differential Equations in Lie Groups," *Philosophical Transactions of the Royal Society of London A: Mathematical, Physical and Engineering Sciences*, vol. 357, no. 1754, pp. 983–1019, 1999.

[46] E. Agrell *et al.*, "Roadmap of Optical Communications," *Journal of Optics*, vol. 18, no. 6, p. 063002, 2016.

[47] S. K. Turitsyn *et al.*, "Nonlinear Fourier Transform for Optical Data Processing and Transmission: Advances and Perspectives," *Optica*, vol. 4, pp. 307–322, Mar 2017.

[48] D. Rourke and P. Morris, "Half-Solitons as Solutions to the Zakharov-Shabat Eigenvalue Problem for rational reflection coefficient with application in the design of selective pulses in nuclear magnetic resonance," *Phys. Rev. A*, vol. 46, no. 7, 1992.

[49] D. Rourke and J. Saunders, "Half-Solitons as Solutions to the Zakharov-Shabat Eigenvalue Problem for Rational Reflection Coefficient. II. Potentials on Infinite Support," *Journal of Mathematical Physics*, vol. 35, pp. 848–872, 1994.

Glossary

List of Acronyms

NSE	Nonlinear Schrödinger Equation
PDE	Partial Differential Equation
SPM	self-phase modulation
NFT	nonlinear Fourier transform
KdV	Korteweg de Vries
CDT	classical Darboux transformation

List of Symbols

Abbreviations

ω_0	Angular carrier frequency
ϕ, ψ	Jost solutions
ζ	Eigenvalue
A	Field amplitude
c	Speed of light in vacuum
$D(x,t,\zeta)$	Darboux matrix
E	Shift operator
$M_n(t,z)$	Discrete Darboux matrix
n	Refractive index
n_0	Frequency dependent refractive index
$q(x,t)$	Complex valued potential
$R(k)$	Reflection coefficient

t	Time
$T(k)$	Transmission coefficient
$v(x,t,\zeta)$	Two dimensional eigenfunction
V_n	Discrete two dimensional eigenfunction
x	Propagation distance
z	Discrete eigenvalue